ANALYSIS OF THE EFFECTS OF CO_2 AND LANDSCAPE CHANGE USING A COUPLED PLANT AND METEOROLOGICAL MODEL

Joseph L. Eastman

NASA Grant No. NAG8-1511, NSF Grant No. ATM-9306754,
EPA Grant No. R824993-01-0, and NSF Grant No. DEB-9524129.
Roger A. Pielke, P.I. and Adviser

Colorado State University

DEPARTMENT OF ATMOSPHERIC SCIENCE

PAPER NO. 686

ANALYSIS OF THE EFFECTS OF CO_2 AND LANDSCAPE CHANGE USING A COUPLED PLANT AND METEOROLOGICAL MODEL

Joseph L. Eastman

Graduate Degree Program in Ecology
Colorado State University
Fort Collins, Colorado
Spring 1999

Atmospheric Science Paper No. 686

ABSTRACT

ANALYSIS OF THE EFFECTS OF CO_2 AND LANDSCAPE CHANGE USING A COUPLED PLANT AND METEOROLOGICAL MODEL

This study outlines the development and subsequent implementation of a meteorological model coupled to a plant-scale model capable of simulating micro to hemispheric scales. For this study, the modeling system was applied to mesoscale (50 km horizontal grid increment) sensitivity studies over a domain covering the central United States. The model was integrated over a single growing season, with observed 1989 meteorology nudging the boundaries. The meteorological model prognosed temperature, momentum, and precipitation processes. The plant model simulates, based on underlying vegetation, the C_3 and C_4 photosynthesis cycles. It was initialized with AVHRR 8 km NDVI data and VEMAP vegetation dataset. Coupling a mechanistic root submodel with a soil submodel, both integrating on a multi-layered grid, represented the below-ground processes. These coupled submodels were employed to simulate water uptake and effluence, heat conduction, and soil respiration.

Eight 210-day integrations were performed using a combination of current and natural vegetation, 1 $\times$ and 2 $\times$ CO_2 both with and without added radiative forcing due to doubling CO_2. In all simulations the CO_2 was treated as a scalar quantity and allowed to advect and diffuse in a manner similar to water vapor. In addition, the plant and soil interfaces provided sources and sinks for the CO_2. The 8 integrations were then analyzed to ascertain the relative contributions to prognosed meteorological and biological fields

due to changing landcover, 2 × CO_2 radiative forcing, 2 × CO_2 with no radiative forcing, and the nonlinear interactions between these factors.

Joseph L. Eastman
Graduate Degree Program in Ecology
Colorado State University
Fort Collins, Colorado 80523
Spring 1999

ACKNOWLEDGEMENTS

I would like to begin my acknowledgments expressing my gratitude and appreciation to Dr. Roger A. Pielke. His unwavering support during my academic career allowed me to complete this journey. In addition, his input into this dissertation from a scientific standpoint has been substantial. I would also like to thank Dr. Micheal B. Coughenour. It was under his diverse guidance that I was able to complete the complex model coupling that made this dissertation possible. Appreciation is also due to my other committee members, Drs. Alan C. Covich and Dennis J. Ojima. It was strong backgrounds in their respective fields that provided considerable insight into this project.

In retrospect, there are more people that deserve thanks for helping me complete this work. The excellent office staff of Dallas McDonald and Tara Pielke made all the papers, supply requests, and administrative logistics as painless as possible. Dr. Bob Walko also deserves mention for his patience in answering countless questions about the RAMS model. Discussions with Drs. Pier Vidale and Thomas Chase provided considerable insight into many components of this dissertation. Dr. Dan Binkley and the excellent academic staff at Colorado State's Graduate Degree Program in Ecology (GDPE) must also be commended for providing me the opportunity to pursue a degree in their excellent program. The head secretary for GDPE, Sally Dunphy, also receives my gratitude for administrative support during my academic pursuit.

Finally, I need to acknowledge the institutions that provided the necessary support allowing me to pursue this degree. These include NASA Grant No. NAG8-1511, NSF Grant No. ATM-9306754, EPA Grant No. R824993-01-0, and NSF Grant No. DEB-9524129.

TABLE OF CONTENTS

LIST OF FIGURES

LIST OF TABLES

Chapter 1

INTRODUCTION AND BACKGROUND

Over the past decade, climate research has tended to focus on carbon dioxide and its role as a greenhouse gas in radiatively forcing an increase in the globe's mean temperature. The term greenhouse gas is actually a misnomer; greenhouse temperatures rise mainly due to the restriction of vertical movement of air. The basic premise of greenhouse gas-induced global warming is that when a gas weakly absorbs shortwave radiation and strongly absorbs longwave radiation, it contributes to a net warming of the surface. This simplistic treatment ignores many complex interactions which take place throughout the depth of the atmosphere and near the surface. Numerous other processes, however, go into any climate change we observe. Two of these other processes are investigated in this dissertation.

The effect of CO_2 levels on plant processes is the subject of considerable investigation, although much of the focus is on agricultural plant species. In general, plants employing the C_3 photosynthesis pathway show a tendency for increased carbon fixation under doubled CO_2, which leads to a higher leaf area index. However, the quality of the biomass in terms of nitrogen content shows a reverse trend. In the case of C_4 photosynthesis, it is believed that the plants are already near CO_2 saturation, and little change in accumulated biomass is observed. However, these generalities are inconclusive and often contradictory. In most studies, a CO_2 enrichment process is used that restricts the feedback to the atmosphere and neglects the radiatively-forced component of increased CO_2. In general, Bazzaz (1990) outlines six expected responses of photosynthesis in natural ecosystems to increased CO_2 levels and include the following.

1. Elevated CO_2 reduces or completely eliminates photorespiration.

2. C_3 plants are more responsive than C_4 plants to elevated CO_2 levels, especially those above ambient concentrations.

3. Photosynthesis is enhanced by CO_2 but this enhancement may decline with time.

4. The response to CO_2 is more pronounced under high levels of other resources, especially water, nutrients, and light.

5. Adjustment of photosynthesis during growth occurs in some species but not in others, and this adjustment may be influenced by resource availability.

6. Species, even of the same community, may differ in their response to CO_2.

It is clear that any climate simulation with doubled CO_2 would have to include at least some of these effects, although there is a lack of pertinent data necessary to model the effect. This dissertation will explicitly address the first two responses.

When modeling the effects of increased CO_2 on the vegetation, it is a general practice to assume constant perturbations to observed climatologies and use the perturbed data to force the plant or ecosystem models. Although this method does provide possible changes due to changing climate, it lacks any real feedback from the underlying vegetation and soil system to the atmosphere.

One such process that is largely ignored is the change in the partitioning of the surface energy budget due to the underlying surface characteristics, which have undergone change due to human and natural activities as outlined in Cotton and Pielke (1995). These include forest management practices, urbanization, agriculture, and grazing. Vitousek et al. (1997), suggested that over 40% of the earth's land surface has been altered by human activity. Pielke and Zeng (1994) estimate that landscape change may have already altered the climate as much as a doubling of CO_2. Inherent in changing landscape is an alteration of the surface energy budget through albedo, soil characteristics, plant physiology, and hydrology. For example, a simple calculation of the blackbody radiative temperature from the Stefan-Boltzmann relationship gives a clear example of the sensitivity to small changes in albedo. Table 1.1 shows the globally-averaged albedo and corresponding radiative equilibrium temperature.

T (K)	Planetary Albedo
276.2521	0.04
274.8019	0.06
273.3283	0.08
271.8306	0.10
270.3077	0.12
268.7586	0.14
267.1822	0.16
265.5775	0.18
263.9431	0.20
262.2777	0.22
260.5800	0.24
258.8485	0.26
257.0815	0.28
255.2773	0.30
253.4340	0.32
251.5496	0.34
249.6219	0.36
247.6485	0.38
245.6267	0.40
243.5537	0.42
241.4264	0.44
239.2413	0.46
236.9947	0.48
234.6822	0.50

Table 1.1: Stefan-Boltzmann radiative equilibrium temperature for a given albedo.

An albedo of around 0.3 is generally an acceptable value for the planet (Otterman 1976). If one looks at a positive or negative change of 0.02, we can see a corresponding equilibrium temperature change of roughly 2.2 degrees. This value is probably within a range roughly corresponding to human impacts and on the order of change in the surface climate record the last 100 years.

Lewis and Wang (1998), examined the change in ground surface temperatures on the northern Vancouver Island and the southern Yukon. These areas have undergone considerable deforestation in the last 5–52 years. Northern Vancouver Island had an increase in the ground surface temperature of 1.8 K, while southern Yukon had a change of 1.2 K. He also found a general trend that the forested areas are coolest, while the grasslands that have taken over after deforestation are the warmest. In addition, the bore hole data used in the study exhibits negligible changes in the years prior to deforestation, or at undisturbed sites. Lewis and Wang (1998) suggest that if the earth is considered to radiate like a black body, the expected increase in ground surface temperatures due to deforestation would be on the order of 1 K.

There have been numerous studies examining the effects of surface patchiness on atmospheric circulations (Dalu et al. 1996; Vidale et al. 1997, Eastman 1994; Pielke et al. 1999a; Avissar 1995). These studies indicate significant effects due to the underlying vegetation on a variety of time scales. Accounting for vegetation in short and long-term integrations is crucial to simulating possible outcomes. The vegetation, and subsequent changes in above- and below-ground processes are closely tied to numerous abiotic factors, including soil characteristics, atmospheric temperature, precipitation, CO_2 concentrations, plant water potential, and other nutrients, such as nitrogen.

Pielke et al. (1999b) investigated the effect of landuse change in more detail. Using the Regional Atmospheric Modeling System (RAMS hereafter), coupled with a plant canopy model (Land Ecosystem Atmospheric Feedback model; LEAF-2) they were able to integrate the biophysical feedback between the vegetation and the atmosphere over south and central Florida using 2 months of meteorology from 1973 to provide the boundary conditions for the weather. Using extensive historical records to construct the vegetative

distribution dating back to 1900, they were able to initialize the vegetation used in LEAF corresponding to 1900, 1973, and the present. The results exhibited a general decrease in precipitation over land, as well as a general warming in most areas. Claussen (1994, 1998), Claussen et al. (1998), Foley (1994), Texier et al. (1997), Sivillo et al. (1997), Ziegler et al. (1997) and Lee (1992) also indicated a strong feedback between the underlying vegetation and precipitative processes.

The altered surface vegetation pattern can also be augmented by large-scale water use for irrigation practices. Examining the potential (natural) and current vegetation patterns over the central U.S., the Great Plains have undergone extensive change, while regions in the Rocky Mountains show considerably less. However, there has been an accompanying shift in moisture, as irrigation practices along the Front Range become commonplace. Shown in Figure 1.1 is a county-level map of irrigation practices. It is clear from this figure, that the western U.S. has undergone large-scale changes in water management.

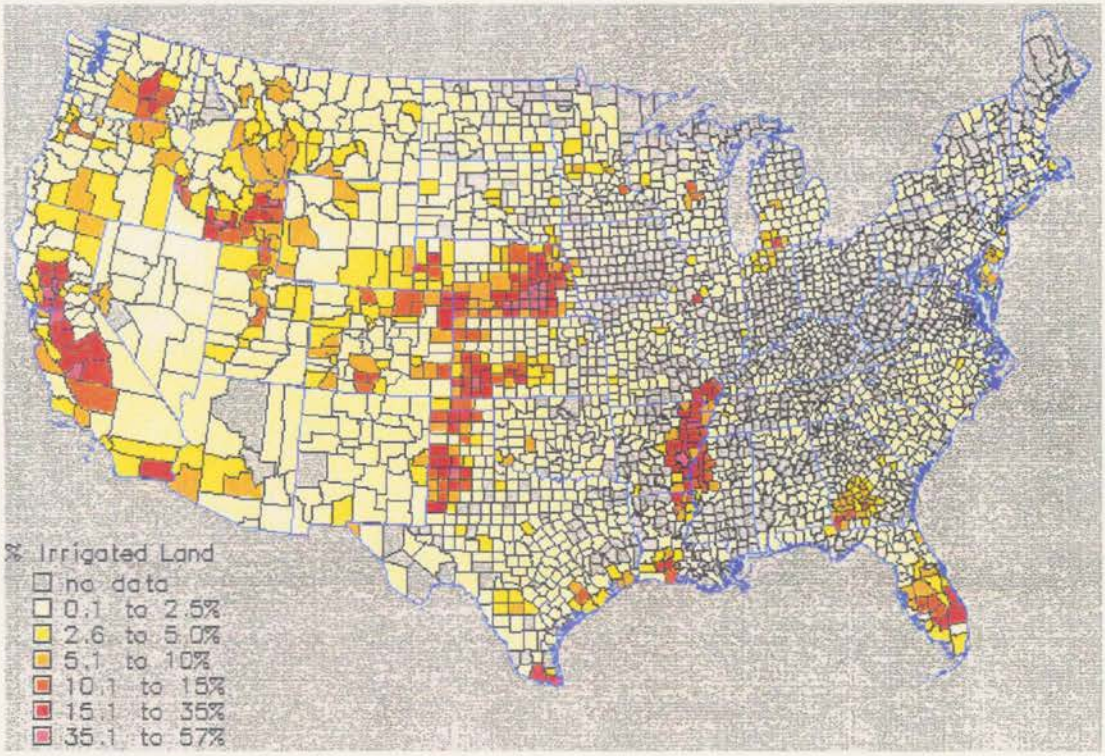

Figure 1.1: County level agricultural irrigation in percent of land.

On a global scale, Chase et al. (1996) used a general circulation model coupled with a simple vegetation parameterization to investigate the effects on large-scale weather patterns. The main study consisted of using presently observed values of leaf area index (LAI) for vegetative forcing and contrasting this to simulations using a potential LAI for the vegetative forcing. The model was integrated for 12 years, and results analyzed using regression and spectral methods for the last 10 years of the simulation. Distinctive patterns resulted from the different LAI distributions. Warm locations, on a regional scale, were found where the LAI had been considerably altered due to human impacts, such as deforestation and urbanization. Some areas showed a cooling, due mainly to a large-scale teleconnected dynamic response to the surface forcing. Detailed work by Henderson-Sellers and McGuffie (1995) also affirms climate dependence due to underlying vegetation. They also assert that "those content to generate vegetation in post facto from climate output will have incomplete results".

It is with the above mentioned studies and hypothesis in mind that this investigation has been designed. The approach here will be a regional modeling study. Using observed meteorology from 1989 as our boundary conditions, attempts are made to specifically address the complications stemming from biological responses to elevated atmospheric CO_2 levels. A modeling system that is highly mechanistic in its formulation is used to ascertain the effects, both meteorological and biological, due to landscape change, radiative CO_2 forcing, changing plant growth patterns due to enhanced CO_2 levels, as well as the nonlinear interactions among these effects. This mechanistic formulation is shown in Reynolds and Acock (1985) where they argued that plant growth models used to investigate elevated CO_2 must be mechanistic or semi-mechanistic in the areas that directly affect plant behavior. This approach is reinforced in Chen et al. (1994) where much of the basis for the plant growth model used here was developed. In their work describing C_4 photosynthesis, they suggest that this mechanistic approach will address the short-term effects of increasing CO_2, as well as the long-term effects resulting from plant acclimation to rising CO_2 levels.

This dissertation is devoted to outlining the coupled model system, its validation, and experiments to quantify the relative importance of CO_2 radiative and biological effects, as well as landscape change. The landscape change is from a potential vegetation as defined by Küchler (1964) relative to the current landuse patterns defined by the Vegetation/Ecosystem Modeling and Analysis Project (VEMAP; Kittel et al. 1995).

Chapter 2

THE COUPLED MODELING SYSTEM

The RAMS model serves as the meteorological platform used in this investigation. The model is a three-dimensional primitive equation model designed for studies of mesoscale processes. It is generally run in a nonhydrostatic mode (Tripoli and Cotton 1980). There are numerous options available for turbulence, radiation parameterization, soil model, boundary conditions, and microphysical parameterizations. For a complete description of all available options, the reader is referred to Walko et al. (1995a,b). The following section will briefly outline the options employed in this study.

2.1 RAMS Configuration

In this investigation, the model was run with a 50 km grid increment in the horizontal. The integrations were 7 months in length. Given these temporal and spatial scales, the choice of some model options becomes rather clear-cut. For example, it is computationally restrictive to run 7-month integrations using the explicit microphysics scheme. In explicit microphysics computations, the different forms of hydrometeors are prognosed every timestep at each gridpoint. Instead, a cumulus parameterization (Kuo and Raymond 1980) was used in conjunction with a dump-bucket precipitation scheme (Cotton et al. 1995). The temporal length also dictates the longwave and shortwave radiation parameterizations incorporated into the model. For these integrations, the Mahrer and Pielke (1977) scheme was used for the radiation model. This parameterization does not take into account the radiative effects of liquid water and ice.

The large horizontal grid increment in conjunction with a fine vertical grid increment (roughly 200 m in the boundary layer) mandates the use of anisotropic (different scale lengths for the vertical and horizontal grids) deformation in the choice of vertical and

horizontal diffusion parameterizations. The submodel is based on the original work of Smagorinsky et al. (1965). The choice of a large horizontal grid increment also allows a fairly long timestep of 90 s. Finally, the large horizontal mesh size permits a fairly small value of upward vertical motion, 0.85 cm s^{-1}, as being necessary to initiate convection in the cumulus parameterization.

The rest of the model options employed for all integrations in this investigation are listed below.

- Explicit multi-layer soil model (Tremback and Kessler 1985). This submodel is capable of representing twelve USGS soil textural classes and accounts for water and heat transport throughout the soil depth to the atmospheric interface.

- Hybrid time differencing scheme. This method calculates the velocity components and pressure by leapfrog differencing, while all other calculations are predicted using forward time differencing. In addition, a time-splitting scheme is employed that partitions the long timestep into an integral number of shorter timesteps. These shorter timesteps are used in calculating the pressure gradient and divergence terms in the model. The speed of sound is also altered internally by the model for increased computational efficiency.

- Newtonian relaxation or nudging in four dimensions. This will be discussed in Section 2.4.

- Addition of CO_2 as a scalar quantity.

- Spatially-variable Coriolis force.

- Rayleigh friction layer in top levels of the model domain. The friction layer allows the dampening of gravity waves that can result in numerical instability. Specifying a dissipation timescale augments the strength of the friction layer.

- Klemp/Wilhelmson (1978a,b) lateral boundary condition which depends on the specification of a phase speed to reduce reflections at the horizontal boundaries.

- A microphysics parameterization that diagnostically computes the condensation of water vapor to cloud water whenever supersaturation occurs. No explicit microphysics were activated for simulations used in this study.

2.1.1 Additional Parameterizations – ClimRAMS

The standard model, described previously, was modified to facilitate longer integrations, such as those used in this research. The basic additions are discussed below, however, the reader is referred to Liston and Pielke (1999) for a complete description. In its standard form, ClimRAMS performs vegetation calculations, such as leaf area index (LAI), and fractional coverage. This parameterization has been replaced by a separate plant model, which will be discussed in the next section.

ClimRAMS also has an enhanced hydrology. In this submodel, the effects of snow are considered in more detail than standard RAMS. Snow accumulation and melt are explicitly calculated at each gridpoint and timestep throughout the simulation. Accompanying the water phase changes, are calculations of thermal properties and their effects on the surface energy budget. The grid-scale albedo is also dependent on the amount of snow cover, although snow age effects are not accounted for. The runoff due to snow melt and other forms of precipitation are diagnosed at each timestep. If there is water available to the soil, it is first allowed to saturate the topsoil layer. If there is excess water beyond that required to saturate the topsoil, it is then stored as runoff and no further calculations are performed.

Finally, ClimRAMS provides a simple calculation for the radiative effects of cloud cover. Cloud cover has direct and indirect effects on the grid-scale meteorology and photosynthesis rates.

2.2 The Plant Model

In order to examine the effects of CO_2 and landcover change, a plant-scale model was coupled to the ClimRAMS meteorological model. This model replaces the standard vegetation model included in ClimRAMS, which was based on the model of Avissar and Mahrer (1988). Instead of using seasonal curves to simulate the seasonal change of biomass

and underlying surface characteristics, the new model prognoses the above and below-ground biomass as well as affecting surface energy calculations though the stoma and fractional coverage. This model is discussed in detail below.

2.2.1 C_3 Photosynthesis Calculation

The plant model is capable of simulating the C_3 and C_4 photosynthesis pathways. The C_3 cycle is based on the model developed by Farquhar et al. (1980). This model simulates the C_3 assimilation as a function of temperature, CO_2 and O_2 concentrations, and photosynthetically active radiation (PAR). The equations presented follow the work of Chen and Coughenour (1994), who modified the Farquhar scheme and developed a C_4 photosynthesis model. The model's ribulose biphosphate carboxylase (Rubisco) dependence, as shown in Chen and Coughenour (1994), is expressed in the following equation:

$$A_n = \left(1 - \frac{0.5O_{bs}}{\tau C_{bs}}\right) \min\{W_c, W_j\} - R_d \tag{2.1}$$

where A_n is the assimilation rate, (a specificity factor for Rubisco), O_{bs} the oxygen concentration inside the bundle sheath, C_{bs} the CO_2 concentration inside the bundle sheath, Rd the dark respiration rate, W_c the Rubisco-limited carboxylation rate, and W_j the ribulose-1,5-biphosphate (RuBP) regeneration limited carboxylation rate. W_c is described by a Michaelis-Menten equation:

$$W_c = \frac{JC_{bs}}{C_{bs} + k_c\left(1 + \frac{O_{bs}}{k_o}\right)} \tag{2.2}$$

where V_{cm} is the maximum carboxylation rate at saturated CO_2, k_c a Michaelis constant for carboxylation, and k_o a Michaelis constant for oxygenation. For the $RuBP$ regeneration dependence, the Chen and Coughenour model uses:

$$W_j = \frac{JC_{bs}}{(C_{bs} + O_{bs}/\tau)} \tag{2.3}$$

where J, the maximum rate of photosynthesis at C_{bs}, is represented by

$$J = \frac{\alpha I_p}{\left(1 + \alpha^2 I_p^2 / J_m^2\right)^{1/2}} \tag{2.4}$$

In this equation, I_p is the incident PAR, α is the quantum efficiency, and J_m is the potential rate of electron transport. This completes the basic set of equations for the C_3 portion of the photosynthesis calculations.

2.2.2 C_4 Photosynthesis Calculation

The C_3 portion of the photosynthesis is also coupled with the C_4 portion of the cycle, following the work of Chen et al. (1994). In this calculation, the limiting factor is the phosphoenolpyruvate carboxylase (PEPcase). The rate of the C_4 cycle, V_4, is again modeled by a Michaelis-Menten equation and is dependent on CO_2 concentration represented by the following equation:

$$V_4 = \frac{V_{4m} C_m}{C_m + k_p}, \tag{2.5}$$

where V_{4m} is this maximum velocity at a given PAR, C_m is the CO_2 concentration in the mesophyll, and k_p a constant. The PAR dependence of V_{4m} is shown in the following equation:

$$V_{4m} = \frac{\alpha_p I_p}{\left(1 + \alpha_p^2 I_p^2 / V_{pm}^2\right)^{1/2}} \tag{2.6}$$

where αp is a constant and V_{pm} is the potential PEPcase activity.

In both photosynthesis cycles, several variables must be solved before the assimilation rates can be determined. For some of the variables, this is accomplished through temperature dependence. C_m and O_m are calculated as a function of temperature after Long (1991), and also multiplied by the ambient air concentration of CO_2 and O_2. In this model, unlike previous modeling efforts, the CO_2 is treated as a scalar quantity that is advected and diffused using the same algorithm as water vapor, for instance. CO_2 is also dependent on the sources and sinks, which vary throughout the modeling period. Examination of the previous equations shows that the dependence on ambient CO_2 concentrations is crucial to the final assimilation rates. Field measurements by Bazzaz and Williams (1991) indicate that the CO_2 concentration in the atmosphere has a healthy seasonal component, as well as a strong diurnal dependence. Both of these dependencies are also regionally variable.

The kinetic parameters k_c, k_o, and k_p, as well, (and dark respiration rates employed in the previous equations) are temperature dependent and are described using Q10 factors (Chen et al. 1994). Finally, an Arrhenius function (Farquhar et al. 1980; Johnson and Thornley 1985) is used to describe the temperature dependence of J_m, V_{cm}, and V_{pm}.

In order to solve for the assimilation rate, a stomatal conductance must be supplied. In this model, the work of Ball et al. (1987) and Chen and Coughenour (1994) was adopted. The model is dependent on the CO_2 concentration and relative humidity at the leaf surface. Here, the relative humidity (RH) and ambient concentration of CO_2 (Ca) calculated by the meteorological model are used in the following equation:

$$g_s = g_b + g_m \left(\frac{A_n RH}{C_a} \right) \tag{2.7}$$

where g_b and g_m are specified parameters.

Chen and Coughenour (1994) also employ diffusion relations to calculate fluxes relevant to our calculations. For the diffusion flux between the bundle sheath and mesophyll, V_b, we have the relation:

$$V_b = (C_{bs} - C_m) / r_{bs} \tag{2.8}$$

where r_{bs} is the resistance to CO_2 between the bundle sheath and mesophyll.

In a similar manner, we can follow the same form described in Berry and Farquhar (1978) and Collatz et al. (1992) to represent the flow of oxygen between the bundle sheath and mesophyll by the equation:

$$f\, A_n = (O_{bs} - O_m) / r_{bso} \tag{2.9}$$

where f is the proportion of total net O_2 production occurring in the bundle sheath, while r_{bso} represents the resistance to O_2 diffusion between the two spaces.

Finally, the exchange of CO_2 between the atmosphere and mesophyll (A_n) can be described by (Chen and Coughenour 1994):

$$A_n = g_s (C_a - C_m) \tag{2.10}$$

In order to solve this system, Chen and Coughenour (1994) assume steady-state photosynthesis (over the timestep) and combine the previous three equations to solve for C_{bs} and O_{bs}. The Newton method, an iterative procedure, is used to solve for these quantities, as well as A_n. Computationally, this method has always closed, however, it can add 25% to the overall model timestep.

Once the available photosynthate has been prognosed, it is accumulated into a daily gross production for the canopy where it must be allocated to roots, shoots, leaves, and seed. This gross production is accumulated into sunlit and shade-produced photosynthate and weighted with the appropriate LAI values. The net available photosynthate is then calculated by subtracting the loss due to total respiration (growth and maintenance) and tissue death. Coefficients for total respiration and death, growth and maintenance, and tissue death rate were multiplied by total photosynthate production to calculate their effects on net carbon assimilation. In order to allocate the net photosynthate, partitioning coefficients were assigned to roots, shoots, leaves, and seeds. In all cases, the partitioning coefficients were further modified by linear interpolation functions that depend on soil water and temperature status. In the case of shoots, leaves, and seeds, the plant canopy temperature is used in place of the soil temperature.

2.2.3 The Root Model

The root model (Chen and Lieth 1993) is a fully three-dimensional interactive system designed to work with the RAMS soil model. At each vertical soil grid level, three components of root resistance are used to simulate the root system's interaction with the surrounding soil medium. There are two components independent of the soil status that follow the works of Chen and Lieth (1992) and Hillel et al. (1976). The radial resistance, R_{rad}, represents the resistance to water flow across the root surface to the xylem. The other component, R_{xyl}, represents the resistance in the xylem. These components are described by the following relations:

$$R_{rad} = R_{rad0}/RLD(\Delta z) \tag{2.11}$$

$$R_{xyl} = R_{xyl0}z/RLD(z) \tag{2.12}$$

where RLD is the root length density, z the absolute value of the depth below the surface, and Δz the spacing between soil levels.

A final component of the root resistance network is dependent on the soil water status through the following relation (Gardner 1960):

$$R_{soil} = ln\left[\left(\frac{1}{RLD\, r_{root}^2}\right)\right] \Big/ \left(4k_w RLD(z)\right) \tag{2.13}$$

where r_{root} is the root radius, and k_w the soil hydraulic conductivity. The soil resistance represents the resistance to water transport across the soil to the root surface. All three resistance components are updated daily in response to changing soil and root length density status.

The resistances are linked to the water by a formulation similar to Chen and Lieth (1992). Soil water uptake, S_w, is a function of plant water potential, ψ_{plant}, and soil water potential, ψ_w, as well as the dynamically-changing resistance functions and is represented by

$$S_w = (\psi_{plant} - \psi_w) / (R_{soil} + R_{rad} + R_{xyl}) \, . \tag{2.14}$$

This equation requires the determination of ψ_{plant}, which requires two assumptions. First, plant water capacity is ignored. This might be a limiting assumption for the woody species in the model, but would require the specification of a quantity that is not fully quantified at the present. The other assumption is that root water uptake is equal to canopy transpiration shown by

$$\int E_{cp} d\, LAI = \int S_w dz \tag{2.15}$$

where E_{cp} is the canopy transpiration rate, and is integrated over LAI. The S_w is integrated over the depth of the root system. Now we can integrate Eq. 2.14 and substitute in $E_{cp} dLAI$ for $S_w dz$ and solve for ψ_{plant} to obtain

$$\psi_{plant} = \frac{\int \psi_w / (R_{soil} + R_{rad} + R_{xyl}) \, dz - \int E_{cp} dl}{\int 1 / (R_{soil} + R_{rad} + R_{xyl}) \, dz} \tag{2.16}$$

This represents the plant water potential at the base of the stem.

Examination of Eq. 2,16 exhibits no control over the direction of flow. In many modeling efforts this is limited to water uptake only. However, as pointed out in Jackson et al. (1996), there are over 20 species that have been shown to output water under gradients reversed from typical water uptake. In Dawson (1993), the effects were clearly demonstrated under drought conditions in upstate New York. The water would move up the xylem from the lowest levels of the root system, where it was efflued in the upper layers where relatively drier soil moisture status exists. This would clearly affect the

surface energy budget. This root model was tested against the standard ClimRAMS root model and found to give superior performance when compared to observations from Dawson's study and over the domain used in the First International Field Experiment (FIFE). The standard root model exhibited a continual overestimation of soil drying that was magnified by the end of the growing season.

The root model also employs a root growth parameterization. This portion of the model simulates root growth by branching and extending. The branching and extension are accomplished through an algorithm developed by Chen and Lieth (1993). The algorithm is rather simplistic in that it only uses soil moisture, temperature, and model-calculated carbohydrate availability. This algorithm ignores the obvious effects introduced by nutrient availability, salt status, and aeration. However, these factors would require the use of a detailed soil organic model, which is currently not available. The algorithm is described in detail in Chen and Coughenour (1994).

A final component of the root model is an algorithm to calculate the flux of CO_2 from the soil to the atmosphere. The empirical relationship of Norman et al. (1992) was used here, as in Chen and Coughenour (1994). The empirical relation is dependent on the soil water content (percent of saturation) at 20 cm below the surface, and the soil temperature at a 10 cm depth.

2.2.4 The Canopy Radiation Model

The radiation transfer in the canopy is a complicated problem due to an extensive list of variables that must be accounted for. For example, the leaves can possess a complicated arrangement as one examines leaf angle distributions. The subsequent effects on reflection are clearly too computationally expensive to model explicitly. The problem is also complicated by the diurnal and seasonal cycle of the sun angle. The effects of diffuse and direct radiation on photosynthesis must also be considered. Clearly a model must be general enough to simulate a wide range of conditions, while at the same time demonstrate the ability to simulate the basic features of radiative transfer in the canopy. The model adapted here was first described by Goudriaan (1977) and further modified by Chen (1983).

The RAMS model according to Mahrer and Pielke (1977) calculates the incident radiation at the top of the canopy. This algorithm was further modified to account for cloud effects. The incident radiation is then used to calculate the flux densities of downward and upward radiation through nine canopy layers. These radiative fluxes are dependent on modified probability functions for interception and transmission for each layer and the zonal distribution of scattered radiation. These quantities are dependent on the inclination of the incident radiation. The layer upward and downward fluxes are also modified reflection and transmission coefficients of the leaves, and by the reflection-transmission distribution function that depends on leaf angle distribution. The effects of the RAMS prognosed soil albedo are also accounted for at the bottom layer of the canopy. In addition, the model explicitly calculates the canopy-soil-surface reflectance and whole canopy transmission coefficient.

The radiation model as presented in Goudriaan (1977) is too computationally expensive to be run in this form for long-term integrations. In his full model, the number of layers used is dependent on LAI. At values of LAI encountered in the simulations performed here, upwards of 100 layers would have to be used to break up the LAI into small components necessary to converge on a solution. Scaling up the results of a detailed multilayer model to fit an exponential extinction function solved this problem. This extinction function was weighted for cumulative LAI, and allows the model to keep track of sunlit and shaded LAI to be used in the photosynthesis and soil surface energy calculations. For a complete description of the finite difference equations, the reader is referred to Chen and Coughenour (1994).

2.3 The Interface Between Plant and Meteorological Models

The previous two sections have outlined the two models employed in this study. Next I discuss how the model's communicate their information to each other. This linkage will be described in this section as well shown schematically.

The plant and meteorological models both simulate processes that cover a wide range of temporal scales. The ClimRAMS simulates large shifts in calculated fluxes and temperatures over the course of a single timestep, which is 90 seconds in this case. At the

same time the various layers of the soil show a slow change that can be observed over several hours in the upper soil layers, to several days in the middle soil layers, to a month for the deepest soil layers. The plant model exhibits similar behavior, with the stoma responding, respiration and death rates operating on a single timestep, and root growth becoming visible on the order of several days.

The interface is largely constrained to the shortest timestep used in the model. This also includes the root model, which calculates the soil and plant water exchange every timestep. The root model is in turn linked to the plant water potential, which affects the photosynthesis rates. The easiest way to demonstrate the linkage is through an outline, which shows the various algorithms used in the model.

1. Call Surface Layer/Soil models
2. Compute Total Precipitation Flux
3. Update Land/Water and Combined Albedos and Shortwave
4. Compute Bare Ground Soil Water, Temperature, and Heat Fluxes
5. Update Vegetation Temperature
6. Compute Shaded Ground Soil Water, Temperature, and Heat Fluxes
7. Update Vegetation Temperature
8. Compute Root Water Uptake and Transpiration
9. Call Main Plant Subroutine
    - Update Photosynthetically-Active Radiation, and Shaded and Sunlit LAI
    - Update Maintenance Respiration
    - Calculate Photosynthesis Rates, and Stomatal Conductance
    - Allocate Photosynthate to Roots, Shoots, and Leaves
    - Update Root, Shoot, and Leaf Death

- Update Plant Dry Weights and LAI
- Distribute Root Photosynthate Vertically and Update Branching and Extension
- Compute Soil Respiration

10. Use LAI, Stomatal Conductance to Compute Effective Vegetation Mixing Ratio
11. Update u_*, θ_*, q_* , Latent/Sensible Heat Fluxes Over Plant
12. Update u_*, θ_*, q_* , Latent/Sensible Heat Fluxes Over Water
13. Update u_*, θ_*, q_*, Latent/Sensible Heat Fluxes Over Bare Dirt
14. Update Bare Dirt Soil Moisture Due to Vertical Transport
15. Update u_*, θ_*, q_*, Latent/Sensible Heat Fluxes Over Shaded Dirt
16. Update Bare Ground Soil Moisture Due to Vertical Transport
17. RETURN to RAMS

The quantities u_*, T_*, and q_* are the friction velocity, flux temperature, and moisture flux, respectively. These quantities are calculated using similarity theory and represent the turbulent transfer of momentum, heat, and moisture, respectively.

Chapter 3

EXPERIMENTAL DESIGN

3.1 Hypothesis

In the Introduction, several contributions to surface temperature fields were mentioned. It is the goal of this study to quantify these contributions with respect to atmospheric and biological variables for a single growing season. In summarizing the mechanistic modeling system used, it is clear that a combination of input variables (initial conditions) and their interaction with each other can produce several nonlinear processes. With this in mind, this investigation will specifically address the following set of hypotheses.

- Significant differences in the domain-averaged predicted meteorological and biological fields will be observable between the control simulation and perturbation simulations when
  - landcover is changed from current to potential vegetation,
  - radiative forcing is changed from $1\times CO_2$ to $2\times CO_2$, and
  - biological CO_2 levels are doubled.
- Significant differences in the domain-averaged predicted meteorological and biological fields will be observable due to the nonlinear interactions between:
  - landcover and doubled CO_2, and
  - radiative forcing at $2\times CO_2$ and landcover.
- Significant differences will be found between the control control and perturbation simulations at individual gridpoints due to each perturbation

- Significant differences will be found between the interaction of perturbations at individual gridpoints.
- Landcover-induced changes will exhibit more significant differences and higher magnitudes of contributions than either CO_2 effect.
- Localized nonlinear interaction effects can be as large as the contributions due to the individual perturbations themselves for some variables.

The demonstration of these hypotheses will be conducted using a factor separation technique outlined in Stein and Alpert (1993) and a variety of statistical tests. This factor separation technique is used to investigate the relative importance of perturbations and their interactions. The statistical tests are designed to examine statistically significant differences in mean, variance, and cumulative distribution.

3.1.1 Separation Methods

In order to quantify the different contributions, a well-documented technique developed by Stein and Alpert (1993) is used. In their work they demonstrate how a contribution due to any factor (or combination of factors) can be extracted from numerical model simulations. In outlining the procedure for n factors, they show that the investigator needs to analyze 2^n simulations. The setup for this investigation is outlined below.

In any numerical model we know that the predicted fields, f, will depend on the models' level of complexity as well as the initial conditions and boundary conditions. First, imagine CO_2 as a factor called ψ in a given model. If the factor continuously changes throughout the modeling domain, then we would expect that the predicted field f will undergo a similar continuous change. Let us now qualitatively investigate a two factor experiment.

Consider a condensed version of this dissertation, in which examination of the landuse change from natural to current states and $2\times CO_2$ effects (combine radiative and biological effects) are examined. This represents a two factor investigation. A widely accepted way to proceed is to run a control simulation with the current vegetation and $1\times CO_2$ (CON).

Another simulation would involve using natural vegetation and $1\times CO_2$ (N1×), while the third simulation would include current vegetation and $2\times CO_2$ (C2×). The investigator might then take a difference between CON and N1× to determine the effect of the change in vegetation. However, the difference fails to address the interaction between the vegetation and CO_2. For instance, much of the tall grass prairie has been replaced by crops and other agricultural practices. The interaction becomes obvious when one considers the stomatal response of a C_4 species (tall grass) and a C_3 species (most crops). To look at the effects of $2\times CO_2$ a difference between CON and C2× might be performed. Again, this difference fails to investigate the interaction of CO_2 and vegetation. According to Stein and Alpert, a fourth simulation is needed. This simulation is needed to separate the interactive effects of vegetation and CO_2. This simulation would include natural vegetation and $2 \times CO_2$. This added simulation suggests that Stein and Alpert's 2^n simulations is correct for this case since it is obvious we must include the interactions of factors.

In the case of three factors, we can outline the simulations and the difference fields necessary to examine them. In this study, we have vegetation change, radiative $1 \times$ and $2 \times CO_2$, and biological $1 \times$ and $2 \times CO_2$ experienced by the plants in photosynthetic production. The term biological is meant to refer to the biota subjected to that CO_2 level, without specifying what level of CO_2 is used for the radiation parameterization. According to Stein and Alpert (1993), we need to perform 2^3 or eight integrations. These are summarized in Table 3.1.

Symbol	Vegetation	CO_2 radiative level	CO_2 biological concentration
f_0	Current	1×	1×
f_1	Natural	1×	1×
f_2	Current	2×	1×
f_3	Current	1×	2×
f_{12}	Natural	2×	1×
f_{23}	Current	2×	2×
f_{13}	Natural	1×	2×
f_{123}	Natural	2×	2×

Table 3.1: Description of the eight simulations and their representative symbols.

The eight simulations in Table 3.1 provide the necessary fields to produce the difference fields needed to ascertain the effects of each factor and their interactions. The contributions are natural vegetation, 2× CO_2 radiation, 2× CO_2 biology concentrations, interaction of natural vegetation and 2× CO_2 radiation, interaction of natural vegetation and 2× CO_2 biological levels, interaction of 2× CO_2 radiation and 2× CO_2 biology, and the triple interaction of natural vegetation with 2× CO_2 radiation and 2× CO_2 biology. The difference fields necessary to ascertain these contributions are summarized in Table 3.2.

Symbol	Difference	Interpretation
$\hat{f}_0$	f_0	Contribution with no factors present, the control run
$\hat{f}_1$	$f_1 - f_0$	Contribution due to natural vegetation
$\hat{f}_2$	$f_2 - f_0$	Contribution due to 2× CO_2 radiation
$\hat{f}_3$	$f_3 - f_0$	Contribution due to 2× CO_2 biology
$\hat{f}_{12}$	$f_{12} - (f_1 + f_2) + f_0$	Contribution due to interaction of natural vegetation and 2× CO_2 radiation
$\hat{f}_{23}$	$f_{23} - (f_2 + f_3) + f_0$	Contribution due to interaction of 2× CO_2 radiation and biology
$\hat{f}_{13}$	$f_{13} - (f_1 + f_3) + f_0$	Contribution due to interaction of natural vegetation and 2× CO_2biology
$\hat{f}_{123}$	$f_{123} - (f_{12} + f_{13} + f_{13})$ $+(f_1 + f_2 + f_3) - f_0$	Contribution due to interaction of natural vegetation, 2× CO_2 radiation and biology

Table 3.2: Description of the difference fields and their representative symbols.

3.1.2 Initialization

The complexity of the modeling system demands a considerable number of variables be initialized. The experimental design requires that all initialized fields be consistent

between the simulations. This consistency is accomplished through well-defined procedures for both plant and meteorological initializations. The procedures are described below.

3.2 Plant Model Initialization

3.2.1 Vegetation Distribution

The current and natural vegetation distributions were directly input from the VEMAP dataset. The vegetation types are assigned the dominant lifeform and leaf characteristics, as well as distinguished by C_3 and C_4 photosynthesis pathways. In the case of natural or potential vegetation, the classes derived by Küchler (1964) were based on current vegetation distributions, historical data, current climate, and CO_2 levels. Figure 3.1 shows the current and Figure 3.2 displays the natural vegetation distribution.

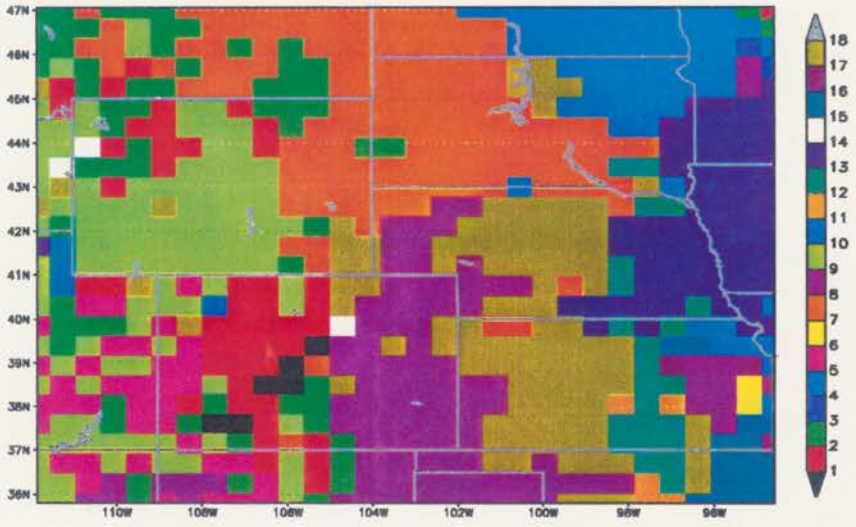

Figure 3.1: Current vegetation distribution. Classes are 1 - tundra, 2 - subalpine, 3 - temperate conifer, 4 - temperate deciduous, 5 - temperate xeromorphic, 6 - temperate coniferous xeromorphic, 7 - savanna and deciduous, 8 - C_3 shortgrass, 9 - C_4 tallgrass, 10 - temperate arid shrub, 11 - spring wheat and small grains, 12 - small grains, 13 - winter wheat, 14 - corn, 15 - irrigated crop, 16 - deciduous forest, crop, 17 - creosote bush, 18 - grassland and grain

3.2.2 NDVI-Derived LAI, Biomass, and Spring Green-up Algorithm

The 8 km Normalized Difference Vegetation Index (NDVI) data are available in a 10-day averaged format and provide an estimation of LAI changes on this timescale. From

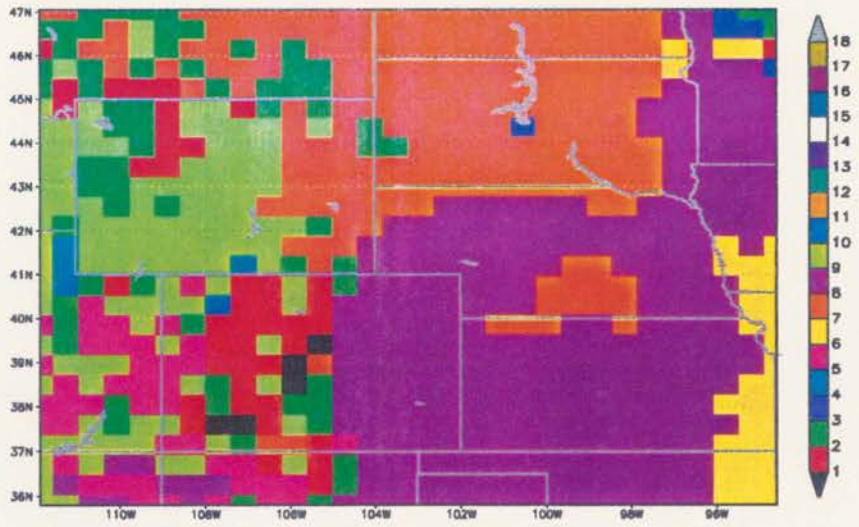

Figure 3.2: Natural vegetation distribution. Classes are 1 - tundra, 2 - subalpine, 3 - temperate conifer, 4 - temperate deciduous, 5 - temperate xeromorphic, 6 - temperate coniferous xeromorphic, 7 - savanna and deciduous, 8 - C_3 shortgrass, 9 - C_4 tallgrass, 10 - temperate arid shrub, 11 - spring wheat and small grains, 12 - small grains, 13 - winter wheat, 14 - corn, 15 - irrigated crop, 16 - deciduous forest, crop, 17 - creosote bush, 18 - grassland and grain.

these data the initial LAI at each gridpoint in the model domain can be calculated. The dataset can also provide an estimation of the rate of increase of LAI over the spring portion of the growing season. First, a LAI was derived from the NDVI data for the April 1 composite, using the following formulas for woody and herbaceous vegetation, respectively.

$$NDVI_{woody} = 0.915(1.0 - 0.83exp(-0.96LAI) \quad \text{(Nemani and Running 1989)} \quad (3.1)$$

$$NDVI_{herbeceous} = ln(LAI/0.1.625) * 0.34 \quad \text{(Asrar et al. 1984)} \quad (3.2)$$

In this experiment, two differing initial underlying vegetation surfaces are set by the NDVI. These surfaces include current and potential vegetation distributions. For each distribution, the above algorithms were used, resulting in slightly different LAI distributions. These distributions are displayed in Figure 3.3 and Figure 3.4. Note that the scale is nonlinear, so that the lower LAI values are distinguishable. It is clear that initial LAI differences are nearly indistinguishable except for a few cells in the southwest of the domain.

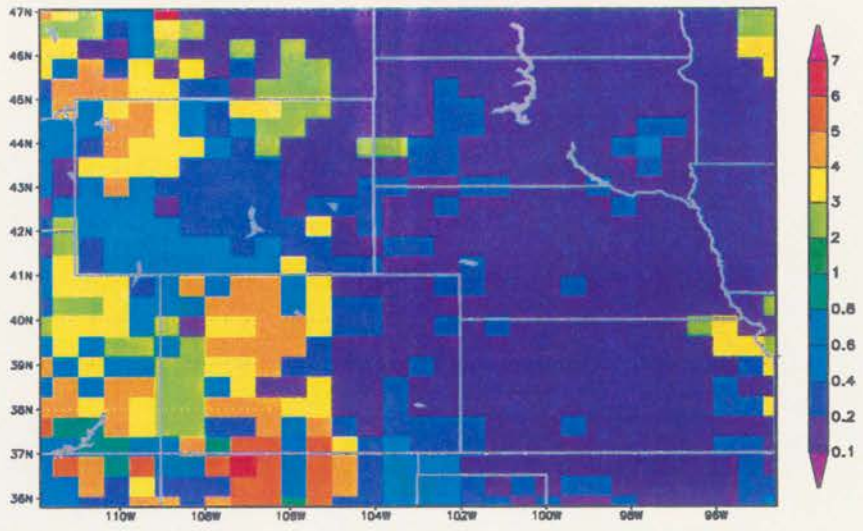

Figure 3.3: NDVI-derived LAI for current vegetation at the initial model time.

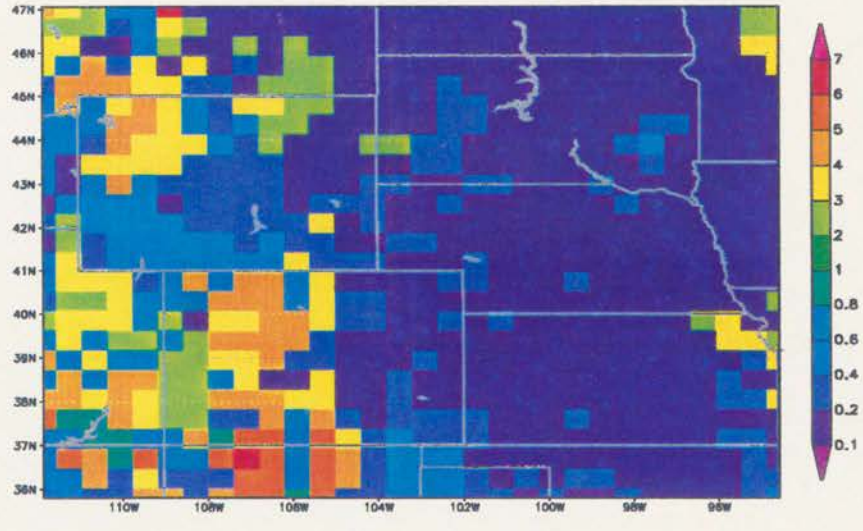

Figure 3.4: NDVI-derived LAI for current vegetation at the initial model time.

After calculating the LAI, which is limited by a user-specified maximum, it is divided by a specific leaf area index (SPLAI, $\frac{m^2}{g}$) for that vegetation type. This quantity gives an estimate of above-ground leaf biomass. From the leaf biomass, one can derive the shoot biomass by using ratios of above-leaf and shoot biomass specified in the plant-input parameter file. Finally, a shoot-to-root ratio can be used to calculate the below-ground biomass (Waring and Running 1998, Chen and Coughenour 1994). The initial mass of above-ground seeds is assumed to be zero. This method will underestimate the below-ground biomass for species other than crops, because the above-ground biomass may not be a good indicator for the woody deciduous species and natural grasses, since they are not at maximum LAI yet. In the case of the forest species and natural grasses, an initial root biomass is specified and the maximum of the NDVI-derived biomass and a specified biomass is taken. The initial distributions of leaf, shoot, and root are shown in Figure 3.5, Figure 3.6, and Figure 3.7 for the current vegetation, which, as in the case of the LAI, is nearly identical to the natural vegetation case.

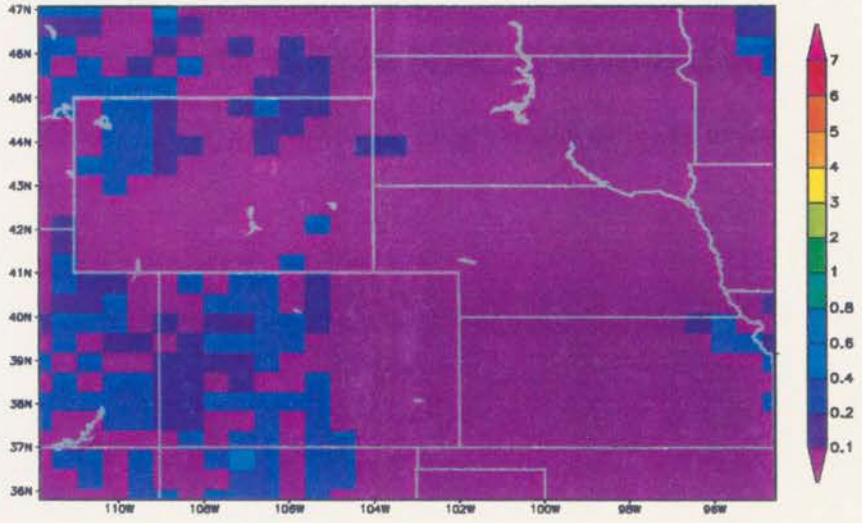

Figure 3.5: The initial distribution of leaf biomass kg m^{-2} for the current vegetation.

One aspect of plant modeling, that is somewhat artificial, involves simulating the observed rapid spring green-up. This is still a biological black box in that it has not been modeled explicitly on a biochemical scale. In addition, when plants emerge from the soil in the spring, they can be subject to the extreme temperatures of the ground

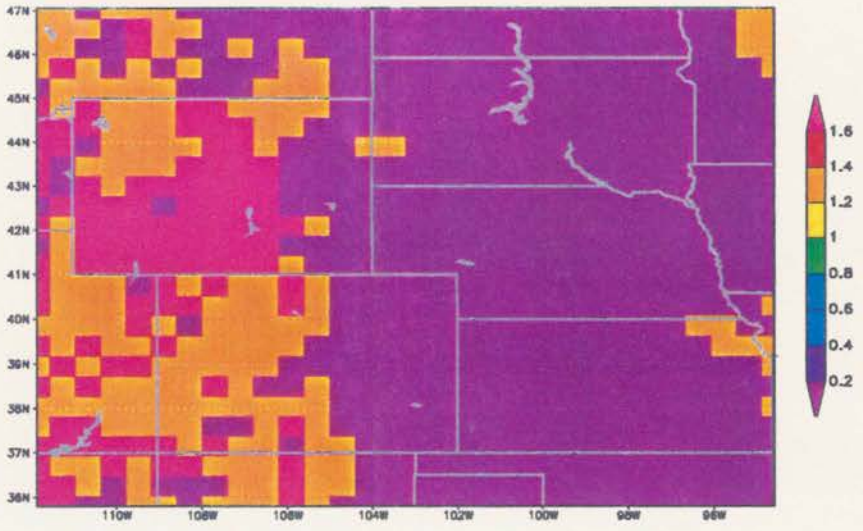

Figure 3.6: The initial distribution of shoot biomass kg m^{-2} for the current vegetation.

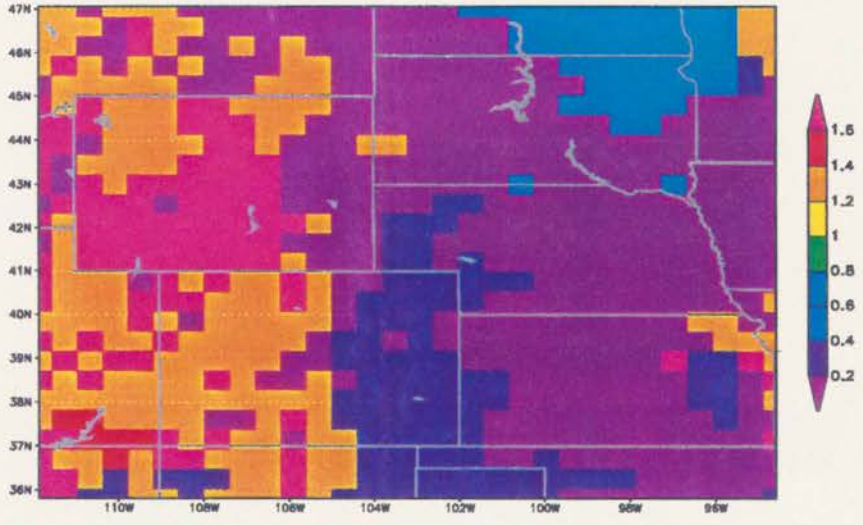

Figure 3.7: The initial distribution of root biomass kg m^{-2} for the current vegetation.

(upwards of 40C), yet manage to survive. One possible mechanism is the plants use of heat shock proteins (H.T. Odum, personal communication), although little is known about their prevalence. In this study, an empirical approach is adopted.

The spring green-up maximum allocation is a difference in biomass and is calculated for each 10-day period beginning 1 April 1989 and continuing until a minimum threshold (a ΔLAI of 0.2) is no longer met. This biomass then provides both a temporal period for rapid spring growth, as well as an estimation of the biomass increase associated with the period. The data are then saved in gridded files that are used as maximum spring growth biomass, and is modified by the allocation algorithms discussed in Section 3.1. The April-averaged maximum biomass allocation fields are shown in Figure 3.8.

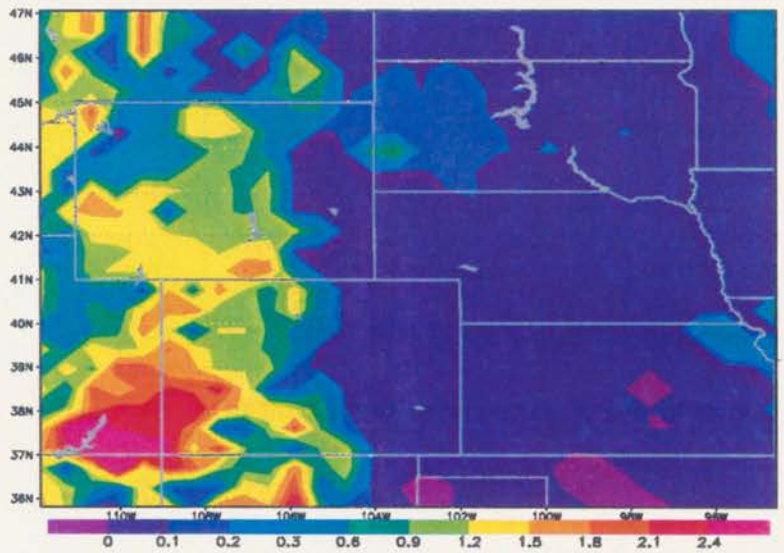

Figure 3.8: The distribution of maximum root to leaf allocation or seed pool in $\frac{\text{kg}}{\text{m}^2}$.

At the other end of the growing season is the fall harvest, which obviously reduces LAI to minimum values over cells containing crops. Using the same dataset and a LAI threshold, one can determine the grid cells where harvest has occurred over the 10-day AVHRR-averaging period. A file containing the Julian day of harvest was then used in the model to set the LAI to 0.1 when this day was reached in the simulation.

3.3 Meteorological Model Initialization

The meteorological model also needs initial fields and lateral boundary conditions to perform the integration. In addition, the bottom boundary is modified by the soil moisture

and temperature profiles. In most cases, the soil moisture and temperature profiles are homogeneously initialized in the model. Homogeneous initialization assumes that the subsequent integration will develop the proper gradients of moisture and temperature. In several seasonal simulations, this was found to be inadequate. The problem lies in the bottom boundary condition, which is kept constant in the ClimRAMS model.

3.3.1 Objective Analysis Procedure

The Isentropic Analysis (ISAN) package performs a blending of multiple data types to the RAMS grid. The three-dimensional variables consist of velocity, temperature, pressure, and moisture. They are processed in two stages to produce fields interpolated to the RAMS model grid. In this investigation, the files are produced at 12-hour intervals. The initial file provides the variable fields used to initialize the model. Subsequent files are employed at the lateral and top boundaries to nudge the predicted model fields for the total integration.

The data source used to create these files was the National Center for Environmental Prediction (NCEP) reanalysis product, Kalney et al. (1996). These data assimilates surface and upper air data onto a 2.5 $\times$ 2.5 global grid. The assimilated data are also processed by a global model to assure the physical consistency between the meteorological variables. The acquired data cover a period of 1 April 1989 through 31 October 1989 at 12-hour intervals.

The next stage consists of performing the task of interpolating the NCEP data to a set of user-specified isentropic surfaces, and the σ-z atmospheric model levels. In addition, a distance related weighting procedure, called the Barnes objective analysis, is performed to blend the data to the RAMS model horizontal coordinates. This procedure requires the input of a user-specified coefficient that smoothes the data in the Barnes analysis. The σ-z and isentropic analysis are then blended by vertical profile weighting above a selected height, while at a lower height the σ-z data is solely used.

3.3.2 Soil Model Initialization

The final component of the modeling system to be initialized is the soil moisture and temperature profiles. It was chosen here to variably initialize the soil moisture and

temperature profiles at each gridpoint. Due to the lack of data, this step is difficult. This course was chosen over a homogeneous initialization after several sensitivity studies exhibited a lack of water stress when homogeneous initialization was used. The reason can be found in the bottom soil boundary condition used in standard RAMS, and ClimRAMS which is fixed in time with the initial value. In general, this initial value is near saturation, which is communicated through time to the upper soil layers.

The data used to variably initialize the soil moisture and temperature profiles are a product of the ECMWF/TOGA Advanced Operational Analysis Data. The soil wetness and temperature are based on climatology following the work of Mintz and Serafini (1981). The surface soil moisture corresponds to a layer from the surface to a depth of 7.2 cm. The deep-layer soil moisture and temperature are derived for a layer at a depth of 42 cm. The data are defined spatially on a 1×1 grid, while the temporal resolution is a one-month averaged field. The initial soil temperature fields are defined by linear interpolation between the 42cm deep soil temperature and the RAMS objectively analyzed surface temperature fields. Soil gridpoints below the 42cm depth are set to the 42cm value.

The gridded data are linearly interpolated to the VEMAP fine grid. This interpolation was done for each month to be integrated. The vertical profile at each gridpoint was produced by linear interpolation for the soil model levels above 42 cm. The values below the deep soils data were set to a 42 cm value. The initial horizontal fields of near surface soil moisture are displayed in Figure 3.9.

The initial near surface temperature field is displayed in Figure 3.10. The interpolated data for subsequent months was then used to provide the values for the bottom soil moisture in the soil model through linear temporal interpolation. Shown in Figure 3.11 is the deep soil moisture for the July, with a similar plot for October displayed in Figure 3.12. Figures 3.11 and 3.12 indicate a drying down of the deep soil moisture. This drying will likely impact the biomes that possess relatively deeper root systems.

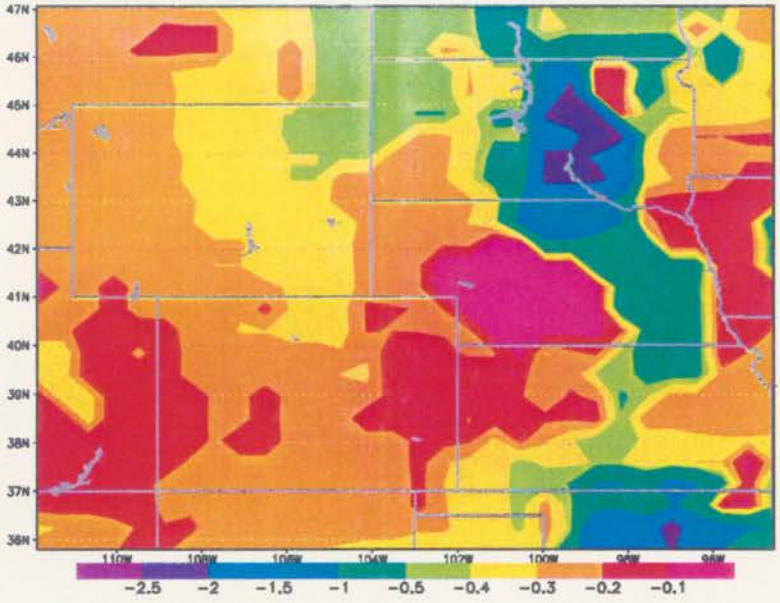

Figure 3.9: The distribution of initial near surface soil moisture in MPa.

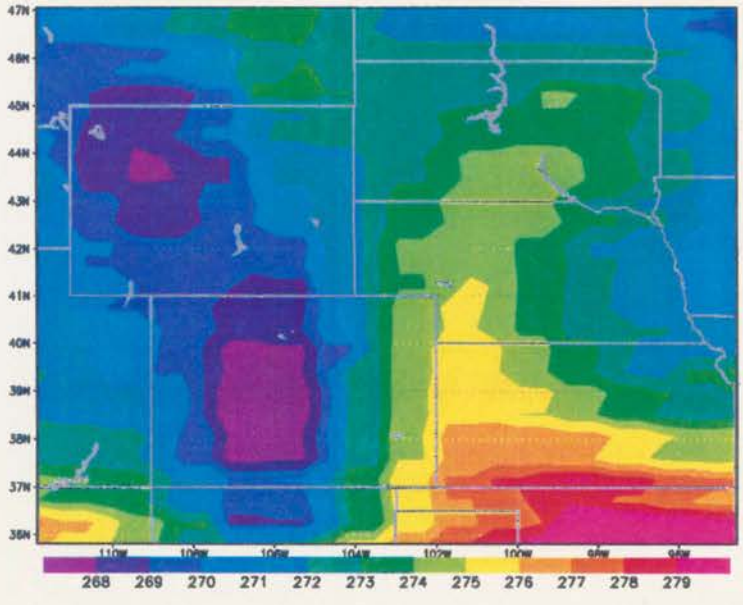

Figure 3.10: The distribution of initial deep soil temperature in K.

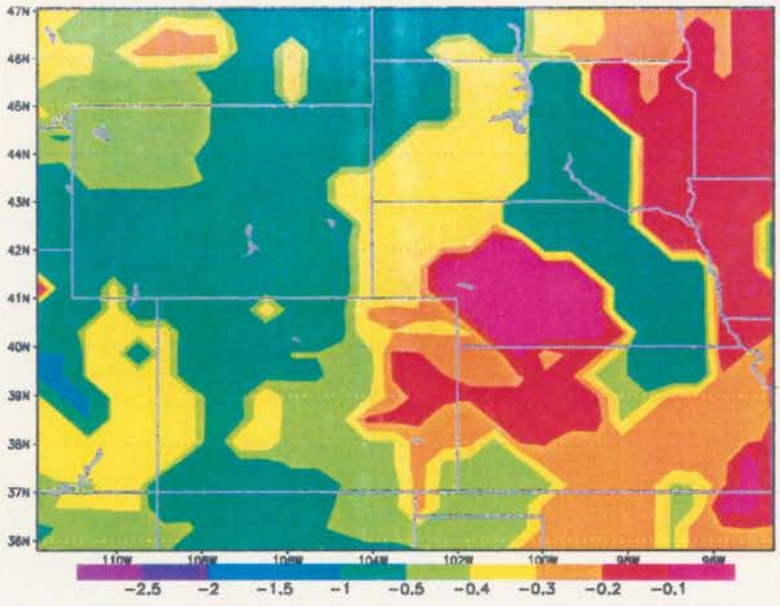

Figure 3.11: The deep soil moisture boundary condition distribution for July in MPa.

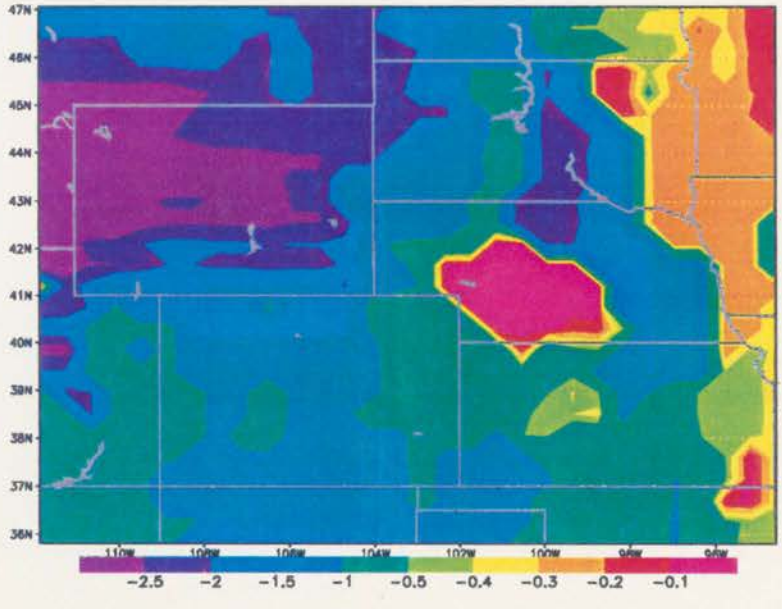

Figure 3.12: The deep soil moisture boundary condition distribution for October in MPa.

Chapter 4

MODEL VALIDATION

4.1 Description of Validation Methods

The validation of gridded modeling systems is an area with a great degree of subjectivity. In general, the density of the data produced by 3D models is at least as dense as any surface data. In the case of the upper air observations it is much more detailed. There are also problems in comparing discrete data to gridded data. Usually linear interpolation is employed. Linear interpolation has its own inherent difficulties, such as topographical considerations and temporal resolution. An objective analysis (a distance weighted interpolation scheme) also contains these difficulties, although the procedure is more robust than simple linear interpolation. There are also numerous approaches to examine gridded data both in temporal and spatial directions. One can employ domain averages, temporal averages, or examine discrete gridpoints temporally. In the case of this investigation, analysis by biome type would also be appropriate for identifying biases.

The validation of the biotic components presents another set of problems. For instance, the LAI is a quantity that can be used. On the domain scale, satellite-derived LAI is one of the most likely choices. However, satellite-derived LAI assumes that algorithms converting NDVI to LAI are accurate. These algorithms are based on exponential relations, and can magnify any inherent errors. In addition, point or site measurements of LAI can be used. This method contains many of the same difficulties presented in analysis of meteorological point data. The FIFE dataset is commonly used for vegetation analysis (Lee 1992, Chen and Coughenour 1994). However, these data represents two biome types, tall and short grass. Examination of the field data indicates a high degree of variability in bio-assays. Temporal measurements are somewhat sparse, and do not cover the entire

growing season. Sites selected for analysis often contain a high degree of heterogeneity in soil characteristics and topographical aspect over even a few meters. The FIFE dataset was originally used to calibrate the tall and short grass parameters used in the model (Chen and Coughenour 1994), and indeed these biomes will be shown to have significant agreement with the observations.

The validation begins with a statistical analysis of the surface data for domain averages, gridpoints, and over biome types. The variables tested include: maximum daily temperature, minimum daily temperature, LAI, and daily precipitation. The meteorological variables are derived from the archived surface data, while the LAI is derived from the previously mentioned NDVI data. There are several different tests and statistical quantities we can use to investigate the relationship between the observations and model output.

4.1.1 Surface Data

The most straightforward quantity used for comparison is Pearson's correlation coefficient, r. This quantity will indicate the degree of association between two paired data sets and is given by the formula

$$r = \frac{\Sigma(x_i - \overline{x})(y_i - \overline{y})}{\sqrt{\Sigma(x_i - \overline{x})^2}\sqrt{\Sigma(y_i - \overline{y})^2}} \tag{4.1}$$

$$bias = \frac{\Sigma(x_i - y_i)}{\#N} \tag{4.2}$$

This quantity by itself is of limited use. We can supplement it by including the bias, mean, variance, standard deviation, skewness, and kurtosis of the distributions. The bias indicates a systematic offset between the 2 distributions. The skewness can describe the asymmetry of a distribution around its mean. The kurtosis indicates whether a distribution is flattened or peaked. These last 2 quantities will also indicate the validity of several other tests used to examine the observational and modeled distributions. If the control run represents the observations, we should see many similarities in the datasets.

Table 4.1 shows the mean, standard deviation, variance, bias, skewness, and kurtosis for the observational and modeled data sets. These numbers were derived from the domain averages excluding the lateral boundary nudging points. The temporal series is taken over a 200-day period and is smoothed with a sliding 5-day averaging filter. The means appear to be quite similar, although the model data are slightly cooler, as indicated by a bias of $-0.98°C$. The model's cool bias is also indicated by a more negative skewness. This indicates the tail extends more towards the lower end of the distribution than its observational counterpart. The variance and standard deviation are also quite similar for the two distributions. In both cases, the kurtosis indicates that both distributions are platykurtic (flattened).

The skewness and kurtosis for both distributions does question the credibility of a student's t test or an F test, which assume a Gaussian distribution. Nevertheless, we will use both tests to examine the two distributions. The t test (Ott 1993) can be used to indicate whether the means are significantly different, while the F test (Lyman 1996) can be used to assess whether the variances are significantly different. A third test, the Kolmogorov-Smirnov test (KS test, Anderson and Darling 1952), will be used to determine whether the two distributions are significantly different. This test is based on the cumulative distributions of the two datasets and their maximum difference. As in the t and F tests a probability is returned. In the case of the t and F test a small value indicates significant differences in the means and variances, respectively. Similarly, small values of the KS probability indicates significant differences in the cumulative distribution functions of the two distributions.

Table 4.2 also shows the linear correlation coefficient, and the probabilities returned from the t, F, and KS tests for the maximum daily temperature. The value of r indicates a strong linear correlation between the datasets, with the model accounting for roughly 89% of variance. The correlation is also calculated from the domain averages excluding the lateral nudging boundary points. The results of the the F test also indicate the variances are not significantly different as does the KS probability. The t test suggests that the means are significantly different. This difference is likely a result of the complex topography in

the western half of the domain. When the model is initialized this topography is set to an average value for the 50 × 50 km grid cells. Often the stations used to derive the observational temperature fields are located at lower elevations than the average model elevation, thus contributing to lower modeled temperature fields. Indeed, when western forested areas are examined by themselves the cool bias ranges from $2 - 8°C$. This bias could also be a result of the weighting procedure used to determine the temperature at 2 m above ground level (AGL). The weighting is determined by the fractional coverage of vegetation and shaded and bare ground temperatures. The locations of the stations are not likely to be directly under a canopy (Ethan Greene, personal communication), while the model uses the fractionally-weighted vegetation temperature in determining these temperatures. A representative weight would further reduce the maximum daily temperatures in the western forest areas where the fractional coverage is high. The effect is opposite for the minimum daily temperatures, where the fractional coverage would tend to increase model predicted temperature fields.

Variable	Mean	σ	Variance	Skewness	kurtosis
TMAX obs	22.658	4.341	18.845	-0.019	-0.798
TMAX control	21.679	4.777	22.816	-0.217	-0.729
TMIN obs	7.205	4.357	18.979	-0.157	-1.050
TMIN control	7.047	4.553	20.731	-0.197	-0.800
PPT obs	1.388	0.702	0.493	0.041	-0.840
PPT control	0.796	0.423	0.179	0.448	-0.491
LAI obs	2.746	1.040	1.082	-0.908	-0.010
LAI control	2.553	0.850	0.722	-1.589	1.687

Table 4.1: Mean, standard deviation, skewness, and kurtosis for a temporal domain-averaged comparison of the control simulation and observational data for the variable listed in the first column. TMAX is the maximum daily temperature, TMIN the minimum daily temperature, PPT the daily total precipitation, and LAI the leaf area index.

The same statistics are shown in Tables 4.2 and 4.1 for the minimum daily temperatures. We see here a similar pattern as was found in the maximum daily temperature results. The means, standard deviations, skewness and kurtosis all exhibit similar values. As suspected the bias has now decreased to $0.16°C$. In the case of the correlation coefficient, it has increased slightly to 0.91. The t test indicates that the means are not

Variable	r	prob F	prob T	KS stat	Bias
TMAX	0.8875	0.1783	0.0325	0.1122	-0.9790
TMIN	0.9057	0.5340	0.7233	0.7112	-0.1579
PPT	0.3479	0.0000	0.0000	0.0000	-0.5922
LAI	0.9016	0.3731	0.5140	0.0423	-0.1930

Table 4.2: Statistical F, t, and KS tests, and bias of the control simulation and observational data for the variable listed in the first column. TMAX is the maximum daily temperature, TMIN the minimum daily temperature, PPT the daily total precipitation, and LAI the leaf area index. Perfect agreement would be indicated by test values of 1 for the statistical tests.

significantly different, while the F test suggests that the variances are also not significantly different. Finally the test for different distributions implies that the distributions are not significantly different. Overall, the various tests and statistical values indicate that the model has done an excellent job of simulating the observed temperature fields.

The statistical evidence for the daily precipitation is not as acceptable as the temperature fields. However, these results are not surprising given the difficulties in predicting precipitation and in objectively analyzing point or station precipitation data to a grid. For single cell precipitation events a cloud scale of roughly 10×10 km is normally expected. Since the model cell in this investigation is 25 times this area, we are not able to resolve these events and are forced to use a parameterization. In general, such parameterized precipitation schemes smooth out the precipitation patterns when compared to observations. One also expects an underprediction at the coarse grid cell resolution used here. This underprediction is the case for the mean value of daily precipitation predicted by the model, which is roughly 57% the observed mean. The correlation is relatively low, 0.35, when compared to the temperature fields. The skewness indicates that the modeled field is more heavy tailed towards the high end of precipitation values. This skewness is not surprising since the dump bucket and Kuo cumulus parameterizations are triggered by thresholds values in liquid water content and vertical motion, respectively. The kurtosis also indicates the role of a threshold, as the observed precipitation distribution is flatter than the modeled counterpart. Also indicative of the observed flatness, it appears that the variance and standard deviation are much smaller for the modeled precipitation. This

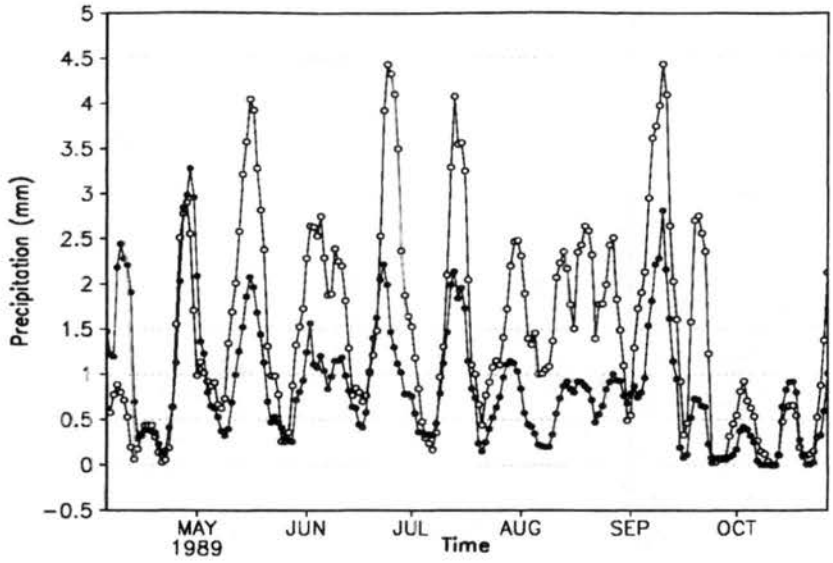

Figure 4.1: Domain-averaged daily precipitation for model (black line) and observations (green line).

evidence of problems with the predicted precipitation is all bore out in the statistical tests, which suggest that the mean, variance, and distribution are significantly different for the modeled and observed datasets. Another way to examine the precipitation is to look at a time series of the observed and modeled precipitation.

Figure 4.1 shows such a plot. Examination indicates what has already been determined in the statistical numbers, that the model underpredicts the daily precipitation. What is apparent from the figure, however, is the ability of the model to capture most of the precipitation events. We see that the peaks and valleys of the model and observations do indeed agree fairly well. There is also some indication that the model predictions degrade during the summer months. This has also been observed in similar modeling studies (Glen Liston, personal communication) using the ClimRAMS model. Apparently this is due to the dump bucket precipitation scheme, which performs best in the cooler months where high saturation levels can be achieved at lower mixing ratios due to the lower temperatures.

Finally, the LAI derived from the NDVI data are used to examine the predicted LAI. The means are quite similar as well as the standard deviation and variance. The skewness indicates that both distributions are more heavily tailed towards smaller LAI values. One surprising figure is the kurtosis which implies the observed LAI is nearly Gaussian, while

the modeled data appear to be leptokurtic, or spiked. The linear correlation coefficient is found to be quite high, with a value of 0.90. In addition, the bias shows the model tends to underpredict the LAI. The F and t tests show that the means and standard deviations are not significantly different. However, the KS test value of 0.042 implies that the distributions may be significantly different, depending what threshold one chooses for this test.

Overall, the domain-averaged comparisons of LAI, maximum daily temperature, and minimum daily temperature are quite good. We see that the variances are not significantly different. The test for significantly different means indicates that only maximum daily temperature is significantly different, while the KS test indicates that only LAI is significantly different. The results of the t and F tests must be examined with caution since the observed and modeled distributions are not truly Gaussian. The KS test is independent of the nature of the distributions. Finally, the correlation coefficients for the temperature and LAI fields are quite high, further increasing the reliability of the model's predictions. As mentioned the precipitation field exhibits the widest discrepancy between the observations and model predictions.

Domain-averaged quantities are indicative of the large-scale integrity of the model. It is also useful to compare spatial plots of quantities evaluated here. Spatial plots aid in evaluating the model at smaller scales than the domain averages. It can also help discern the skill of the model over different biome types. For this portion of the analysis, modeled maximum daily temperature, minimum daily temperature, and LAI are spatially evaluated against the observations. Instead of a single statistical number, spatial plots will be examined for correlation and bias.

Figure 4.2 shows the correlation coefficient at each gridpoint for maximum daily temperature. The color bar indicates that values of r range from 0.7 to 1.0. The western half of the domain consistently exhibits values ranging from 0.8 to 1.0. The southeastern portion of the domain indicates values around 0.7 to 0.8. This portion of the domain, dominated by the mixed class of grains, wheat, and grasslands, will be shown to have the lowest correlations for the rest of the fields analyzed. It could be possible that the high

correlations in the west and northern portions of the domain are due to their proximity to the nudged boundary points combined with westerly and northerly prevailing flow. The southeast region is not downwind of the nudging points in general.

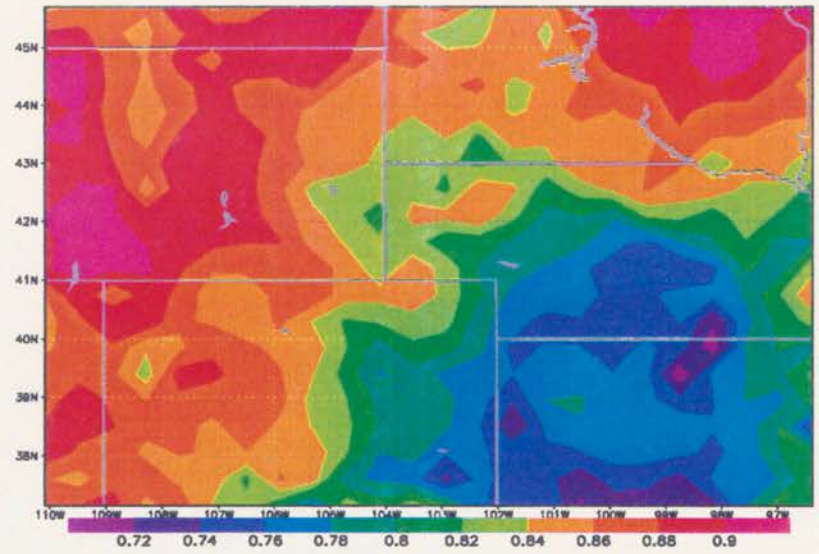

Figure 4.2: 210 day-day domain-averaged maximum daily temperature correlation between the model and observations at each gridpoint.

The bias for maximum daily temperature is displayed in Figure 4.3. The figure indicates the cool bias found in the forested regions in the western mountainous regions. Some areas, collocated with the temperate conifers and temperate coniferous xeromorphic classes have bias of nearly $-8°C$. As mentioned previously, this could be due to the complex topography and actual placement of the surface weather stations used in the objective analysis procedure. The eastern portions indicate a warm bias ranging from $1 - 4°C$.

The correlations for daily minimum temperature fields are exhibited in Figure 4.4. Again, the southeastern portion of the domain shows the lowest correlations. The values are still acceptable, with a minimum of 0.72. Overall, large portions of the domain are above 0.86 and is consistent with the larger domain-averaged correlation when compared to the maximum daily temperature value. The daily minimum temperature bias is shown in Figure 4.5. Large portions of the domain, generally in the east, exhibit a biases of $\pm 1°C$. The largest biases are seen the western mountainous areas, again coinciding with the high LAI biomes of temperate coniferous species. This concentration of high bias values reaffirms the suggestion that station placement is playing a large role in the calculation

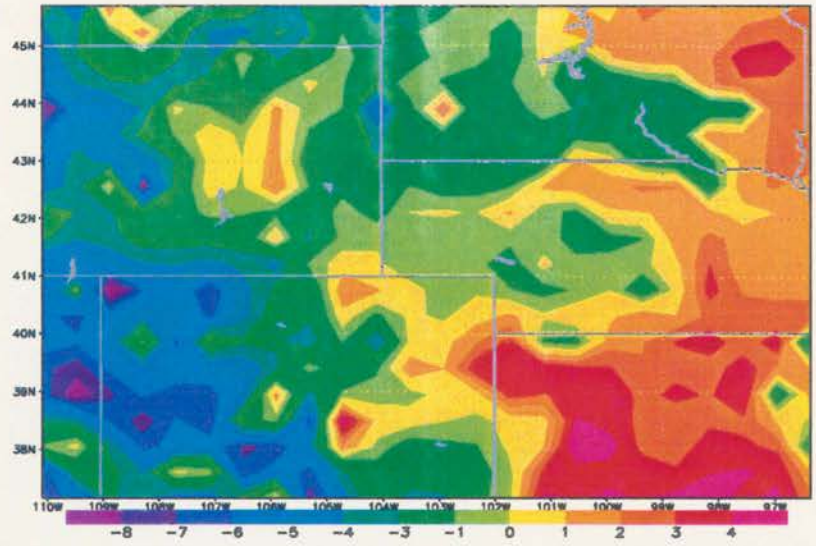

Figure 4.3: 210 day-day domain-averaged maximum daily temperature bias between the model and observations at each gridpoint.

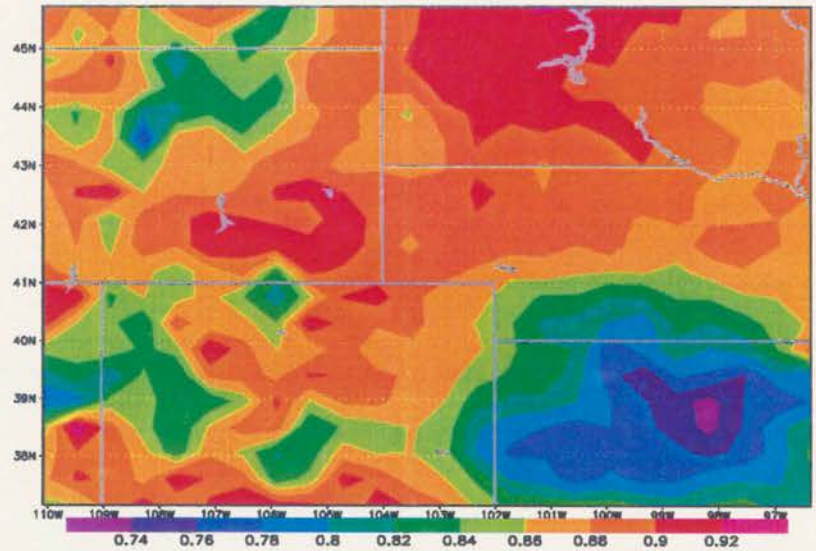

Figure 4.4: 210 day-day minimum daily temperature correlation between the model and observations at each gridpoint.

of the temperature fields. One would expect that under a high LAI species the minimum temperature would be greater due to less radiative cooling.

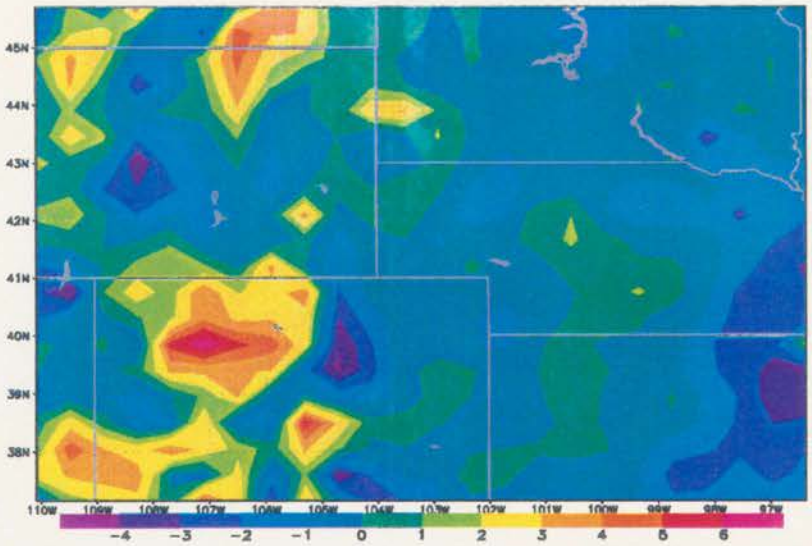

Figure 4.5: 210 day-day minimum daily temperature bias between the model and observations at each gridpoint.

The LAI correlations and biases are exhibited in Figures 4.6 and 4.7, respectively. The fields calculated are the NDVI-derived 10-day averaged LAI values. The correlation fields indicate that values of 0.7 and higher dominate most of the domain. This is interesting in that it shows that the slowly changing temporal dynamics of LAI are well captured. In any given grid cell a large number of processes could be occurring in the real world. This includes extreme weather events, herbivory, harvesting, and senescence. The third process is accounted for to some degree by the harvest parameterization discussed in Chapter 3. Intense herbivory and extreme weather could be captured by analyzing the events where large LAI changes are detected at a given grid cell. The senescence is dependent on the death allocation algorithms which are closely tied to temperature and soil water fields. The lowest correlation coefficients are found at gridpoints where biome type are relatively infrequent compared to other classes. These would also be the hardest to calibrate because there are a small number of points. The LAI bias is small over large portions of the domain. Nearly the entire eastern half of the domain shows values of ± 1. However, this area also contains most of the lower LAI values, ranging from 0.1 to 1.0. The mountainous areas of the west, with a large conifer population has peak LAI values from about 5 to 11. These

relatively large values suggest the negative bias bullseyes in the western half of the domain are relatively insignificant in terms of percentage of total LAI.

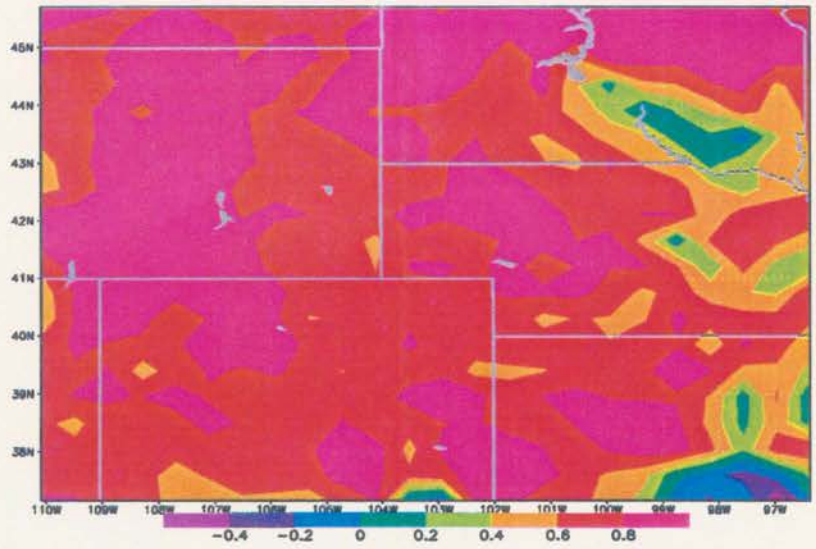

Figure 4.6: 210 day-day LAI correlation between the model and observations at each gridpoint.

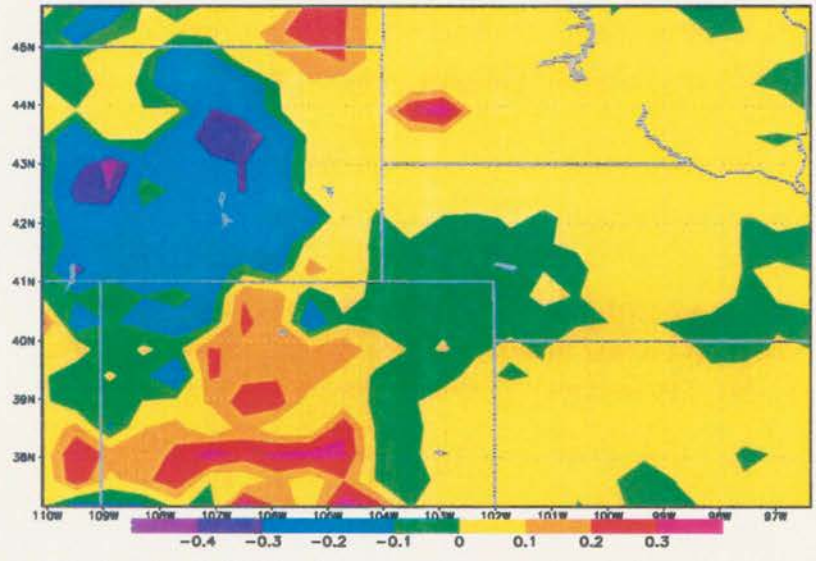

Figure 4.7: 210 day-day LAI bias between the model and observations at each gridpoint.

We can illustrate the model's ability to predict LAI by qualitatively comparing the 1 July LAI values predicted by the model to the NDVI-derived LAI. These are shown in Figures 4.8 and 4.9, respectively. The observed field exhibit some questionably low values for some crop areas in the eastern portion of the domain. Over corn areas, LAI values

of 0–0.2 are indicated. The model fields exhibit values of 0.2–0.4. Overall, the fields are quite similar however. The most striking contrast is the short grass areas over central and southeastern South Dakota. The model predicts a value roughly double that of the NDVI-derived LAI. The modeled short grass also lacks the west-to-east gradient in short grass LAI. The areas of underprediction observed in the bias field can be seen to occur over areas with LAI values greater than 9, which corresponds to a deficit of about 5%. Overall the model does a good job in capturing the spatial similarities, as was found in the statistical analysis.

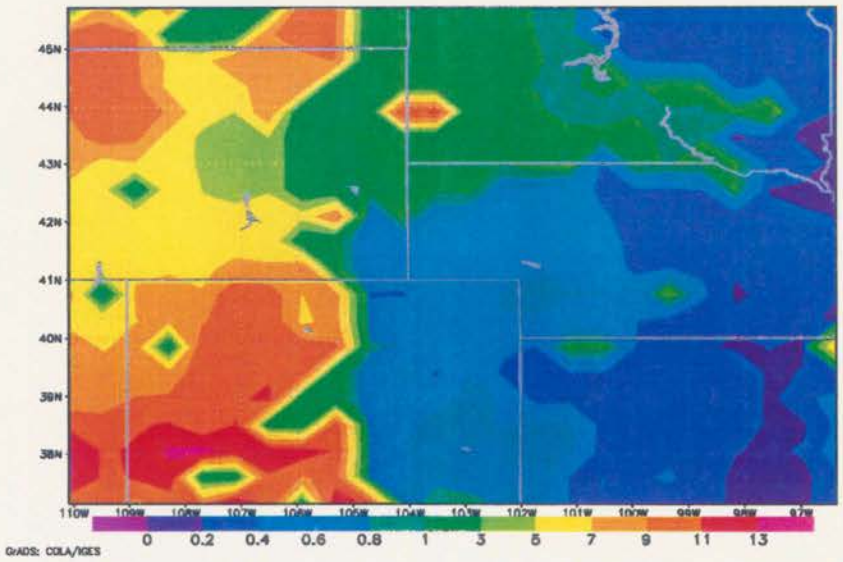

Figure 4.8: Modeled LAI at each gridpoint for 1 July 1989.

An analysis over biome type was also performed to assess the models ability over these biomes. LAI was analyzed for these biomes and compared to the observations. In this analysis only biomes with more than $n = 25$ points are shown. This includes sub-alpine ($n = 46$), temperate conifer ($n = 65$), temperate coniferous xeromorphic ($n = 37$), short grass ($n = 135$), tall grass ($n = 98$), temperate arid shrub ($n = 105$), spring wheat and small grains ($n = 51$), corn ($n = 66$), and grassland, mixed grains and wheat ($n = 102$). The plots range from 10 April through 20 October and show the model points (open circles) and observations (solid green circles). The graph for sub-alpine species, Figure 4.10 indicates a slight overprediction by the model. There is also a lack of the rapid falloff observed in early fall and the secondary peak in LAI observed in late August. The LAI for

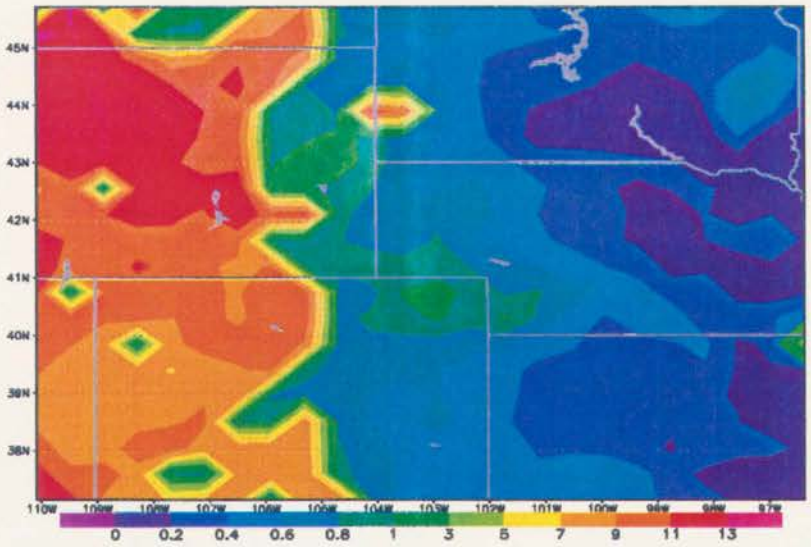

Figure 4.9: Observed LAI at each gridpoint for 1 July 1989.

temperate conifers is shown in Figure 4.11 and follows the observed LAI closely until the fall, where rapid death is observed. The peak values are well represented. In Figure 4.12 we see that the model does a fair job of capturing the peak LAI for the temperate coniferous xeromorphic species, as well as the leveling off in growth observed in the mid-summer months. As in the previous classes the rapid fall death is underpredicted. The short grass LAI shown in Figure 4.13 indicates the model overpredicts LAI, with a peak value of 1.15 versus the observed value of 0.88. As in previous biome types, the fall senescence is underpredicted, although the decline in LAI after 1 July is well captured. The predicted and observed LAI for the tall grass biome is displayed in Figure 4.14. The model again overpredicts the LAI. The temporal distribution is fairly well captured, including a fairly rapid decline in the fall. LAI values for temperate arid shrub are shown in 4.15 . The plot for spring wheat is shown in Figure 4.16 displays good temporal agreement to the observations capturing the early summer peak and steady decline the rest of the growing season. In this case the model underpredicts the observed LAI. Figure 4.17 also exhibits the underprediction seen in spring wheat. There is also a secondary peak in observed LAI that is not represented by the model. Figure 4.18 represents observed and modeled LAI for grasslands, grain, and winter wheat. As is the case for the other agricultural biomes analyzed, there is an underprediction in the peak LAI values, although the model does

represent a fairly rapid fall decline in LAI. When considering the LAI analysis of these different biome types it is useful to consider the numerous processes occurring within a given grid cell as mentioned previously. Within a given grid cell there are actually many other species present that cannot be captured by a cell of homogeneous content. Qualitatively the model does an acceptable job of modeling these different vegetation classes.

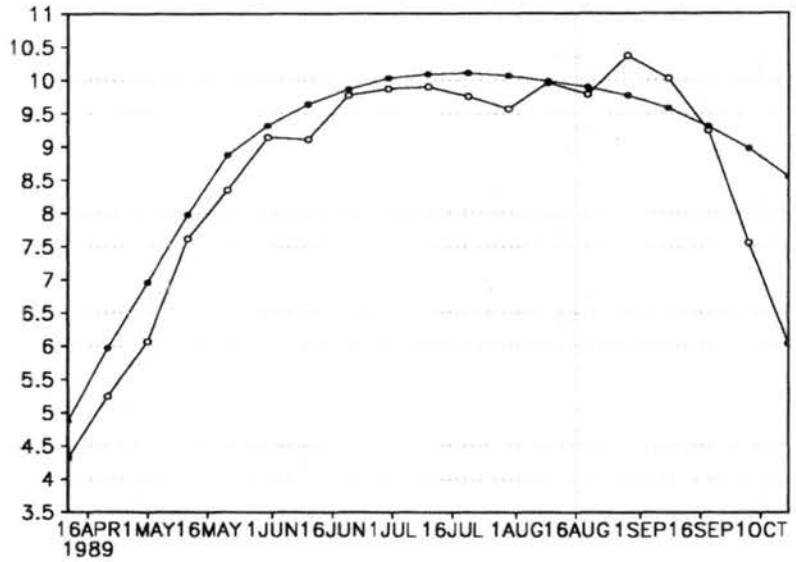

Figure 4.10: 210-day averaged sub-alpine biome LAI average. Model – green, Observed – black.

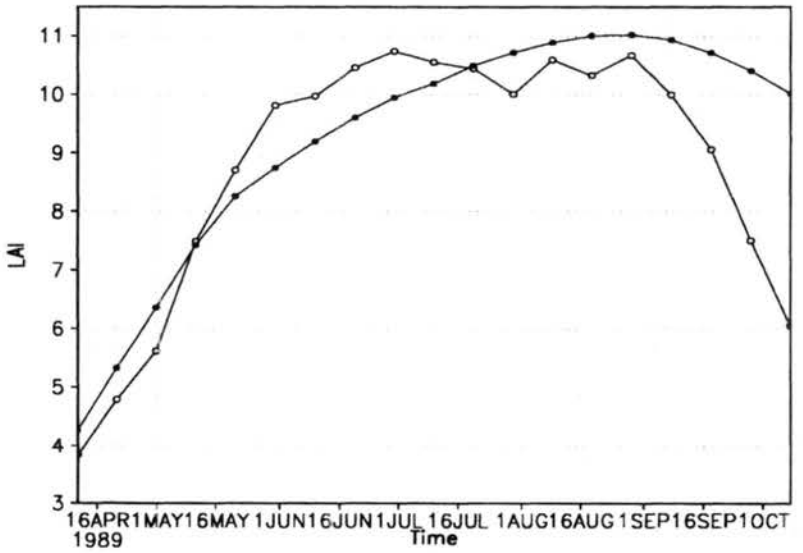

Figure 4.11: 210-day averaged temperate conifer biome LAI average. Model – green, Observed – black.

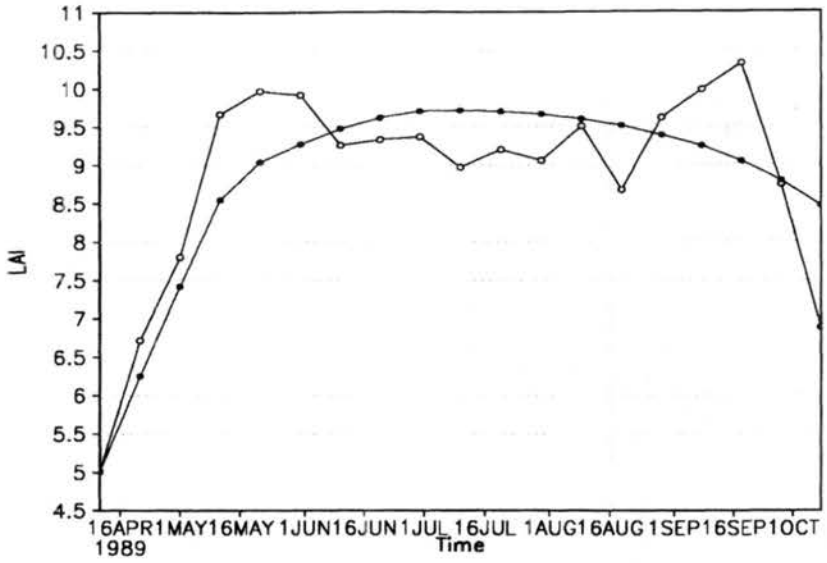

Figure 4.12: 210-day averaged temperate coniferous xeromorphic biome LAI average. Model – green, Observed – black.

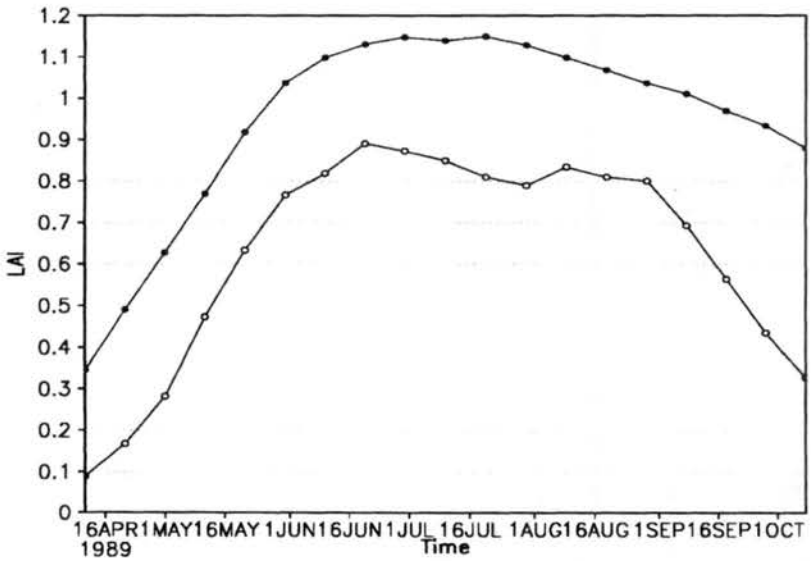

Figure 4.13: 210-day averaged shortgrass biome LAI average. Model – green, Observed – black.

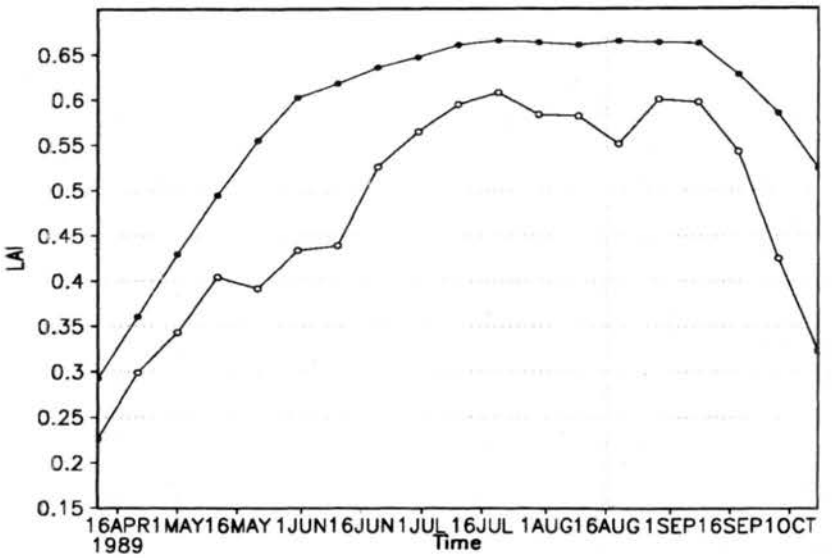

Figure 4.14: 210-day averaged tall grass biome LAI average. Model – green, Observed – black.

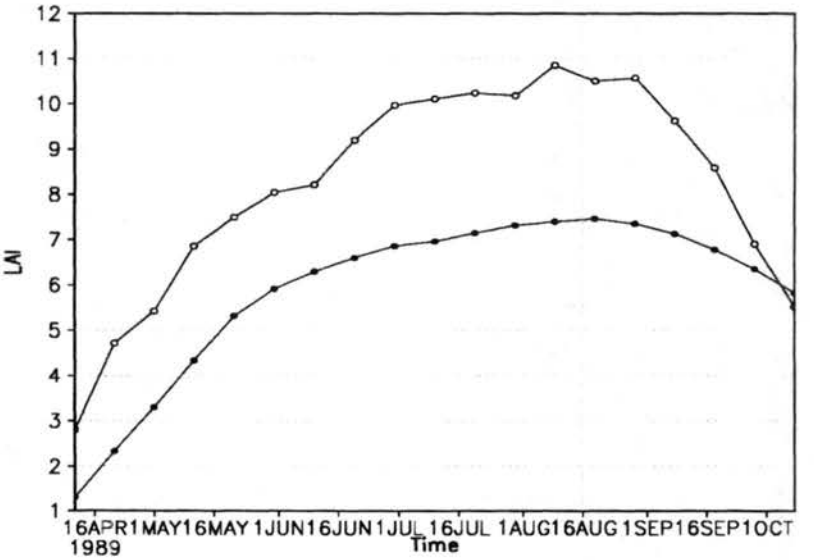

Figure 4.15: 210-day averaged temperate arid shrub biome LAI average. Model – green, Observed – black.

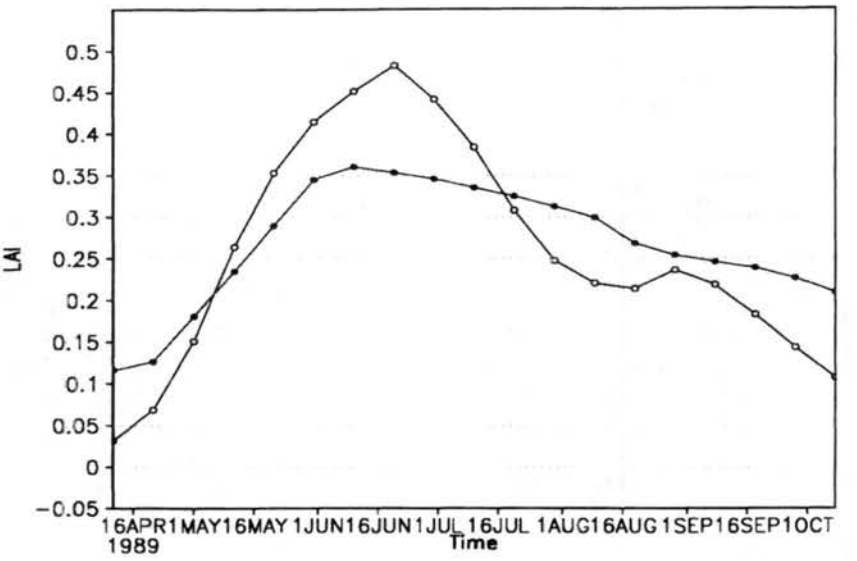

Figure 4.16: 210-day averaged spring wheat/ small grains biome LAI average. Model – green, Observed – black.

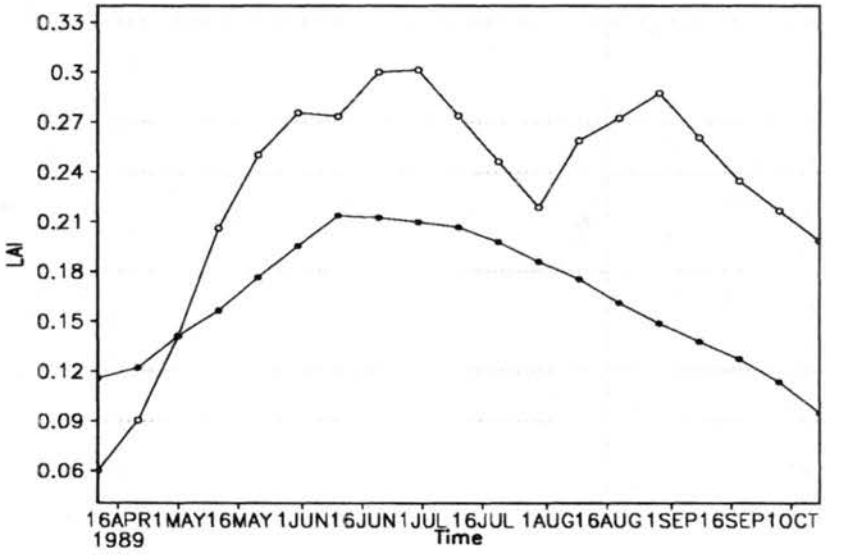

Figure 4.17: 210-day averaged corn biome LAI average. Model – green, Observed – black.

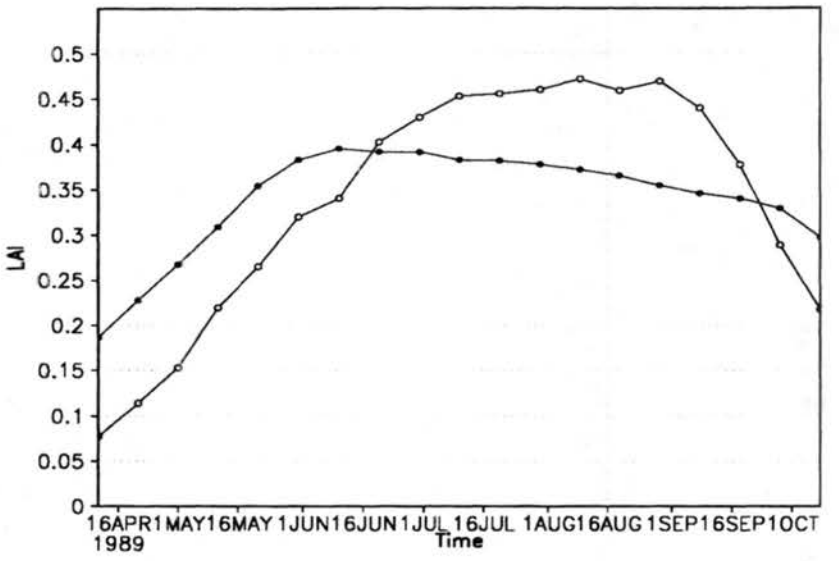

Figure 4.18: 210-day averaged mixed grains biome LAI average. Model – green, Observed – black.

Chapter 5

PURE FACTOR CONTRIBUTION TO MODELED FIELDS

The results from the previous chapter indicate that the modeling system has reproduced observed fields with an acceptable degree of accuracy. Given these results a total of 7 more simulations were conducted. The runs were summarized in the hypothesis section of the paper and are discussed here for review. The data from these simulations can then be used to separate various factors and their combinations in order to discern their impact on various meteorological and biological quantities.

The control run, f_0, consists of current landscape with free atmosphere $1\times CO_2$ levels used for both the biological air concentration and longwave radiative forcing. Biological air CO_2 levels are actually allowed to change due to sources and sinks as well as advection and diffusion. In the next simulation, f_1, the landscape was changed to a theoretical natural landscape as described earlier. All other conditions were kept the same and the simulation was integrated over the same time period. The next integration, f_2, was performed with the same conditions as the control run with the exception that radiative CO_2 levels were doubled. A fourth simulation, f_3, was performed with identical conditions to the control run except doubled biological CO_2 levels. These four simulations can be used to extract the contribution to prognosed fields due to the factor that has been changed. These include landscape change, doubled radiative CO_2 forcing, and doubled CO_2 biological air levels. Alone, these contributions can provide valuable information for putting the forcing magnitudes in perspective. It was pointed out in the hypothesis section that significant differences will be exhibited in domain-averaged and individual gridpoint-prognosed variables. It hypothesized that there will also be significant differences due to the interactions of the aforementioned factors. This hypothesis was the impetus for the 4 additional simulations specified in Chapter 4. These include various combinations of the 3 factors studied

here and are shown in Table 5.1. The final hypothesis was that the results would indicate that seasonal modeling should be treated as an initial value problem as discussed in Pielke et al. (1998) and Pielke (1998). Although this will not be demonstrated explicitly it can be inferred from the simulation results.

As in any complex mesoscale modeling system, the number of variables available for analysis is large. The saved information represents over a gigabyte of data, with 16 3D variables over 100 2D variables, and 13 3D soil variables saved. Clearly an analysis of every variable is to voluminous for this study. Instead, a subset of variables is chosen for the 2D variables. The data will be averaged for the entire season. Domain averages will first be examined followed by a spatial analysis of the selected variables. The various tests employed in the model validation will also be used.

5.1 Separation of Domain-Averaged Fields

The data from the simulation f_0 combined with a difference field using f_1, f_2, and f_3 can be used to extract the contributions to a given variable from natural vegetation, $2\times CO_2$ radiation, and $2\times CO_2$ biological air, respectively. These differences will be done before the separation of the factor's interaction is performed, mainly because it is more straightforward to interpret. The pure factor contributions can also be used as a measuring stick for the interaction fields. This set of difference calculations will address the first hypothesis stated in Chapter 4.

- Significant differences in the domain-averaged prognosed meteorological fields, biophysical, and biogeochemical processes will be observable when:
  - landcover is changed from current to potential vegetation,
  - radiative forcing is changed from $1\times CO_2$ to $2\times CO_2$, and
  - biological CO_2 levels are doubled.

As mentioned in the introduction to this chapter, the number of variables is immense. Domain averages simplify this task to some degree in that a single number, or test result, can be assigned to each variable. Using a similar procedure as that used in Chapter 5, the

results will be shown in tabular format. For example, the pure due to natural vegetation can easily be extracted by taking a difference with the control simulation. In addition, since the hypothesis states "significant differences" a series of statistical tests can be used to examine this. For domain averages, a time series will be compared covering the entire integration as well as monthly values. The monthly values will aid in discerning any short term trends.

5.1.1 Contributions to Daily Variables

The first set of variables tested were the surface daily variables. They are listed in Table 5.1. These variables are meteorological and biological in their nature, and vary over the growing season over several temporal scales. Displayed in Table 5.2 are the results for the contribution due to natural vegetation. For the different tests, small values indicate significant differences in the domain-averaged distributions. A threshold of $\alpha = 0.05$ was chosen and those values meeting this criteria have an asterisk next to them. It should be noted this is a 2-sided test for t and F tests; thus the probability must be less than $\frac{\alpha}{2}$. The variables that have significant differences in variance are fractional coverage, leaf biomass, and total accumulated carbon. The root biomass is also close to the $\alpha = 0.025$ threshold. For the t test, in addition to these variables, total accumulated precipitation, LAI, shoot biomass, root biomass, and transpiration have significantly different means between the natural and current vegetation simulations. The results indicate that the maximum daily temperature is 1.23°C warmer under the current vegetation distribution. There is roughly 2.81 mm more rainfall under the current vegetation. For the KS test for significantly different distributions, the table shows that maximum daily temperature, total accumulated precipitation, LAI, daily LAI change, leaf biomass, shoot biomass, transpiration, and total accumulated carbon all are significantly different.

The same calculations are shown in Table 5.3 for the $2\times CO_2$ radiation simulation. In this table, none of the variables exhibit significant differences for variance and mean. The only significant result is for the cumulative distribution for root biomass. The minimum daily temperature shows a general warming of nearly 0.1°C under this scenario. On the domain-averaged scale, the contribution of $2\times CO_2$ is insignificant. The cumulative root

Variable Symbol	Description
TMAX	Maximum daily temperature (C)
TMIN	Minimum daily temperature (C)
ACCUMALL	Total accumulated precipitation (mm)
VFRAC	Fraction of vegetation cover (percent)
FLAI	Leaf Area Index
DLAI	Daily change in LAI
WL	Leaf biomass (kg m^{-2})
WSH	Shoot biomass (kg m^{-2})
WR	Root biomass (kg m^{-2})
EVAPOTR	Transpiration (mm day^{-1})
SUMALL	Total accumulated biomass (kg m^{-2})

Table 5.1: Variable symbols and descriptions for the daily 2D variable analysis.

Variable Symbol	F test	t test	KS test	Mean	σ	difference
TMAX	0.374E+00	0.354E-01	*0.298E-01	0.224E+02	0.463E+01	-0.123E+01
TMIN	0.868E+00	0.968E+00	0.100E+01	0.767E+01	0.455E+01	-0.221E-01
ACCUMALL	0.443E+00	0.583E+00	*0.864E-02	0.107E+03	0.427E+02	-0.281E+01
VFRAC	*0.147E-06	*0.484E-37	0.100E+01	0.610E+00	0.658E-01	0.106E+00
FLAI	0.141E+00	*0.621E-03	*0.505E-19	0.292E+01	0.469E+00	0.200E+00
DLAI	0.519E+00	0.521E+00	*0.879E-01	0.763E-02	0.161E-01	0.125E-02
WL	*0.216E-01	*0.772E-08	*0.108E-30	0.214E+00	0.351E-01	0.251E-01
WSH	0.427E+00	*0.174E-04	*0.220E-14	0.509E+00	0.311E-01	0.177E-01
WR	0.667E-01	*0.000E+00	0.100E+01	0.521E+00	0.134E-01	0.572E-01
EVAPOTR	0.299E+00	*0.133E-02	*0.671E-03	0.243E+02	0.575E+01	0.228E+01
SUMALL	*0.619E-03	*0.212E-03	*0.199E-04	0.199E+00	0.853E-01	0.336E-01

Table 5.2: Natural vegetation table of indicated statistical test, mean, standard deviation, and average difference (relative to control simulation) for the listed variable.

distribution function however, was found to be significantly different. This significance would suggest that soil water relations would likely be significantly different and will be addressed later in this chapter.

Variable Symbol	F test	t test	KS test	Mean	σ	difference
TMAX	0.983E+00	0.981E+00	0.100E+01	0.237E+02	0.494E+01	0.144E-01
TMIN	0.985E+00	0.863E+00	0.100E+01	0.779E+01	0.461E+01	0.961E-01
ACCUMALL	0.890E+00	0.855E+00	0.792E+00	0.111E+03	0.459E+02	0.963E+00
VFRAC	0.999E+00	0.974E+00	0.923E+00	0.504E+00	0.440E-01	0.194E-03
FLAI	0.976E+00	0.990E+00	0.987E+00	0.272E+01	0.425E+00	0.716E-03
DLAI	0.952E+00	0.976E+00	0.100E+01	0.643E-02	0.155E-01	0.574E-04
WL	0.974E+00	0.988E+00	0.987E+00	0.189E+00	0.302E-01	0.610E-04
WSD	0.960E+00	0.964E+00	0.100E+01	0.492E+00	0.328E-01	0.189E-03
WR	0.922E+00	0.872E+00	*0.618E-02	0.464E+00	0.155E-01	0.365E-03
EVAPOTR	0.995E+00	0.897E+00	0.100E+01	0.221E+02	0.532E+01	0.875E-01
SUMALL	0.918E+00	0.954E+00	0.100E+01	0.166E+00	0.670E-01	0.458E-03

Table 5.3: $2\times CO_2$ radiation simulation table of indicated statistical test, mean, standard deviation, and bias (relative to control simulation) for the listed variable.

Under $2\times CO_2$ biological air concentrations displayed in Table 5.4, results are similar to the natural vegetation contribution. For the variances, fractional coverage, LAI, daily change in LAI, leaf and root biomass, and total accumulated carbon indicate significant differences from the control run. Significant differences in means are exhibited for fractional coverage, LAI, leaf, shoot and root biomass, and total accumulated carbon. The LAI has increased by a domain average of 0.589 under $2\times CO_2$ biological air concentrations. This LAI increase likely contributes to a domain-averaged decrease in maximum daily temperature of 0.764°C and an increase in minimum daily temperature of 0.263°C. The CO_2 enhancement is accounted for in two separate algorithms. The effect on maintenance respiration follows the work of Idso et al. (1992), and is related to the difference between the CO_2 levels and a base state of 350 ppm. The CO_2 levels are also directly involved in the iterative photosynthesis calculations described in Chapter 3. The calculated assimilation rate is also directly involved in the stomatal conductance, through Equation 2.7. Unlike the natural vegetation simulation where the majority of variables indicated significant differences, the results show that only total accumulated precipitation, LAI,

daily change in LAI, shoot biomass, and total daily accumulated carbon are significantly different.

Variable Symbol	F test	t test	KS test	Mean	σ	difference
TMAX	0.620E+00	0.195E+00	0.393E+00	0.229E+02	0.474E+01	-0.764E+00
TMIN	0.897E+00	0.640E+00	0.923E+00	0.795E+01	0.466E+01	0.263E+00
ACCUMALL	0.340E+00	0.395E+00	0.618E-02	0.105E+03	0.422E+02	-0.432E+01
VFRAC	0.990E-05	0.332E-13	0.100E+01	0.560E+00	0.626E-01	0.556E-01
FLAI	0.145E-05	0.612E-16	0.222E-41	0.331E+01	0.606E+00	0.589E+00
DLAI	0.199E-01	0.950E-01	0.307E-02	0.986E-02	0.184E-01	0.348E-02
WL	0.153E-06	0.488E-18	0.100E+01	0.235E+00	0.443E-01	0.456E-01
WSH	0.255E+00	0.264E-08	0.741E-20	0.516E+00	0.315E-01	0.245E-01
WR	0.145E-01	0.543E-09	0.100E+01	0.477E+00	0.137E-01	0.133E-01
EVAPOTR	0.910E+00	0.221E+00	0.465E+00	0.229E+02	0.534E+01	0.834E+00
SUMALL	0.242E-15	0.587E-19	0.104E-20	0.277E+00	0.122E+00	0.111E+00

Table 5.4: $2\times CO_2$ biology simulation table of indicated statistical test, mean, standard deviation, and average difference (relative to control simulation) for the listed variable.

5.1.2 Diurnal Analysis of Hourly Variables

So far only daily variables have been analyzed. A similar analysis will now be conducted for the 2D hourly data, with the variables and their description displayed in Table 5.5. Since the computing power necessary to test all of these variables hourly would be immense, 4 daily times are chosen. These times correspond to 0, 6, 12, and 18 GMT (roughly corresponding to 18, 0, 6, and 12 LST). Through analysis of the diurnal cycle, significant differences on shorter temporal scales should be apparent. The significant differences on the shorter timescale would be an obvious conclusion based on the diurnal cycle of many of the variables investigated. It would also be intuitive that the nocturnal results might include fewer significant results, given the previous results from the minimum daily temperature; that there is stronger forcing during the daylight hours.

The results for the natural vegetation simulations are shown in Table 5.6 through Table 5.9 corresponding to 6 GMT through 0 GMT at 6-hour intervals. At 6 GMT there are 3 variables with significant differences in variance; the latent heat flux, the average soil water potential, and the near surface soil water potential. The t test indicates significant

Variable Symbol	Description
QFZ	2-hour averaged surface latent heat flux (W m^{-2})
TFZ	2-hour averaged surface sensible heat flux (W m^{-2})
WFZ	2-hour averaged surface momentum heat flux (kg m^{-1} s^{-1})
SOIL1	2-hour averaged soil temperature at 1m below the surface (K)
SOIL2	2-hour averaged soil temperature at the surface (K)
SWPAVG	2-hour averaged soil water potential averaged over the root profile (MPa)
SWPTOP	2-hour averaged soil water potential averaged over the top 0.25 m (MPa)
PLWP	2-hour averaged plant water potential at the base of the xylem (MPa)
GS	2-hour averaged whole canopy stomatal conductance
AN	2-hour averaged assimilation rate *micro* mol m^{-2} s^{-1}
RESS	2-hour averaged soil respiration rate *micro* mol m^{-2} s^{-1}
CO2FLX	2-hour averaged surface CO_2 flux *micro* mol m^{-2} s^{-1}
CO2SFC	2-hour averaged surface CO_2 (ppm)
U500	2-hour averaged U-component of geostrophic wind (m s^{-1})
V500	2-hour averaged V-component of geostrophic wind (m s^{-1})
RHAIR	2-hour averaged relative humidity (percent)
RVAPPL	2-hour averaged vapor mixing ratio at the leaf surface (kg kg^{-1})

Table 5.5: Variable symbols and descriptions for the 2-hour averaged 2D variable analysis.

differences in means for the same soil water potentials and also includes whole canopy stomatal conductance. For the KS test, Table 5.6 indicates that the same variables as for the t test meet the significance threshold. Table 5.7, corresponding to 12 GMT, includes the same variables as the previous time for the F test. The only difference is that the t and KS tests no longer indicate a significant difference for plant water potential, although they are close to the 95% confidence limits.

The midday analysis shown in Table 5.8 displays a change in the variables exhibiting significant differences. In addition to the soil water potentials, momentum flux and plant water potential are now significantly different for the variance test. What is most dramatic is the number of variables now meeting the threshold for the t and KS test. As mentioned previously, variables with strong diurnal signals are significantly different in the t and KS tests. These include the latent heat flux, sensible heat flux, momentum flux, soil water potentials, plant water potential, whole canopy stomatal conductance, assimilation rates, and surface CO_2 flux. In addition, the near-surface soil temperature shows significant differences in means. The 0 GMT results, displayed in Table 5.9 are quite similar to the

Variable Symbol	F test	t test	KS test	Mean	σ	difference
QFZ	*0.214E-01	0.653E-01	0.393E+00	0.825E+01	0.437E+01	0.942E+00
TFZ	0.695E+00	0.100E+01	0.100E+01	-0.144E+02	0.674E+01	-0.203E-02
WFZ	0.856E+00	0.962E+00	0.100E+01	0.140E+00	0.643E-01	0.390E-03
SOIL1	0.677E+00	0.832E+00	0.987E+00	0.288E+03	0.460E+01	-0.120E+00
SOIL2	0.758E+00	0.708E+00	0.270E+00	0.281E+03	0.431E+01	-0.195E+00
SWPAVG	*0.208E-01	*0.224E-01	*0.222E-01	-0.379E+00	0.775E-01	0.224E-01
SWPTOP	*0.219E-01	*0.129E-01	*0.164E-01	-0.406E+00	0.105E+00	0.337E-01
PLWP	0.110E+00	0.696E-01	0.397E-01	-0.371E+00	0.741E-01	0.164E-01
GS	0.572E-01	*0.418E-06	*0.120E-27	0.526E-02	0.682E-03	0.406E-03
AN	0.486E+00	0.438E+00	0.879E-01	-0.724E+01	0.192E+01	-0.182E+00
RESS	0.994E+00	0.491E+00	0.864E+00	0.187E+00	0.595E-01	-0.499E-02
CO2FLX	0.537E+00	0.562E+00	0.327E+00	-0.874E+01	0.232E+01	-0.163E+00
CO2SFC	0.868E+00	0.859E+00	0.997E+00	0.319E+03	0.119E+02	-0.259E+00
U500	0.988E+00	0.868E+00	0.100E+01	0.147E+01	0.325E+00	-0.646E-02
V500	0.918E+00	0.975E+00	0.100E+01	0.272E+01	0.392E+01	0.155E-01
RHAIR	0.930E+00	0.105E+00	0.178E+00	0.474E+00	0.850E-01	0.172E-01
RVAPPL	0.562E+00	0.404E+00	0.711E+00	0.681E-02	0.163E-02	0.160E-03

Table 5.6: Natural simulation table of indicated statistical test, mean, standard deviation, and average difference (relative to control simulation) for the listed 2D 2-hourly variable at 6 GMT. The asterisk indicates significant difference for the various tests at the 95% confidence level.

Variable Symbol	F test	t test	KS test	Mean	σ	difference
QFZ	*0.433E-01	0.839E-01	0.627E+00	0.699E+01	0.364E+01	0.744E+00
TFZ	0.808E+00	0.695E+00	0.627E+00	-0.116E+02	0.515E+01	0.273E+00
WFZ	0.679E+00	0.652E+00	0.987E+00	0.158E+00	0.731E-01	0.408E-02
SOIL1	0.856E+00	0.691E+00	0.987E+00	0.285E+03	0.454E+01	0.220E+00
SOIL2	0.755E+00	0.702E+00	0.220E+00	0.281E+03	0.429E+01	-0.199E+00
SWPAVG	*0.216E-01	*0.226E-01	*0.222E-01	-0.379E+00	0.777E-01	0.224E-01
SWPTOP	*0.227E-01	*0.129E-01	*0.120E-01	-0.406E+00	0.105E+00	0.338E-01
PLWP	0.111E+00	0.688E-01	0.681E-01	-0.372E+00	0.743E-01	0.165E-01
GS	0.551E-01	*0.340E-06	*0.376E-29	0.527E-02	0.685E-03	0.409E-03
AN	0.511E+00	0.577E+00	0.270E+00	-0.637E+01	0.215E+01	-0.141E+00
RESS	0.987E+00	0.480E+00	0.923E+00	0.210E+00	0.672E-01	-0.566E-02
CO2FLX	0.559E+00	0.654E+00	0.270E+00	-0.797E+01	0.251E+01	-0.132E+00
CO2SFC	0.835E+00	0.766E+00	0.100E+01	0.328E+03	0.135E+02	-0.492E+00
U500	0.983E+00	0.859E+00	0.997E+00	0.148E+01	0.326E+00	-0.690E-02
V500	0.889E+00	0.864E+00	0.100E+01	0.192E+01	0.337E+01	-0.737E-01
RHAIR	0.941E+00	0.219E+00	0.465E+00	0.591E+00	0.924E-01	0.141E-01
RVAPPL	0.771E+00	0.607E+00	0.964E+00	0.693E-02	0.172E-02	0.105E-03

Table 5.7: Natural simulation table of indicated statistical test, mean, standard deviation, and average difference (relative to control simulation) for the listed 2D 2-hourly variable at 12 GMT. The asterisk indicates significant difference for the various tests at the 95% confidence level.

Variable Symbol	F test	t test	KS test	Mean	σ	difference
QFZ	0.438E+00	*0.111E-01	*0.164E-01	0.109E+03	0.234E+02	0.771E+01
TFZ	0.695E+00	*0.206E-04	*0.176E-06	0.143E+03	0.276E+02	-0.156E+02
WFZ	*0.237E-01	*0.118E-11	*0.113E-13	0.990E+00	0.128E+00	-0.114E+00
SOIL1	0.344E+00	*0.246E-01	0.522E-01	0.293E+03	0.460E+01	-0.131E+01
SOIL2	0.754E+00	0.700E+00	0.327E+00	0.281E+03	0.427E+01	-0.199E+00
SWPAVG	*0.223E-01	*0.228E-01	*0.222E-01	-0.379E+00	0.780E-01	0.224E-01
SWPTOP	*0.235E-01	*0.130E-01	*0.120E-01	-0.407E+00	0.105E+00	0.338E-01
PLWP	*0.998E-12	*0.695E-31	*0.130E-18	-0.453E+00	0.946E-01	0.191E+00
GS	0.572E+00	*0.940E-12	*0.255E-08	0.251E+00	0.406E-01	0.356E-01
AN	0.674E+00	*0.433E-21	*0.515E-17	0.168E+02	0.196E+01	0.261E+01
RESS	0.988E+00	0.991E+00	0.100E+01	0.143E+00	0.608E-01	-0.806E-04
CO2FLX	0.825E+00	*0.289E-26	*0.306E-16	0.154E+02	0.203E+01	0.287E+01
CO2SFC	0.977E+00	0.773E+00	0.100E+01	0.323E+03	0.122E+02	-0.433E+00
U500	0.987E+00	0.858E+00	0.964E+00	0.148E+01	0.325E+00	-0.693E-02
V500	0.944E+00	0.979E+00	0.100E+01	0.912E+00	0.282E+01	0.946E-02
RHAIR	0.433E+00	0.327E-01	0.681E-01	0.463E+00	0.743E-01	0.200E-01
RVAPPL	0.464E+00	0.270E+00	0.627E+00	0.702E-02	0.160E-02	0.208E-03

Table 5.8: Natural simulation table of indicated statistical test, mean, standard deviation, and average difference (relative to control simulation) for the listed 2D 2-hourly variable at 18 GMT. The asterisk indicates significant difference for the various tests at the 95% confidence level.

midday results. For the test on variance, the momentum flux is no longer significant, possibly indicating a decay or decoupling of the boundary layer from the surface. Still at this time, the same variables for the significantly different means at 18 GMT are present with the exception of momentum flux and latent heat flux. The KS statistics indicate a similar pattern, with the same variables as 18 GMT. As hypothesized previously, there appears a strong diurnal component for the variables tested. The soil water potentials are the only two quantities that indicate significant differences throughout the diurnal cycle. This is not surprising in light of differing root distributions for natural and current vegetation. It is also clear that most variables that are strongly affected by solar insolation appear significantly different in the daylight hours.

Variable Symbol	F test	t test	KS test	Mean	σ	difference
QFZ	0.932E+00	0.317E-01	*0.146E-02	0.697E+02	0.153E+02	0.430E+01
TFZ	0.216E+00	*0.312E-03	*0.671E-03	0.750E+02	0.212E+02	-0.991E+01
WFZ	0.518E+00	0.929E-01	*0.164E-01	0.453E+00	0.116E+00	-0.261E-01
SOIL1	0.302E+00	*0.174E-01	*0.397E-01	0.296E+03	0.458E+01	-0.137E+01
SOIL2	0.763E+00	0.718E+00	0.393E+00	0.281E+03	0.433E+01	-0.189E+00
SWPAVG	*0.201E-01	*0.223E-01	*0.222E-01	-0.378E+00	0.773E-01	0.223E-01
SWPTOP	*0.207E-01	*0.126E-01	*0.164E-01	-0.406E+00	0.104E+00	0.337E-01
PLWP	0.699E-01	*0.241E-06	*0.269E-05	-0.395E+00	0.752E-01	0.481E-01
GS	0.572E+00	*0.294E-11	*0.111E-10	0.180E+00	0.308E-01	0.275E-01
AN	0.304E+00	*0.143E-19	*0.733E-16	0.134E+02	0.194E+01	0.243E+01
RESS	0.938E+00	0.917E+00	0.997E+00	0.155E+00	0.588E-01	0.765E-03
CO2FLX	0.507E+00	*0.849E-12	*0.123E-12	0.114E+02	0.226E+01	0.214E+01
CO2SFC	0.922E+00	0.888E+00	0.997E+00	0.308E+03	0.104E+02	0.178E+00
U500	0.999E+00	0.882E+00	0.997E+00	0.147E+01	0.324E+00	-0.577E-02
V500	0.891E+00	0.868E+00	0.100E+01	0.138E+01	0.310E+01	0.644E-01
RHAIR	0.678E+00	0.337E-01	0.298E-01	0.365E+00	0.705E-01	0.188E-01
RVAPPL	0.360E+00	0.168E+00	0.393E+00	0.642E-02	0.144E-02	0.234E-03

Table 5.9: Natural vegetation simulation table of indicated statistical test, mean, standard deviation, and average difference (relative to control simulation) for the listed 2D 2-hourly variable at 0 GMT. The asterisk indicates significant difference for the various tests at the 95% confidence level.

Tables 5.10 through 5.13 show the same variables and time series as used in the natural vegetation analysis and corresponds to the results obtained for the $2\times CO_2$ radiation simulation. The most significant result from the tests performed is a complete lack of significant differences for variances, means, and distributions. In these tests, none of the

variables are even close to suggesting significant differences. A similar result was found in the analysis of the 2D daily variables, although a few variables tested significantly different in that analysis. This null result further indicates the relatively weak contribution due to $2\times CO_2$ radiation.

Variable Symbol	F test	t test	KS test	Mean	σ	difference
QFZ	0.905E+00	0.847E+00	0.100E+01	0.740E+01	0.377E+01	0.902E-01
TFZ	0.982E+00	0.992E+00	0.100E+01	-0.144E+02	0.662E+01	0.789E-02
WFZ	0.950E+00	0.925E+00	0.100E+01	0.140E+00	0.639E-01	0.774E-03
SOIL1	0.987E+00	0.884E+00	0.100E+01	0.289E+03	0.474E+01	0.830E-01
SOIL2	0.993E+00	0.948E+00	0.100E+01	0.281E+03	0.443E+01	0.342E-01
SWPAVG	0.911E+00	0.963E+00	0.100E+01	-0.400E+00	0.919E-01	0.484E-03
SWPTOP	0.885E+00	0.963E+00	0.100E+01	-0.439E+00	0.125E+00	0.671E-03
PLWP	0.917E+00	0.959E+00	0.100E+01	-0.387E+00	0.834E-01	0.485E-03
GS	0.991E+00	0.995E+00	0.100E+01	0.486E-02	0.582E-03	0.500E-06
AN	0.951E+00	0.941E+00	0.100E+01	-0.707E+01	0.182E+01	-0.169E-01
RESS	0.983E+00	0.985E+00	0.100E+01	0.192E+00	0.593E-01	-0.133E-03
CO2FLX	0.952E+00	0.933E+00	0.100E+01	-0.860E+01	0.220E+01	-0.231E-01
CO2SFC	0.959E+00	0.979E+00	0.100E+01	0.319E+03	0.116E+02	-0.370E-01
U500	0.986E+00	0.940E+00	0.100E+01	0.148E+01	0.324E+00	0.291E-02
V500	0.996E+00	0.993E+00	0.100E+01	0.270E+01	0.395E+01	-0.406E-02
RHAIR	0.986E+00	0.984E+00	0.100E+01	0.457E+00	0.861E-01	0.205E-03
RVAPPL	0.986E+00	0.991E+00	0.100E+01	0.665E-02	0.155E-02	0.213E-05

Table 5.10: $2\times CO_2$ radiation simulation table of indicated statistical test, mean, standard deviation, and average difference (relative to control simulation) for the listed 2D 2-hourly variable at 6 GMT. The asterisk indicates significant difference for the various tests at the 95% confidence level.

The analysis was next applied to the $2\times CO_2$ biological simulation. Following the same format as the natural vegetation and $2\times CO_2$ radiation analysis, the results are displayed in Tables 5.14 through 5.17. The 6 GMT analysis indicates that significant differences exist in the means and variances of whole canopy conductance, assimilation rate, surface CO_2 flux, and CO_2 surface concentrations between the $2\times CO_2$ biological and control simulations. The same can be said of the KS test with the exception of CO_2 surface concentration. These results are expected, considering the only change to the control simulation was to double the free atmosphere CO_2 concentration involved in the biotic processes. Clearly a difference in CO_2 surface concentration would be expected for variance and mean. The fact that a significant result does not appear in the KS test is an artifact of the test's

Variable Symbol	F test	t test	KS test	Mean	σ	difference
QFZ	0.911E+00	0.815E+00	0.100E+01	0.634E+01	0.317E+01	0.936E-01
TFZ	0.975E+00	0.974E+00	0.100E+01	-0.119E+02	0.532E+01	0.230E-01
WFZ	0.967E+00	0.918E+00	0.100E+01	0.155E+00	0.711E-01	0.918E-03
SOIL1	0.982E+00	0.843E+00	0.100E+01	0.285E+03	0.461E+01	0.110E+00
SOIL2	0.994E+00	0.948E+00	0.100E+01	0.281E+03	0.441E+01	0.342E-01
SWPAVG	0.910E+00	0.963E+00	0.100E+01	-0.401E+00	0.921E-01	0.493E-03
SWPTOP	0.884E+00	0.963E+00	0.100E+01	-0.439E+00	0.126E+00	0.679E-03
PLWP	0.916E+00	0.959E+00	0.100E+01	-0.388E+00	0.836E-01	0.486E-03
GS	0.990E+00	0.993E+00	0.100E+01	0.486E-02	0.582E-03	0.568E-06
AN	0.955E+00	0.910E+00	0.100E+01	-0.626E+01	0.204E+01	-0.278E-01
RESS	0.983E+00	0.993E+00	0.100E+01	0.216E+00	0.667E-01	-0.714E-04
CO2FLX	0.968E+00	0.911E+00	0.100E+01	-0.787E+01	0.240E+01	-0.323E-01
CO2SFC	0.980E+00	0.984E+00	0.100E+01	0.328E+03	0.132E+02	0.318E-01
U500	0.986E+00	0.940E+00	0.100E+01	0.149E+01	0.325E+00	0.293E-02
V500	0.999E+00	0.100E+01	0.100E+01	0.199E+01	0.341E+01	0.532E-03
RHAIR	0.968E+00	0.953E+00	0.100E+01	0.578E+00	0.927E-01	0.681E-03
RVAPPL	0.994E+00	0.989E+00	0.100E+01	0.682E-02	0.168E-02	0.280E-05

Table 5.11: $2\times CO_2$ radiation simulation table of indicated statistical test, mean, standard deviation, and average difference (relative to control simulation) for the listed 2D 2-hourly variable at 12 GMT. The asterisk indicates significant difference for the various tests at the 95% confidence level.

Variable Symbol	F test	t test	KS test	Mean	σ	difference
QFZ	0.990E+00	0.829E+00	0.100E+01	0.102E+03	0.248E+02	0.669E+00
TFZ	0.948E+00	0.966E+00	0.100E+01	0.159E+03	0.284E+02	0.157E+00
WFZ	0.905E+00	0.952E+00	0.100E+01	0.110E+01	0.109E+00	-0.853E-03
SOIL1	0.995E+00	0.957E+00	0.100E+01	0.295E+03	0.492E+01	0.324E-01
SOIL2	0.994E+00	0.948E+00	0.100E+01	0.281E+03	0.440E+01	0.342E-01
SWPAVG	0.909E+00	0.962E+00	0.100E+01	-0.401E+00	0.923E-01	0.498E-03
SWPTOP	0.883E+00	0.963E+00	0.100E+01	-0.440E+00	0.126E+00	0.679E-03
PLWP	0.847E+00	0.919E+00	0.100E+01	-0.642E+00	0.159E+00	0.182E-02
GS	0.999E+00	0.836E+00	0.100E+01	0.216E+00	0.385E-01	0.979E-03
AN	0.793E+00	0.643E+00	0.987E+00	0.143E+02	0.192E+01	0.115E+00
RESS	0.996E+00	0.988E+00	0.100E+01	0.143E+00	0.608E-01	0.115E-03
CO2FLX	0.767E+00	0.619E+00	0.864E+00	0.126E+02	0.198E+01	0.120E+00
CO2SFC	0.972E+00	0.996E+00	0.100E+01	0.323E+03	0.121E+02	-0.758E-02
U500	0.986E+00	0.940E+00	0.100E+01	0.149E+01	0.324E+00	0.292E-02
V500	0.993E+00	0.993E+00	0.100E+01	0.899E+00	0.280E+01	-0.290E-02
RHAIR	0.993E+00	0.981E+00	0.100E+01	0.443E+00	0.794E-01	-0.236E-03
RVAPPL	0.977E+00	0.995E+00	0.100E+01	0.681E-02	0.150E-02	0.141E-05

Table 5.12: 2 $\times CO_2$ radiation simulation table of indicated statistical test, mean, standard deviation, and average difference (relative to control simulation) for the listed 2D 2-hourly variable at 18 GMT. The asterisk indicates significant difference for the various tests at the 95% confidence level.

Variable Symbol	F test	t test	KS test	Mean	σ	difference
QFZ	0.986E+00	0.860E+00	0.100E+01	0.657E+02	0.152E+02	0.350E+00
TFZ	0.941E+00	0.950E+00	0.100E+01	0.851E+02	0.231E+02	0.178E+00
WFZ	0.961E+00	0.918E+00	0.100E+01	0.480E+00	0.124E+00	0.163E-02
SOIL1	0.985E+00	0.977E+00	0.100E+01	0.297E+03	0.493E+01	0.172E-01
SOIL2	0.993E+00	0.949E+00	0.100E+01	0.281E+03	0.446E+01	0.341E-01
SWPAVG	0.912E+00	0.964E+00	0.100E+01	-0.400E+00	0.917E-01	0.472E-03
SWPTOP	0.887E+00	0.965E+00	0.100E+01	-0.439E+00	0.125E+00	0.638E-03
PLWP	0.972E+00	0.100E+01	0.100E+01	-0.444E+00	0.878E-01	0.913E-05
GS	0.993E+00	0.864E+00	0.100E+01	0.153E+00	0.297E-01	0.641E-03
AN	0.786E+00	0.739E+00	0.964E+00	0.110E+02	0.209E+01	0.844E-01
RESS	0.100E+01	0.980E+00	0.100E+01	0.155E+00	0.592E-01	0.182E-03
CO2FLX	0.823E+00	0.792E+00	0.997E+00	0.936E+01	0.244E+01	0.777E-01
CO2SFC	0.958E+00	0.969E+00	0.100E+01	0.308E+03	0.103E+02	-0.493E-01
U500	0.986E+00	0.941E+00	0.100E+01	0.147E+01	0.323E+00	0.289E-02
V500	0.997E+00	0.995E+00	0.100E+01	0.131E+01	0.306E+01	-0.294E-02
RHAIR	0.994E+00	0.995E+00	0.100E+01	0.346E+00	0.739E-01	-0.614E-04
RVAPPL	0.976E+00	0.992E+00	0.100E+01	0.619E-02	0.134E-02	0.166E-05

Table 5.13: $2\times CO_2$ radiation simulation table of indicated statistical test, mean, standard deviation, and average difference (relative to control simulation) for the listed 2D 2-hourly variable at 0 GMT. The asterisk indicates significant difference for the various tests at the 95% confidence level.

ignorance of magnitude; only a reliance on the cumulative distribution. The increased concentrations would also directly impact the stomatal conductance, which is related to CO_2 surface concentration. The stomatal conductance also is tied into the photosynthesis calculations and thus impacts the assimilation rates. Finally, assimilation rate is one of the source/sink terms for the net CO_2 flux calculation and is likely the chief contributer to the difference. Notice that the test results at 12 GMT show that the same variables have significant differences. It should be noted that at both of these times we would not have the solar influence on the prognosed variables.

Variable Symbol	F test	t test	KS test	Mean	σ	difference
QFZ	0.412E+00	0.319E+00	0.864E+00	0.779E+01	0.393E+01	0.479E+00
TFZ	0.815E+00	0.727E+00	0.987E+00	-0.141E+02	0.646E+01	0.298E+00
WFZ	0.876E+00	0.952E+00	0.100E+01	0.140E+00	0.640E-01	0.491E-03
SOIL1	0.885E+00	0.950E+00	0.100E+01	0.288E+03	0.469E+01	0.358E-01
SOIL2	0.867E+00	0.918E+00	0.923E+00	0.281E+03	0.436E+01	-0.541E-01
SWPAVG	0.754E+00	0.854E+00	0.792E+00	-0.403E+00	0.906E-01	-0.192E-02
SWPTOP	0.316E+00	0.822E+00	0.923E+00	-0.436E+00	0.118E+00	0.317E-02
PLWP	0.904E+00	0.653E+00	0.864E+00	-0.392E+00	0.847E-01	-0.430E-02
GS	*0.110E-07	*0.415E-18	*0.886E-41	0.574E-02	0.907E-03	0.883E-03
AN	*0.143E-02	*0.691E-07	*0.306E-16	-0.848E+01	0.231E+01	-0.142E+01
RESS	0.947E+00	0.556E+00	0.964E+00	0.187E+00	0.597E-01	-0.427E-02
CO2FLX	*0.603E-02	*0.350E-05	*0.113E-13	-0.100E+02	0.272E+01	-0.144E+01
CO2SFC	*0.856E-19	*0.000E+00	0.100E+01	0.637E+03	0.230E+02	0.318E+03
U500	0.839E+00	0.851E+00	0.997E+00	0.147E+01	0.318E+00	-0.724E-02
V500	0.986E+00	0.935E+00	0.100E+01	0.266E+01	0.395E+01	-0.398E-01
RHAIR	0.937E+00	0.780E+00	0.100E+01	0.460E+00	0.856E-01	0.296E-02
RVAPPL	0.932E+00	0.906E+00	0.100E+01	0.667E-02	0.156E-02	0.222E-04

Table 5.14: $2\times CO_2$ biology simulation table of indicated statistical test, mean, standard deviation, and average difference (relative to control simulation) for the listed 2D 2-hourly variable at 6 GMT. The asterisk indicates significant difference for the various tests at the 95% confidence level.

The next two times analyzed, 18 and 0 GMT, begin to show more variables with significant differences. The incoming solar radiation, combined with the biomass and fractional coverage differences outlined in the previous section, have contributed to significant differences in some of the surface energy fluxes. At 18 GMT all tests indicate significant differences in the momentum flux. By 0 GMT none of the tests indicate the momentum flux is significantly different. The tables also exhibit t and KS test results that indicate

Variable Symbol	F test	t test	KS test	Mean	σ	difference
QFZ	0.230E+00	0.174E+00	0.711E+00	0.682E+01	0.342E+01	0.565E+00
TFZ	0.847E+00	0.785E+00	0.711E+00	-0.117E+02	0.521E+01	0.190E+00
WFZ	0.809E+00	0.880E+00	0.100E+01	0.155E+00	0.718E-01	0.136E-02
SOIL1	0.951E+00	0.596E+00	0.923E+00	0.285E+03	0.463E+01	0.296E+00
SOIL2	0.862E+00	0.911E+00	0.864E+00	0.281E+03	0.434E+01	-0.580E-01
SWPAVG	0.754E+00	0.855E+00	0.792E+00	-0.403E+00	0.908E-01	-0.191E-02
SWPTOP	0.318E+00	0.821E+00	0.964E+00	-0.437E+00	0.118E+00	0.319E-02
PLWP	0.905E+00	0.654E+00	0.864E+00	-0.393E+00	0.849E-01	-0.430E-02
GS	*0.112E-07	*0.441E-18	*0.886E-41	0.574E-02	0.908E-03	0.882E-03
AN	*0.261E-02	*0.178E-05	*0.174E-15	-0.758E+01	0.255E+01	-0.135E+01
RESS	0.956E+00	0.534E+00	0.923E+00	0.211E+00	0.674E-01	-0.499E-02
CO2FLX	*0.730E-02	*0.256E-04	*0.574E-12	-0.920E+01	0.291E+01	-0.136E+01
CO2SFC	*0.778E-17	*0.000E+00	0.100E+01	0.651E+03	0.249E+02	0.323E+03
U500	0.833E+00	0.842E+00	0.987E+00	0.148E+01	0.319E+00	-0.769E-02
V500	0.981E+00	0.961E+00	0.100E+01	0.197E+01	0.342E+01	-0.211E-01
RHAIR	0.985E+00	0.100E+01	0.100E+01	0.577E+00	0.927E-01	-0.854E-05
RVAPPL	0.950E+00	0.920E+00	0.100E+01	0.684E-02	0.169E-02	0.205E-04

Table 5.15: $2\times CO_2$ biology simulation table of indicated statistical test, mean, standard deviation, and average difference (relative to control simulation) for the listed 2D 2-hourly variable at 12 GMT. The asterisk indicates significant difference for the various tests at the 95% confidence level.

the sensible heat flux is significantly different at both times. The four variables showing significantly different results at 6 and 12 GMT have changed under the daylight heating. The tests that are no longer significant for these variables are generally close to meeting the threshold. Remembering that these are domain averages, it might be suspected that large areas in a spatial analysis might exhibit significant differences. This will be the subject of the next section.

Variable Symbol	F test	t test	KS test	Mean	σ	difference
QFZ	0.483E+00	0.205E+00	0.327E+00	0.977E+02	0.235E+02	-0.384E+01
TFZ	0.395E+00	*0.274E-02	*0.437E-02	0.147E+03	0.306E+02	-0.114E+02
WFZ	*0.250E-02	*0.223E-04	*0.159E-05	0.104E+01	0.135E+00	-0.687E-01
SOIL1	0.656E+00	0.266E+00	0.627E+00	0.294E+03	0.475E+01	-0.657E+00
SOIL2	0.861E+00	0.909E+00	0.964E+00	0.281E+03	0.432E+01	-0.591E-01
SWPAVG	0.757E+00	0.854E+00	0.711E+00	-0.403E+00	0.910E-01	-0.192E-02
SWPTOP	0.320E+00	0.822E+00	0.923E+00	-0.437E+00	0.118E+00	0.318E-02
PLWP	0.301E+00	0.322E+00	0.270E+00	-0.626E+00	0.149E+00	0.173E-01
GS	*0.303E-08	*0.987E-09	*0.310E-06	0.190E+00	0.251E-01	-0.250E-01
AN	*0.646E-02	0.000E+00	0.100E+01	0.213E+02	0.218E+01	0.713E+01
RESS	0.960E+00	0.854E+00	0.987E+00	0.142E+00	0.607E-01	-0.135E-02
CO2FLX	0.122E+00	*0.000E+00	0.100E+01	0.200E+02	0.217E+01	0.753E+01
CO2SFC	*0.841E-19	*0.000E+00	0.100E+01	0.646E+03	0.239E+02	0.323E+03
U500	0.833E+00	0.839E+00	0.987E+00	0.148E+01	0.319E+00	-0.781E-02
V500	0.973E+00	0.943E+00	0.100E+01	0.928E+00	0.281E+01	0.253E-01
RHAIR	0.816E+00	0.535E+00	0.792E+00	0.449E+00	0.774E-01	0.591E-02
RVAPPL	0.836E+00	0.863E+00	0.100E+01	0.684E-02	0.153E-02	0.319E-04

Table 5.16: $2\times CO_2$ biology simulation table of indicated statistical test, mean, standard deviation, and average difference (relative to control simulation) for the listed 2D 2-hourly variable at 18 GMT. The asterisk indicates significant difference for the various tests at the 95% confidence level.

This section of the analysis has included several interesting results. It was found for the natural vegetation contribution that a strong diurnal signal was present for the t and KS tests. This would be expected since the underlying vegetation has been altered. Coinciding with this change are different albedos, photosynthesis characteristics, emissivities, and root distributions to name a few changes. The next analysis on the $2\times CO_2$ radiation simulation found a complete lack of significant results. The last analysis concerning the $2\times CO_2$ biological simulation exhibited results in-between the prior two analyses. Some

Variable Symbol	F test	t test	KS test	Mean	σ	difference
QFZ	0.849E+00	0.397E+00	0.544E+00	0.637E+02	0.149E+02	-0.167E+01
TFZ	0.748E+00	*0.189E-02	*0.307E-02	0.761E+02	0.229E+02	-0.879E+01
WFZ	0.881E+00	0.844E-01	0.298E-01	0.452E+00	0.121E+00	-0.273E-01
SOIL1	0.581E+00	0.168E+00	0.270E+00	0.296E+03	0.472E+01	-0.806E+00
SOIL2	0.873E+00	0.924E+00	0.987E+00	0.281E+03	0.438E+01	-0.499E-01
SWPAVG	0.753E+00	0.853E+00	0.792E+00	-0.403E+00	0.904E-01	-0.192E-02
SWPTOP	0.315E+00	0.822E+00	0.923E+00	-0.436E+00	0.117E+00	0.316E-02
PLWP	0.985E+00	0.960E+00	0.987E+00	-0.444E+00	0.876E-01	-0.491E-03
GS	*0.121E-08	0.211E+00	0.142E+00	0.148E+00	0.189E-01	-0.395E-02
AN	0.771E-01	*0.000E+00	0.100E+01	0.180E+02	0.236E+01	0.709E+01
RESS	0.969E+00	0.825E+00	0.997E+00	0.153E+00	0.592E-01	-0.162E-02
CO2FLX	*0.700E-02	*0.000E+00	0.100E+01	0.163E+02	0.281E+01	0.702E+01
CO2SFC	*0.822E-22	*0.000E+00	0.100E+01	0.620E+03	0.217E+02	0.312E+03
U500	0.847E+00	0.860E+00	0.987E+00	0.146E+01	0.318E+00	-0.677E-02
V500	0.980E+00	0.965E+00	0.100E+01	0.133E+01	0.305E+01	0.170E-01
RHAIR	0.867E+00	0.419E+00	0.627E+00	0.353E+00	0.724E-01	0.720E-02
RVAPPL	0.806E+00	0.735E+00	0.964E+00	0.624E-02	0.137E-02	0.560E-04

Table 5.17: $2\times CO_2$ biology simulation table of indicated statistical test, mean, standard deviation, and average difference (relative to control simulation) for the listed 2D 2-hourly variable at 0 GMT. The asterisk indicates significant difference for the various tests at the 95% confidence level.

variables exhibited a diurnally-varying significance, while others were consistently different throughout the diurnal cycle. Given the abrupt changes introduced by changing the vegetation it would be expected that shorter time scales are going to be apparent for many of the variables. In the case of $2\times CO_2$ radiation, these results indicate that a diurnal manifestation is not there and could indicate that long time scale analysis might be needed to see significant differences. Indeed, the 2D daily variables exhibited some significant differences, and it is possible that the integrated effect of these differences could lead to further differences. In the case of $2\times CO_2$ biological forcing, there appears to be several scales at work. The cumulative effect of $2\times CO_2$ on the biomass accumulation and other related variables is concentrated on the seasonal time scale to a large degree. In the case of agricultural systems, the effect would be reduced by annual harvest and herbivory. Some of the results also suggest, by the proximity of several variables to meeting the significance threshold, that spatial analysis might exhibit areas of significant differences. It is with this in mind that the next section presents a spatial analysis of some of the variables analyzed thus far.

5.2 Spatial Analysis of Factor Contributions

In this section on the spatial analysis of factor contributions, a series of spatial test results will be examined for significant differences. In addition a subset of the variables and their spatial plots will be presented. This will be accomplished by forming a time series at each gridpoint and subjecting it to the same tests used for variance, mean, and distribution. This will be presented in the same order as used in the previous section. This portion of the analysis is meant to address one of the hypothesis presented in Chapter 4 that "grid-scale differences will be significant".

The natural vegetation contribution to the listed variables is analyzed first. In addition to spatial plots, a single number can be used to describe the percentage of gridpoints with significant differences from the control simulation. The percentage of gridpoints changing vegetation class between the two simulations is 41%. This is a similar percentage as that obtained when the boundary nudging points are included, which is 42.9%.

However, the nudging could influence the test results for the prognosed variables at these points and they are excluded from the analysis. The 41% is an important number to keep in mind as the variables are analyzed. The change is displayed explicitly in Figure 5.1. Areas that are green have been changed, while the blue shade indicates no change.

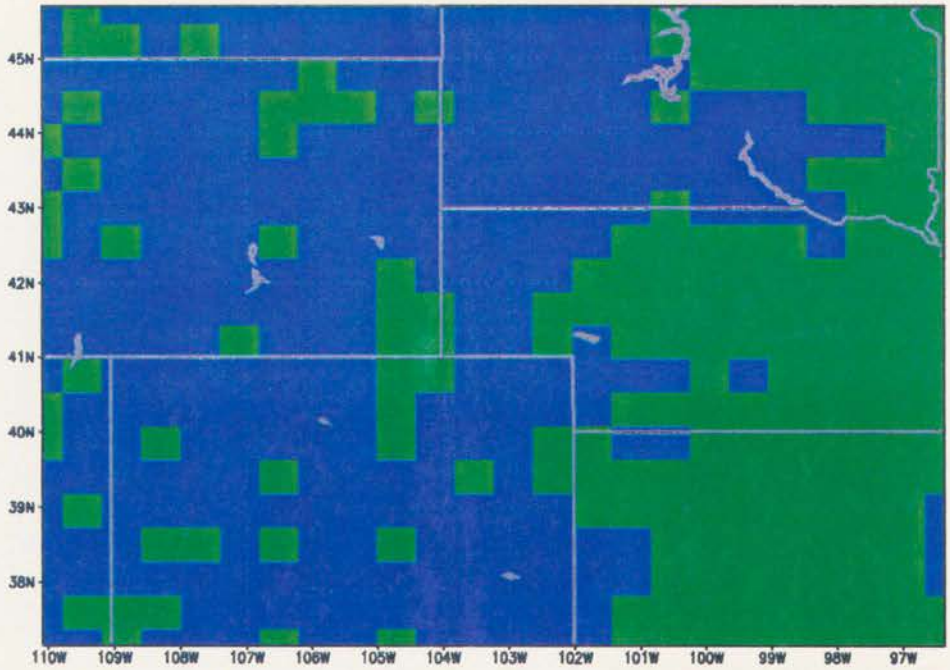

Figure 5.1: XY plot of vegetation change between natural and current vegetation. Blue areas represent no change, while the green areas represent change.

Those 2D daily variables tested in the previous section and their corresponding percentages that are not displayed in spatially explicit plots, are included in Table 5.18. One variable has been added, total daily precipitation (PPT in mm), for reasons that will become apparent as the analysis proceeds.

Table 5.18 contains several interesting results. Keeping in mind that the percentage of cells changed from natural to current vegetation is 41%, we see several variables that exceed this percentage for several tests. In the case of the t tests all but 5 variables exceed 41% of the cells with significant differences. For the variance test, 8 variables out of the 12 indicate a higher percentage of the cells have significant differences than the total percentage of cells with changed vegetation. The KS test results show 6 out of 12 with

Variable Symbol	t test %	F test %	KS test %
TMAX	39.8	17.7	40.6
TMIN	3.1	0.0	3.1
ACCUMALL	16.9	16.0	78.1
PPT	0.2	3.1	81.5
VFRAC	52.1	47.1	24.2
FLAI	50.8	44.2	25.8
DLAI	37.5	39.0	50.0
WL	50.6	43.5	25.6
WSD	46.3	46.7	57.9
WR	49.8	36.0	27.3
EVAPOTR	45.6	36.3	43.5
SUMALL	52.7	52.9	36.5

Table 5.18: Variable and percentage of cells significantly different for the given test between the natural vegetation and control simulations using a daily time series for each gridpoint.

greater totals than the percentage of changed cells. Taking the 3 results together, they generally indicate that the means, variance, and distributions are significantly different at a higher percentage of gridpoints relative to the number of cells with changed vegetation. The accumulated precipitation and daily precipitation are different because the distribution test indicates a much higher percentage than the t and F tests. The KS test indicates 81.5% of the cells have significantly different distributions for total accumulated precipitation, while the means and variance are significantly different at roughly 16% of cells. Considering that the KS test is on a temporal distribution, the results suggest that it rains nearly the same amount at most gridpoints but the time of the precipitation events has changed. Thus the seasonal distribution of precipitation has changed. This high percentage of distributional change was also indicated in the last section on domain averages (KS statistic = 0.0086). We can graphically demonstrate the timing of precipitation events by examining domain averages of the difference in daily precipitation between the control and natural simulations. This is displayed in Figure 5.2.

The plot indicates that the largest difference occurs in mid-July. The LAI data would suggest the trend would be the opposite, that the natural vegetation with increased LAI would lead to more transpiration and enhanced precipitation. However, there is

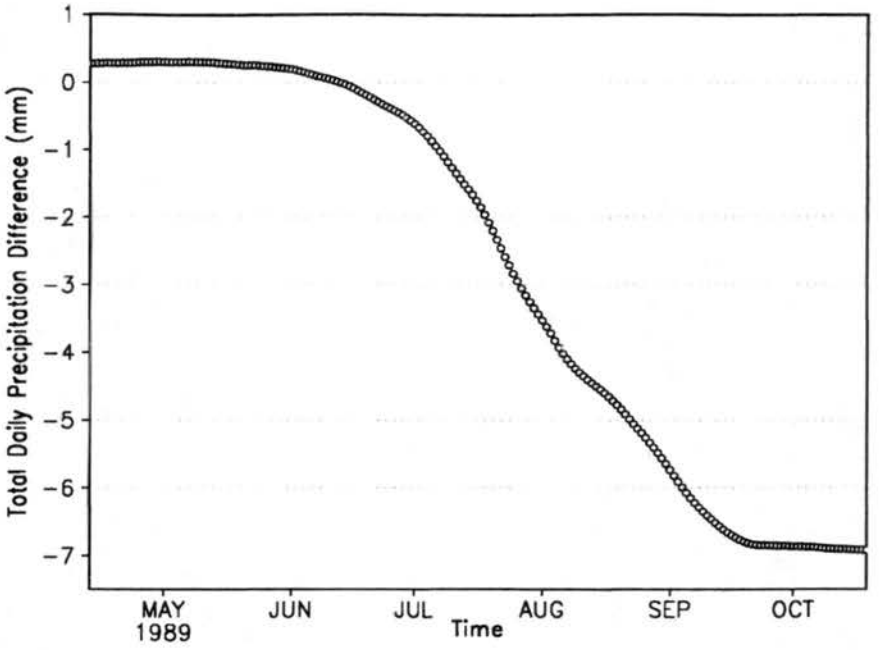

Figure 5.2: Domain-averaged difference in daily precipitation (mm) between the control run and the natural vegetation simulation.

an important mechanism that would offset this. The smaller LAI values in the current simulation have been shown to have higher maximum daily temperatures. This would lead to higher temperatures and result in more precipitation due to enhanced convergence. This makes sense since the summertime precipitation is frequently convective. Overall, it must be kept in mind that the precipitation is a noisy field that possesses high nonlinearity.

An example of the spatial plots is shown in Figure 5.3, which displays the t test results for maximum daily temperature. In this case it was found that nearly the same percentage of cells with changed vegetation contained significantly different means. It is evident from the figure that the contour lines roughly coincide with the areas where significant differences exist.

The data also indicates in some cases that the percentages of significantly different cells is larger than the percent of cells with changed vegetation. An example of this is shown for biomass in Figure 5.4. The figure is intriguing for several reasons. First, it is clear that there are numerous cells where there are significantly different cells outside of the areas of vegetation change. Second, many of these gridpoints are several points removed from the boundaries of areas where there has been changes in the vegetation. Finally,

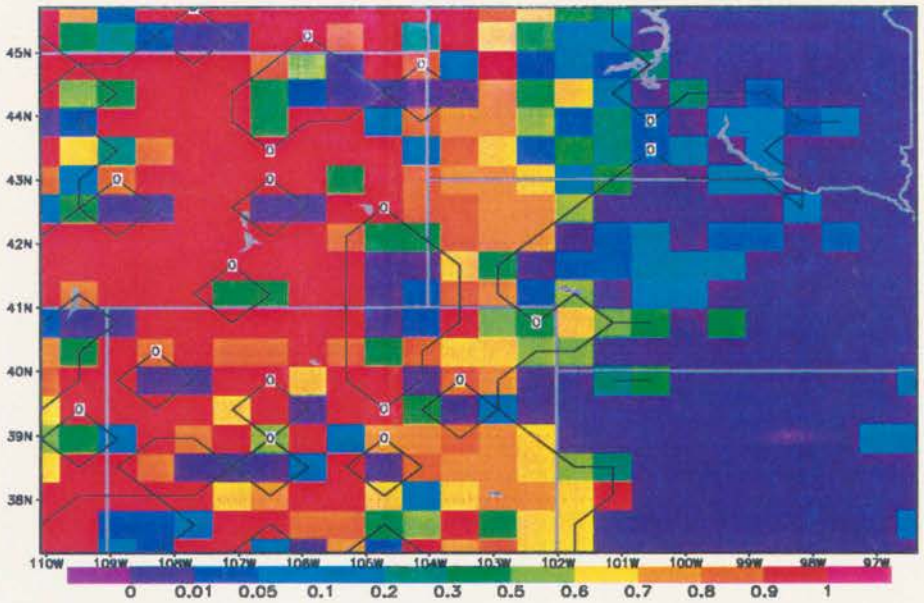

Figure 5.3: Gridded t test results for maximum daily temperature between the natural and control simulation. Contour line encloses unchanged vegetational areas.

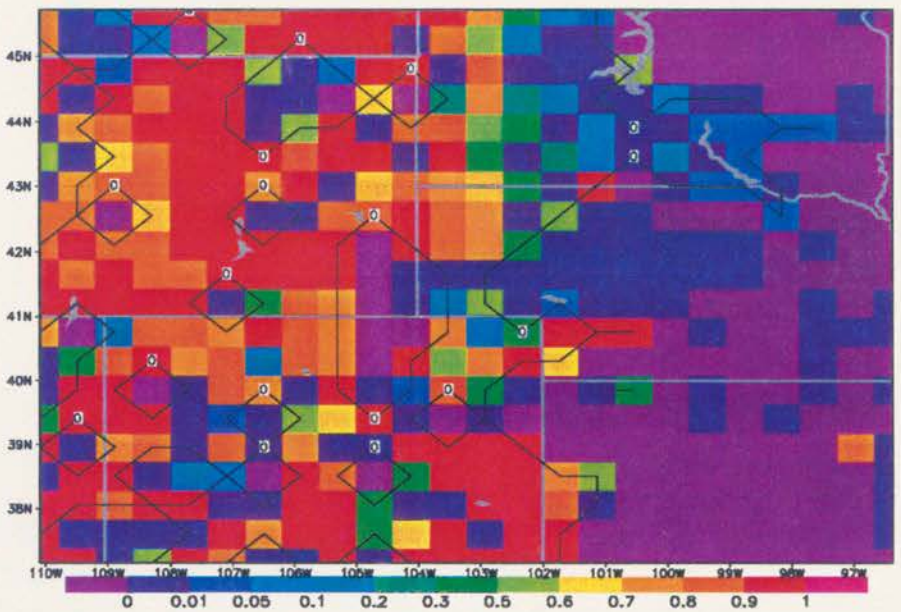

Figure 5.4: Gridded t test results for accumulated biomass between the natural and control simulations. Contour line encloses unchanged vegetational areas.

for reasons not understood from this analysis, this is a biological field that is exhibiting characteristics of teleconnection. This is surprising since the maximum daily temperature field is not exhibiting the same characteristics. It is possible that the temporal shift in precipitation is a contributor, although further study is required.

The next series of tests were performed on the $2\times CO_2$ radiation simulation and are shown in Table 5.19.

Variable Symbol	t test %	F test %	KS test %
TMAX	0.0	0.0	0.0
TMIN	0.0	0.0	0.0
ACCUMALL	0.4	0.0	49.0
PPT	0.0	0.4	77.3
VFRAC	4.8	1.0	24.2
FLAI	6.0	1.3	15.6
DLAI	1.3	0.6	6.9
WL	6.0	1.3	15.6
WSD	6.0	5.0	16.0
WR	5.0	4.4	25.2
EVAPOTR	1.5	0.2	1.5
SUMALL	8.3	9.0	21.7

Table 5.19: Variable and percentage of cells significantly different for the given test between the $2\times CO_2$ radiation and control simulations.

The table exhibits a strikingly smaller percentage of cells with significant differences. The KS test for the daily precipitation has the largest percentage at 77.3%, followed by the total accumulated precipitation. This suggests a sensitivity of precipitation to small perturbations in prognosed fields. The difference in domain-averaged precipitation is displayed in Figure 5.5. Comparison with the same plot for the natural vegetation run indicates that the differences are roughly an order of magnitude smaller in the $2\times CO_2$ radiation comparison. When compared to the magnitudes of the total precipitation, not the difference, this average is less than 2% of the total. In the natural vegetation case however, the totals were on the order of 10%. The largest differences are again found in the mid-July time period.

A spatial plot of the KS test for total accumulated precipitation is displayed in Figure 5.6. This figure shows that the areas not significantly different are largely contained in

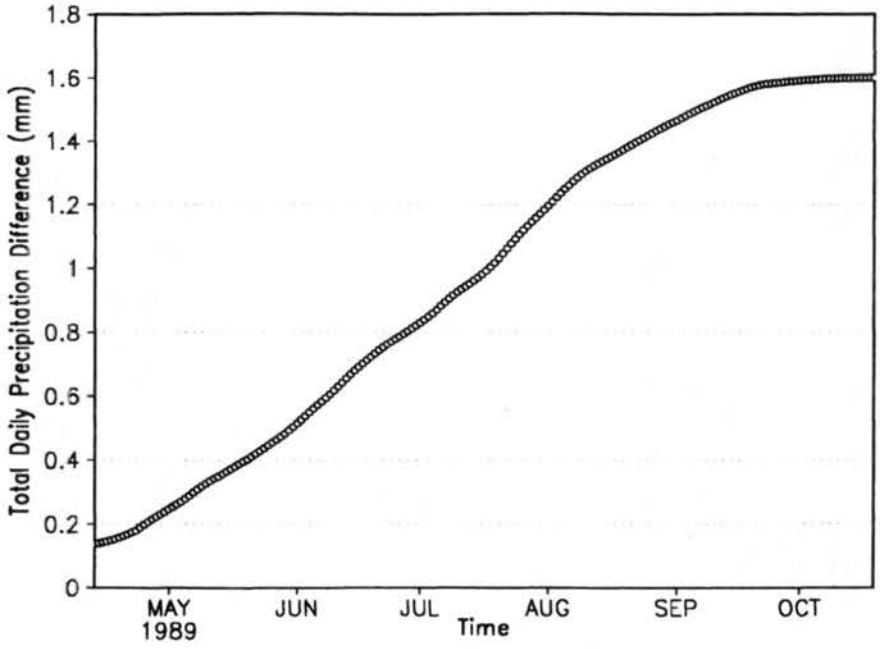

Figure 5.5: Domain-averaged difference in daily precipitation (mm) for the control run minus the $2\times CO_2$ radiation simulation.

the northwest quadrant of domain. These points are, in general, downstream from the western boundary conditions. As mentioned earlier, the precipitation is again showing sensitivity to rather small perturbations in other fields.

The precipitation differences are also likely contributors to the biomass results. However, these are again small when compared to the natural vegetation simulations when the significant differences in the means and variance are examined. The biomass would be impacted by the soil water potential and temperature, which in turn are affected by the precipitation. We also note a well-known statement in atmospheric science, it rains where it is wet. This is a simple way of stating that there is likely a feedback between the atmosphere and the land surfaces.

Finally, the results for the $2\times CO_2$ biological simulations are displayed in Table 5.20. As in the case of the natural simulation comparison, a high percentages of cells exhibit significant differences for most biological variables, with the mean and variance tests generally higher than the distribution test. The meteorological variables exhibit a smaller percentage of significantly different cells for maximum and minimum daily temperatures when compared to the natural vegetation contribution previously analyzed. However, the

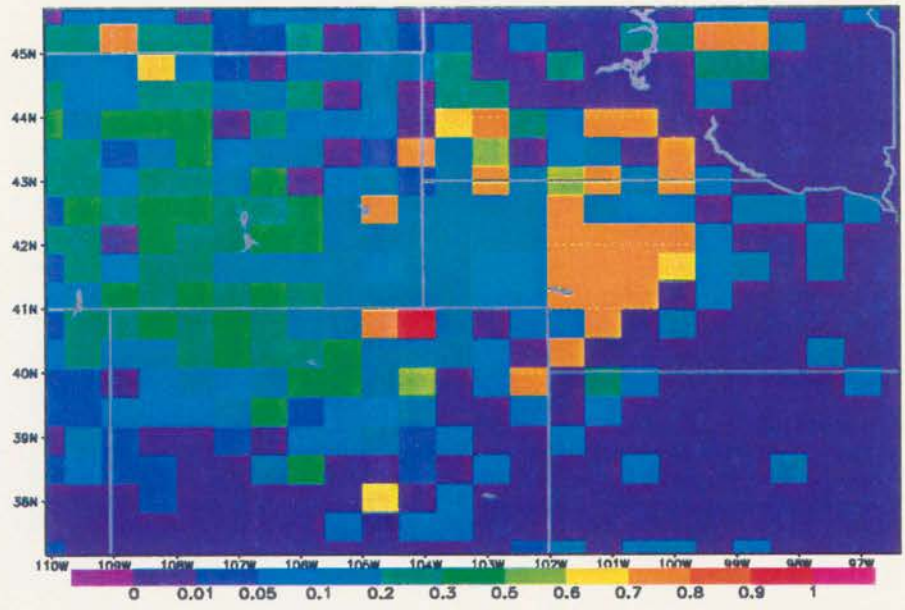

Figure 5.6: Horizontal plot of KS test for total accumulated precipitation between the control run minus the $2\times CO_2$ radiation simulation.

Variable Symbol	t test %	F test %	KS test %
TMAX	14.6	0.0	18.1
TMIN	0.0	0.0	0.6
ACCUMALL	11.7	12.3	89.6
PPT	0.0	2.1	84.2
VFRAC	86.7	65.4	58.8
FLAI	97.5	80.4	66.7
DLAI	40.0	46.9	91.5
WL	97.5	80.4	66.7
WSD	89.4	60.4	81.7
WR	77.7	58.1	57.5
EVAPOTR	20.0	2.9	20.8
SUMALL	99.8	95.8	66.0

Table 5.20: Variable and percentage of cells significantly different for the given test between the $2\times CO_2$ biological and control simulations.

precipitation displays a large percentage of significant cells for the KS test. Previous analysis indicated that the mean was generally less in the natural and $2\times CO_2$ biological simulations, while the $2\times CO_2$ radiation simulation indicated a higher mean for precipitation. The domain-averaged daily precipitation difference between the $2\times CO_2$ biological and control simulation is shown in Figure 5.7. Notice a signal close to that seen for the natural vegetation simulation. For reasons similar to the natural simulation, it is believed the maximum daily temperature and the enhanced total daily transpiration are contributors to the precipitation differences. It should also be noted that the percentage of cells with a significantly different mean is roughly the same as the natural case. This suggests that while the natural vegetation forcing is restricted to 41% of the cells and the $2\times CO_2$ biological is felt everywhere, the impact on precipitation is observed at nearly the same number of gridpoints.

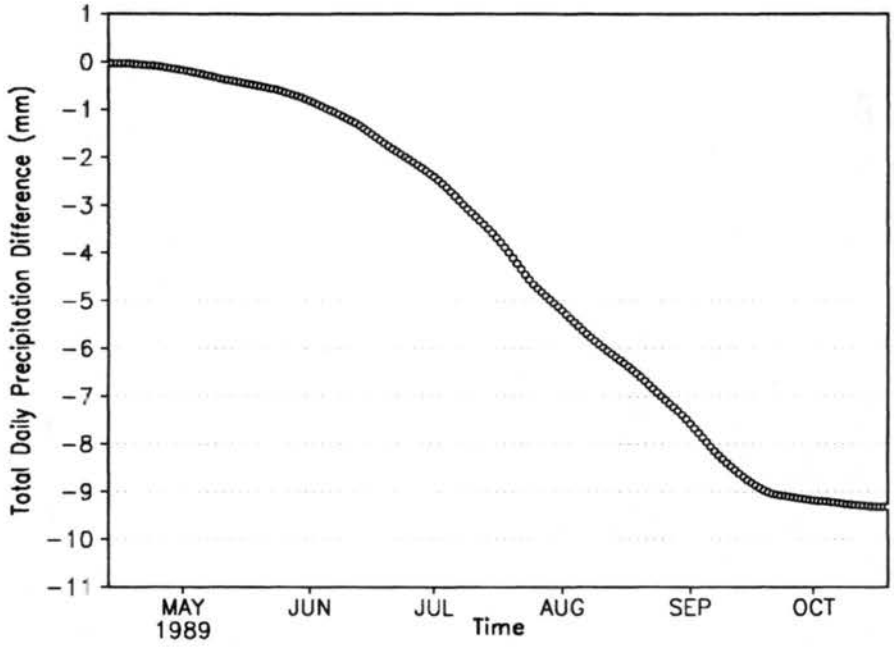

Figure 5.7: Domain-averaged difference in daily precipitation (mm) between the control run and the $2\times CO_2$ radiation simulation.

Since the two variables, domain-averaged daily maximum temperature and daily total transpiration have been mentioned so frequently, it would be instructive to examine their spatial fields for the season. Their domain averages are displayed in Figures 5.8 and 5.9, respectively. The figures indicate a similar pattern for both maximum daily temperature

and total daily transpiration. In both plots the natural simulation contribution is the largest in magnitude followed by the $2\times CO_2$ biology contribution. Both exhibit a strong seasonal cycle with peaks sometime after July. The maximum daily temperature contributions, however, exhibit different seasonal patterns. For the natural factor, a temperature difference is present from the beginning of the simulation and reaches a local peak by 1 July. The $2\times CO_2$ biology displays a general increase through the integration, with a maximum achieved in late September. In the case of transpiration the natural contribution peaks in mid-July, while the $2\times CO_2$ biology contribution appears to peak and flatten out around the beginning of August. The $2\times CO_2$ radiation contribution is minimal for both variables, with the plot showing a relative flatness. Clearly there is a complicated set of interactions between the biota and meteorology that cannot be explained in simple linear terms.

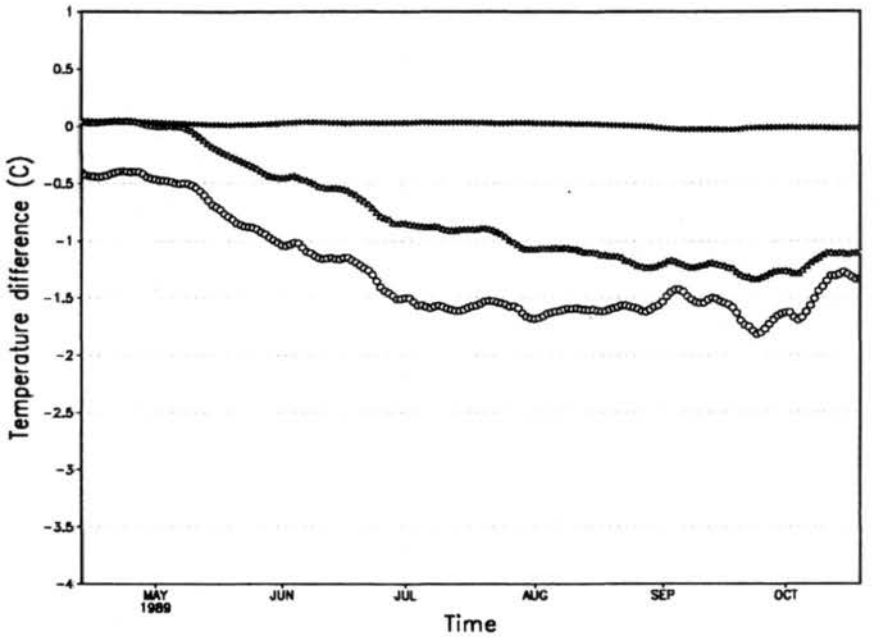

Figure 5.8: Domain-averaged difference in maximum daily temperature (C) between the control run and natural (open circle), $2\times CO_2$ radiation (cross), and $2\times CO_2$ biology (triangle) simulations.

The spatial plot of significantly different maximum daily temperature means for the $2\times CO_2$ biology contribution is shown in Figure 5.10. This figure indicates a spatial response concentrated over short grass areas in the north central and southern portions of

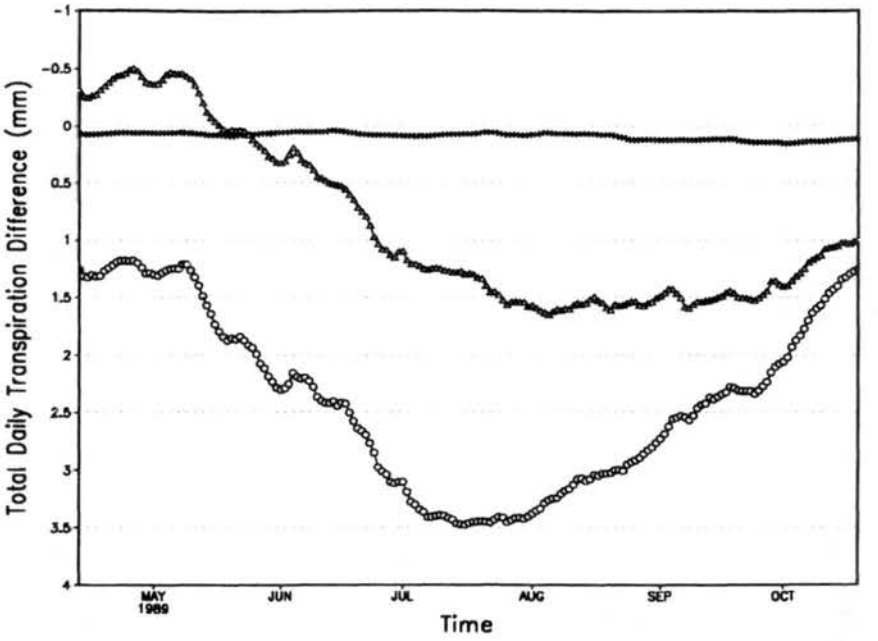

Figure 5.9: Domain-averaged difference in total daily transpiration (mm) between the control run and natural (open circle), $2\times CO_2$ radiation (cross), and $2\times CO_2$ biology (triangle) simulations.

the domain with a few cells interspersed throughout the rest of the model grid. There is also a considerable portion of the temperate arid shrub cells that are less than 0.1. It is possible that under longer integrations or with further adjustments to the precipitation schemes that even more cells would exhibit significant differences at the 0.05 level of significance. The figure also indicates that the areas with the least significance are in the northeastern portion of the grid.

Figures 5.11 and 5.12 show the t test fields for transpiration and total accumulated precipitation. Notice that the significantly changed grid cells for transpiration are collocated with the significant cells for the maximum daily temperature t test. However, the total accumulated precipitation plot indicates that more gridpoints with significant differences are located in the western portion of the domain. The points exhibiting a collocation of significant or near significant differences with the maximum daily temperature and daily transpiration are over the north central short grasslands and to some degree over the temperate arid shrublands. This raises the question as to why the western areas, with orographic forcing the main mechanism producing precipitation, would produce the

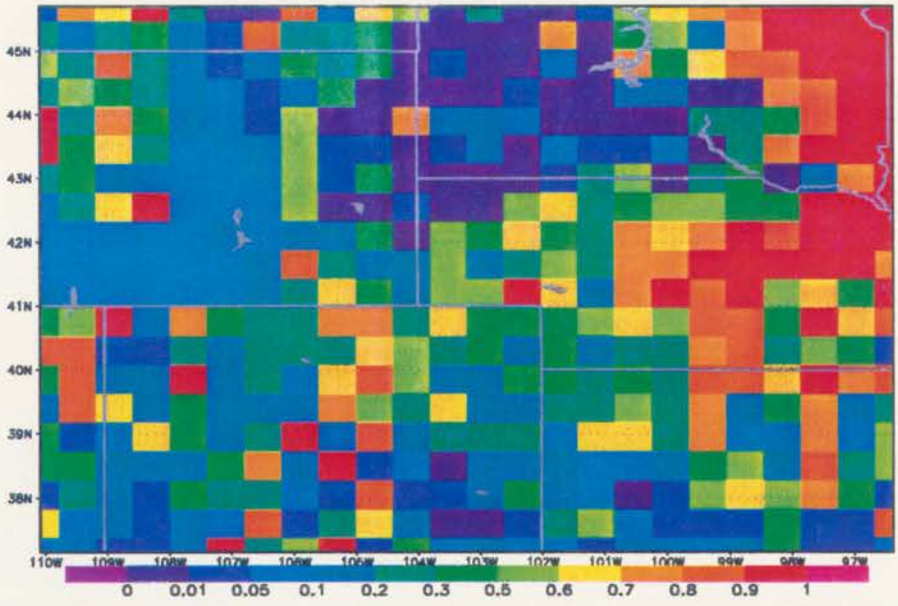

Figure 5.10: Horizontal fields of t test results for maximum daily temperature between the $2\times CO_2$ biology and control simulations.

most significant differences. This general area also possesses vegetation with relatively large LAI values.

There is a difference between the mechanism forcing precipitation over the plains and topography. In general, the $2\times CO_2$ biology will produce higher transpiration and lower maximum temperatures due to higher LAI despite the stomates closing. This could produce a dampening effect on the orographically forced precipitation in the mountainous regions through enhanced stability. A simple way to examine the differences in the mountainous regions and those areas over the plains would be to examine a product of the maximum daily temperature and daily transpiration averaged over the season. This is shown in Figure 5.13, with t test values indicated at 0.05, 0.1, and 0.11 intervals. There is a clear pattern that follows the general terrain of the domain.

This chapter has examined the factor contributions to meteorological and biological fields. In the case of natural vegetation, the results exhibited strong relationships to changes in the vegetation, and at the same time showed that more gridpoints were affected than the number of changed gridpoints. This suggested an analogy to meteorological teleconnection for plants, with the atmospheric flow being the mechanism to transfer

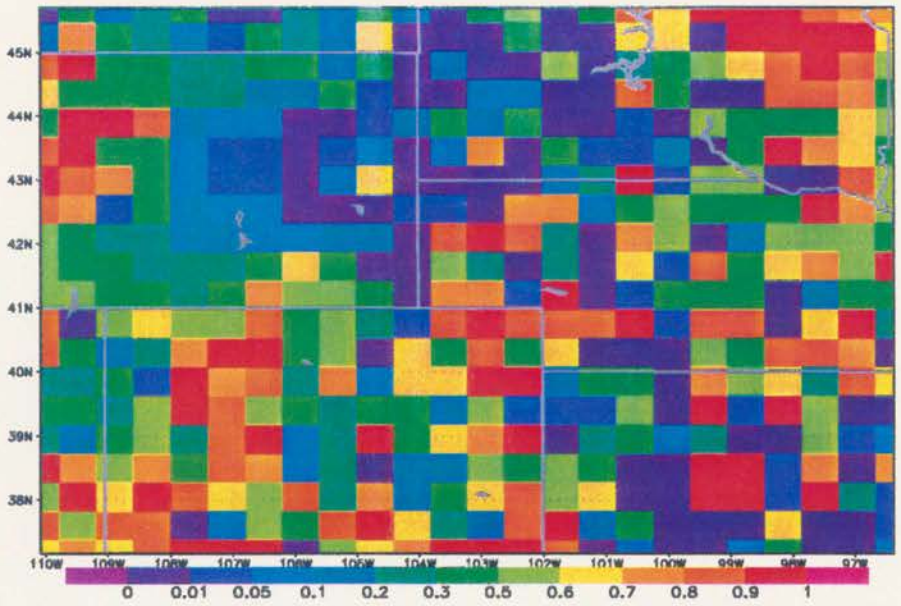

Figure 5.11: Horizontal fields of t test results for daily net transpiration between the $2\times CO_2$ biology and control simulations.

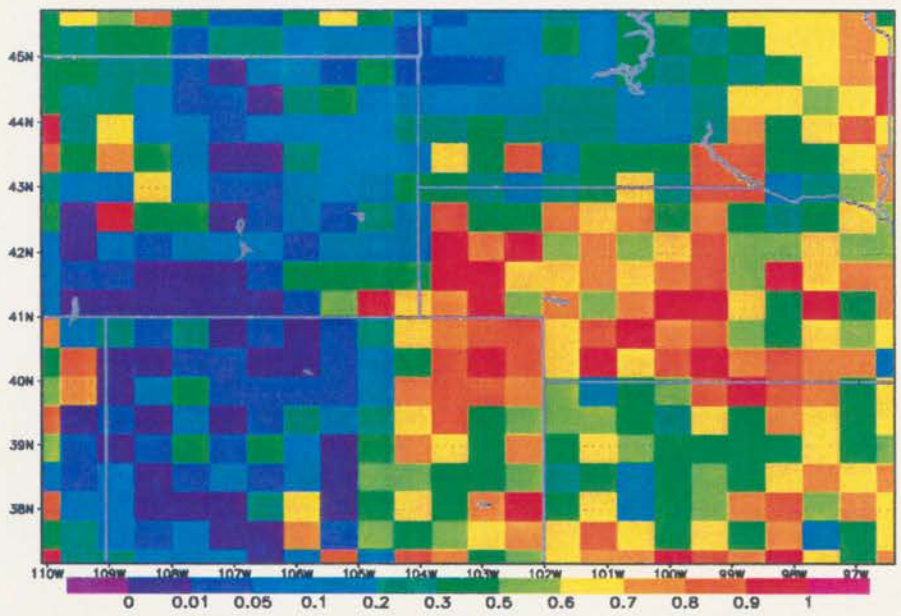

Figure 5.12: Horizontal fields of t test results for total accumulated precipitation between the $2\times CO_2$ biology and control simulations.

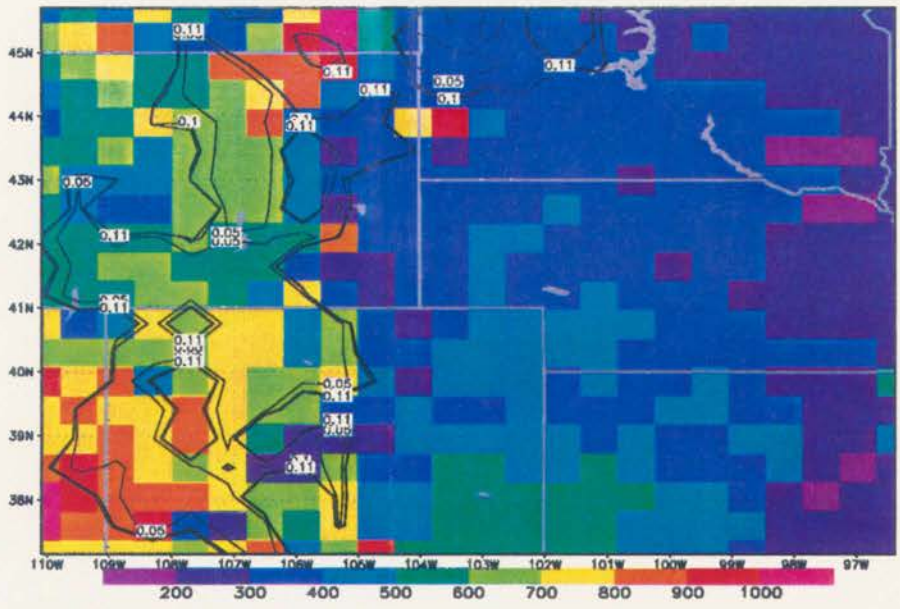

Figure 5.13: Horizontal seasonally-averaged fields of the product of maximum daily temperature and daily transpiration rates for the $2\times CO_2$ biology simulation. T test results are plotted at 0.05, 0.1, and 0.11 values.

horizontally the effect of landuse change. The $2\times CO_2$ biology experiment also indicated significant differences for meteorology, and in the case of the biota, the effect was nearly domain wide. Finally, the $2\times CO_2$ radiation contribution was much smaller than the previous two factors. In the next chapter, the interaction of these various factors will be examined.

Chapter 6

ANALYSIS OF FACTORS AND THEIR INTERACTIONS

It is difficult to describe just exactly what kind of physical process is occurring in the interactions. The factors are much simpler to explain. How does $2\times CO_2$ radiation and biology interact? We cannot really explain this explicitly. This is inherent due to the nonlinearity of nature itself. For instance, take the most extreme perturbation applied in this study; a difference for maximum daily temperature between the control simulation and one including natural vegetation, $2\times CO_2$ radiation, and $2\times CO_2$ biology. What does this represent? Clearly this represents the contribution to maximum daily temperature due to forcing by natural vegetation, $2\times CO_2$ radiation, and $2\times CO_2$ biology. However, for example, what is the role of the interaction between the vegetation and $2\times CO_2$ biology? The perturbation experiment actually represents a combination of the forcing due to:

- natural vegetation,
- $2\times CO_2$ radiation,
- $2\times CO_2$ biology,
- double interaction of natural vegetation and $2\times CO_2$ radiation,
- double interaction of natural vegetation and $2\times CO_2$ biology,
- double interaction of $2\times CO_2$ biology and $2\times CO_2$ radiation,
- triple interaction of natural vegetation, $2\times CO_2$ radiation, and $2\times CO_2$ biology.

Indeed, after applying Stein and Alpert's technique, the same difference field can be constructed by adding each of these components together as would be obtained by subtracting the simulations themselves. Through the separation process considerable knowledge is gained however.

In more qualitative terms, Stein and Alpert cite a work by Uccellini et al. (1987), in which the authors suggest that "the rapid development phase of extratropical cyclones is dependent not on the processes, but on a synergistic interaction among them." If this was not important, we could successfully model numerous processes with simple linear relations and curve fitting. The best that can be done at the present is to quantify the contribution through a series of statistical tests and plots.

This section of the analysis will show the significance and magnitudes of the interaction of factors. Significance in this case must be done with Z tests, since there is really no distribution to compare the separated interactions. That is, the mean of the interaction significantly different from zero. The relative contribution of each interaction is compared to the control field. Contributions among interactions will also be completed to place the magnitudes in relative importance.

As in the last section, the focus will be on the 2D surface variables. This will include the daily and hourly variables. The contributions to the variables will be shown for a time series of domain averages and spatial time averages to investigate large- and finer-scale contributions. The main impetus for this section was outlined in the second set of hypotheses in Chapter 3. These include:

- Significant differences in the domain-averaged prognosed meteorological fields, biophysical, and biogeochemical processes will be observable due to the nonlinear interactions between:
  - landcover and doubled CO_2, and
  - radiative forcing at $2\times CO_2$ and landcover.
- Grid-scale differences will be significant.

6.1 Domain-Averaged Contributions and Significance

6.1.1 Statistical Results

The Z test for significantly different means will be applied to the variables listed in Table 5.1. The test is designed to reject the null hypothesis, H_0. In this case H_0 is that

the means computed for each variable are equal to zero. When this test is done, it is also suggested that power, β, be computed to access the chance of accepting H_0 when it is actually false and the alternate hypothesis, H_a, is true. This is called a Type II error and its probability is β. Similarly, a Type I error is committed if we reject the H_0 when it is actually true. The probability of a type one error is denoted as α, and represents an acceptable rate of Type I error. As before, $\alpha = 0.05$ is chosen. Since this is a two-tailed test with $\alpha = 0.05$, the value of $z_{\frac{\alpha}{2}}$ is 1.96. There might be questions of the validity of using a Z test since this test assumes the distribution is normal. However, at large n this assumption is not as critical. In addition, for the domain averages, as samples of means are collected from a distribution of varying degrees of skewness or kurtosis, the distribution of the means themselves becomes Gaussian (Ott 1993).

The test results for each factor and factor interaction, reported as probabilities, are shown in Tables 6.1 through 6.7. In addition, the Tables indicate the percent of grid cells significantly different from zero, mean, standard deviation, and percent contribution relative to the control run mean. The percent contribution relative to the control run mean was included since a significant difference from zero would not be that surprising. This is also the reasoning behind inclusion of the individual factor results, even though they were extensively analyzed in the last chapter. In addition, this test has not been applied to the individual factors. Finally, it should be mentioned that the power, β, of the majority of the tests was so large that it is not reported in these results. It was over 95% in nearly all significant results.

Table 6.1 exhibits near unanimous rejections of the null hypothesis. The exception is the minimum daily temperature. Also of note is the high percentage of individual gridpoints with the same result. As mentioned, this is not surprising since the null is $H_0 = 0$. The main impetus of this, and subsequent tables, is to demonstrate that the separated signals are not noise. The ratio of mean factor contribution to control mean is the most pertinent result. The table indicates that there is a 5% decrease in the maximum daily temperature. This was also seen in the last section. The total daily accumulated precipitation and transpiration also show at least single digits for percent contribution.

Variable Symbol	Probability	% cells significantly different	mean	σ	100% x ratio of factor and control means
TMAX	0.000E+00	0.894E+02	-0.119E+01	0.564E+00	-5.150
TMIN	0.168E+00	0.738E+02	-0.167E-01	0.174E+00	-0.055
ACC	0.920E-30	0.971E+02	-0.284E+01	0.301E+01	-2.039
PPT	0.227E-12	0.471E+02	-0.348E-01	0.641E-01	-0.025
FLAI	0.000E+00	0.977E+02	0.198E+00	0.887E-01	0.139
DLAI	0.653E-29	0.688E+02	0.122E-02	0.132E-02	0.001
WL	0.000E+00	0.971E+02	0.248E-01	0.987E-02	0.017
WSD	0.000E+00	0.931E+02	0.177E-01	0.368E-02	0.012
WR	0.000E+00	0.975E+02	0.571E-01	0.405E-02	0.040
TRAN	0.000E+00	0.685E+02	0.220E+01	0.974E+00	1.331
SUMAS	0.000E+00	0.981E+02	0.339E-01	0.231E-01	0.020

Table 6.1: Z test probabilities for rejecting the null hypothesis, H_0, percentage of cells rejecting H_0, mean, variance, and percent contribution relative to the control run for domain averages due to natural vegetation.

Tables 6.2 and 6.3 represent the analysis of the other factor contributions. As in the natural vegetation case, they both show rejections of the null for domain averages and individual cells for all variables. The results also show that only the $2\times CO_2$ biological simulation exhibits percent contributions in the single digits, for maximum daily temperature and accumulated precipitation.

Examining the remaining tables for factor interactions, similar results for the rejection of the null is prevalent throughout. This includes domain averages and individual grid cell results. The null for daily precipitation is not rejected in any of the interaction analysis, yet is rejected for the factor contributions. We can also see that the triple interaction results have the highest failure to reject numbers, including transpiration, daily precipitation, minimum daily temperature, shoot biomass, LAI, and total accumulated carbon. This is followed by the interaction of $2\times CO_2$ radiation and biology, followed by a tie between the other two factors. There is a clear drop-off in the percent contribution due to a given interaction. The highest value for any interaction, in this case natural vegetation and $2\times CO_2$ biology, is 0.304%, followed by the same interactions contribution to minimum daily temperature. It is difficult to quantify just exactly what kind of physical process is occurring in the interactions. How do $2\times CO_2$ radiation and biology interact?

Variable Symbol	Probability	% cells significantly different	mean	σ	100% x ratio of factor and control means
TMAX	0.352E-10	0.802E+02	0.141E-01	0.292E-01	0.061
TMIN	0.000E+00	0.931E+02	0.972E-01	0.349E-01	0.319
ACC	0.000E+00	0.967E+02	0.956E+00	0.539E+00	0.687
PPT	0.690E-25	0.158E+02	0.783E-02	0.936E-02	0.006
FLAI	0.452E-02	0.971E+02	0.969E-03	0.488E-02	0.001
DLAI	0.467E-07	0.494E+02	0.558E-04	0.142E-03	0.000
WL	0.169E-02	0.971E+02	0.790E-04	0.359E-03	0.000
WSD	0.861E-41	0.979E+02	0.196E-03	0.165E-03	0.000
WR	0.000E+00	0.971E+02	0.365E-03	0.223E-03	0.000
TRAN	0.000E+00	0.502E+02	0.868E-01	0.639E-01	0.052
SUMAS	0.189E-15	0.971E+02	0.495E-03	0.799E-03	0.000

Table 6.2: Z test probabilities for rejecting the null hypothesis, H_0, percentage of cells rejecting H_0, mean, variance, and percent contribution relative to the control run for domain averages due to $2\times CO_2$ radiation.

Variable Symbol	Probability	% cells significantly different	mean	σ	100% x ratio of factor and control means
TMAX	0.000E−00	0.933E+02	-0.747E+00	0.502E+00	-3.227
TMIN	0.000E−00	0.688E+02	0.261E+00	0.143E+00	0.856
ACC	0.316E-41	0.985E+02	-0.434E+01	0.362E+01	-3.115
PPT	0.726E-24	0.729E+02	-0.460E-01	0.565E-01	-0.033
FLAI	0.000E+00	0.100E+03	0.578E+00	0.274E+00	0.405
DLAI	0.277E-21	0.946E+02	0.328E-02	0.433E-02	0.002
WL	0.000E+00	0.100E+03	0.449E-01	0.222E-01	0.031
WSD	0.000E+00	0.998E+02	0.241E-01	0.122E-01	0.017
WR	0.000E+00	0.100E+03	0.134E-01	0.908E-02	0.009
TRAN	0.137E-28	0.821E+02	0.799E+00	0.870E+00	0.483
SUMAS	0.000E+00	0.100E+03	0.111E+00	0.672E-01	0.067

Table 6.3: Z test probabilities for rejecting the null hypothesis, H_0, percentage of cells rejecting H_0, mean, variance, and percent contribution relative to the control run for domain averages due to $2\times CO_2$ biology.

Based on the results of these tables, especially the small percent contributions, one might be tempted to dismiss the results as insignificant. In other words, none of the factors or interactions lead to interesting results. This would be a mistake obviously, since a single number based on domain average is misleading. We saw in the last chapter a complicated pattern when a spatial analysis was undertaken.

Variable Symbol	Probability	% cells significantly different	mean	σ	100% x ratio of factor and control means
TMAX	0.964E-19	0.733E+02	0.264E-01	0.379E-01	0.114
TMIN	0.821E-03	0.329E+02	-0.894E-02	0.381E-01	-0.029
ACC	0.000E+00	0.933E+02	-0.131E+00	0.380E-01	-0.094
PPT	0.357E+00	0.542E+01	-0.797E-03	0.125E-01	-0.001
FLAI	0.366E-29	0.956E+02	-0.706E-02	0.758E-02	-0.005
DLAI	0.576E-04	0.535E+02	-0.596E-04	0.210E-03	0.000
WL	0.237E-30	0.956E+02	-0.510E-03	0.532E-03	0.000
WSD	0.264E-38	0.952E+02	-0.362E-03	0.320E-03	0.000
WR	0.222E-11	0.944E+02	-0.552E-04	0.107E-03	0.000
TRAN	0.162E+00	0.340E+02	-0.853E-02	0.879E-01	-0.005
SUMAS	0.154E-25	0.960E+02	-0.895E-03	0.105E-02	-0.001

Table 6.4: Z test probabilities for rejecting the null hypothesis, H_0, percentage of cells rejecting H_0, mean, variance, and percent contribution relative to the control run for domain averages due to interaction of natural vegetation and $2\times CO_2$ radiation.

6.1.2 Temporal Results

Before examining spatial patterns of the various contributions, a temporal analysis is instructive. The last section demonstrated that the contributions are not merely noise, but are significant. It would also seem likely that a temporal signal would be present in some of the distributions. In all figures the scale will be kept the same so that the reader can see the relative contribution of each factor and factor interactions. The control simulation will also be shown to aid in gauging the magnitude of the contributions.

The first series of plots in Figure 6.1 display the control run domain-averaged daily maximum temperature and the contributions of the factors. The plot of the domain-averaged maximum daily temperature, (Figure 6.1a) exhibits a clear seasonal trend. The

Variable Symbol	Probability	% cells significantly different	mean	σ	100% x ratio of factor and control means
TMAX	0.391E-17	0.854E+02	0.703E-01	0.107E+00	0.304
TMIN	0.479E-25	0.531E+02	0.743E-01	0.884E-01	0.244
ACC	0.480E-25	0.963E+02	-0.463E-01	0.550E-01	-0.033
PPT	0.799E+00	0.123E+02	0.321E-03	0.183E-01	0.000
FLAI	0.000E+00	0.969E+02	0.559E-01	0.339E-01	0.039
DLAI	0.253E-04	0.654E+02	0.255E-03	0.855E-03	0.000
WL	0.000E+00	0.971E+02	0.602E-02	0.351E-02	0.004
WSD	0.000E+00	0.956E+02	0.151E-02	0.109E-02	0.001
WR	0.339E-17	0.960E+02	0.327E-03	0.495E-03	0.000
TRAN	0.196E-18	0.617E+02	-0.171E+00	0.248E+00	-0.103
SUMAS	0.000E+00	0.965E+02	0.768E-02	0.499E-02	0.005

Table 6.5: Z test probabilities for rejecting the null hypothesis, H_0, percentage of cells rejecting H_0, mean, variance, and percent contribution relative to the control run for domain averages due to interaction of natural vegetation and $2\times CO_2$ biology.

Variable Symbol	Probability	% cells significantly different	mean	σ	100% x ratio of factor and control means
TMAX	0.137E-11	0.738E+02	0.179E-01	0.342E-01	0.077
TMIN	0.126E+00	0.290E+02	-0.381E-02	0.359E-01	-0.013
ACC	0.000E+00	0.956E+02	0.107E+00	0.427E-01	0.077
PPT	0.311E+00	0.646E+01	0.772E-03	0.110E-01	0.001
FLAI	0.661E-11	0.948E+02	-0.299E-02	0.594E-02	-0.002
DLAI	0.246E-08	0.563E+02	-0.666E-04	0.155E-03	0.000
WL	0.253E-13	0.948E+02	-0.310E-03	0.547E-03	0.000
WSD	0.360E-13	0.954E+02	-0.165E-03	0.293E-03	0.000
WR	0.383E-40	0.958E+02	-0.172E-03	0.146E-03	0.000
TRAN	0.511E-05	0.371E+02	-0.224E-01	0.691E-01	-0.014
SUMAS	0.576E-17	0.960E+02	-0.792E-03	0.121E-02	0.000

Table 6.6: Z test probabilities for rejecting the null hypothesis, H_0, percentage of cells rejecting H_0, mean, variance, and percent contribution relative to the control run for domain averages due to interaction of $2\times CO_2$ radiation and biology.

Variable Symbol	Probability	%cells significantly different	mean	σ	100% x ratio of factor and control means
TMAX	0.128E-02	0.771E+02	-0.989E-02	0.438E-01	-0.043
TMIN	0.816E+00	0.310E+02	0.740E-03	0.460E-01	0.002
ACC	0.000E+00	0.948E+02	-0.248E+00	0.120E+00	-0.178
PPT	0.169E+00	0.583E+01	-0.150E-02	0.157E-01	-0.001
FLAI	0.341E-01	0.963E+02	-0.955E-03	0.647E-02	-0.001
DLAI	0.513E-07	0.602E+02	-0.113E-03	0.288E-03	0.000
WL	0.134E-02	0.958E+02	0.113E-03	0.504E-03	0.000
WSD	0.170E-28	0.963E+02	0.206E-03	0.225E-03	0.000
WR	0.265E-02	0.958E+02	-0.373E-04	0.177E-03	0.000
TRAN	0.760E+00	0.448E+02	-0.264E-02	0.125E+00	-0.002
SUMAS	0.416E-01	0.965E+02	0.106E-03	0.746E-03	0.000

Table 6.7: Z test probabilities for rejecting the null hypothesis, H_0, percentage of cells rejecting H_0, mean, variance, and percent contribution relative to the control run for domain averages due to interaction of all factors.

maximum occurs around early-July and the minimum at the beginning of the simulation. The synoptic component is evident in the spring and fall, as weekly fluctuations of $5-10°C$ are apparent. Notice the signal is fairly steady throughout August.

Figure 6.1b exhibits the seasonal synoptic fluctuations evident in Figure 6.1a. The contribution of natural vegetation indicates a steady decline from the beginning of the simulation until early July, where it begins to level off at $-1.6°$. This is also the same time period where steady growth in the biomass takes place. From July through early September the signal is fairly consistent. At this point, the current simulation begins to undergo the harvesting schedule for the crops, while the natural vegetation is not subjected to this human impact. After a brief rise due to a synoptic event, the natural vegetation shows an even stronger cooling in maximum daily temperature through the end of September, bottoming out at $-2.1°C$. At this point the death and senescence of the natural vegetation likely leads to LAI values approaching the control simulation, and the signal shows a rise to the end of the simulation to around $-1°C$. Still, at this point, the short and tall grasses still have considerable ground cover in the form of senescent grass, while the current vegetation would be replaced by fairly barren fields.

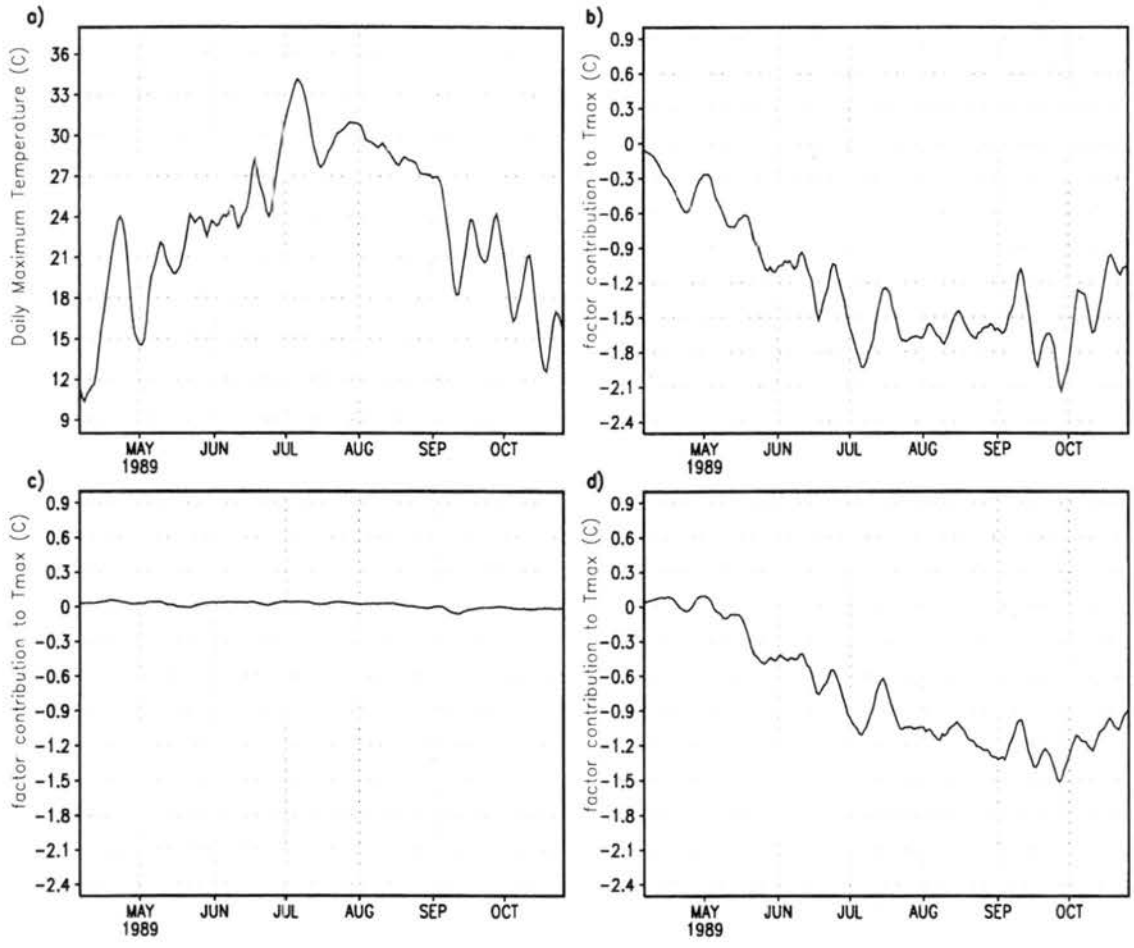

Figure 6.1: a) Domain-averaged maximum daily temperature. Contribution to domain-averaged maximum daily temperature due to: b) natural vegetation, c) $2\times CO_2$ radiation, and d) $2\times CO_2$ biology.

The $2\times CO_2$ radiation component is displayed in Figure 6.1c. There is a relatively consistent contribution of 0.1°C until the harvest period, of early to late September. There are still fluctuations associated with synoptic-scale patterns, however the signal is smaller than that of the natural vegetation and they are not as apparent. During the harvest period the sign of the signal switches and finally levels off at less than −0.05°C.

The last factor contribution, $2\times CO_2$ biology, is shown in Figure 6.1d. This figure exhibits many similarities to the natural vegetation component in that there is a steady increase in the magnitude of the forcing. In this case, the increase appears to last until early September, where it reaches the local maximum magnitude of −1.3°C. At this time the effect of the crop scheduling is not clear, although it appears that a leveling in the signal has occurred. There appears to be an upward trend from the end of September until the end of the simulation for reasons not clearly understood. One explanation would be that the added leaf coverage, which is still present in the $2\times CO_2$ biology in areas not affected by the harvest, would proportionally effect the cooling, while the harvest areas would exhibit maximum daily temperature quite close to one another for the two simulations. Other considerations would be the onset of higher death rates and maintenance coefficients.

The interaction contributions are displayed in Figure 6.2a-d, and represent the input due to the interaction of natural vegetation and $2\times CO_2$ radiation, natural vegetation and $2\times CO_2$ biology, $2\times CO_2$ radiation and $2\times CO_2$ biology, and all three, respectively. As expected from the domain- and seasonally-averaged analysis of the last section, the magnitudes of these are considerably smaller than the natural vegetation and $2\times CO_2$ biology effects. Still visible in all plots are harvest effects. The strongest signal, shown in Figure 6.2b, is present in the interaction of natural vegetation and $2\times CO_2$ biology, varying between −0.2°C and 0.3°C. This should come as no surprise, since the enhanced growth due to the doubling of CO_2 was readily apparent in the $2\times CO_2$ biology simulation. One must also keep in mind what this field really represents. This field is created by the natural vegetation with $2\times CO_2$ biology interaction minus the sum of the separate effects of the natural vegetation and $2\times CO_2$ biology simulations, plus the control simulation (see Table 3.2). This represents their interaction. The high prevalence of C_4 tall grass in the

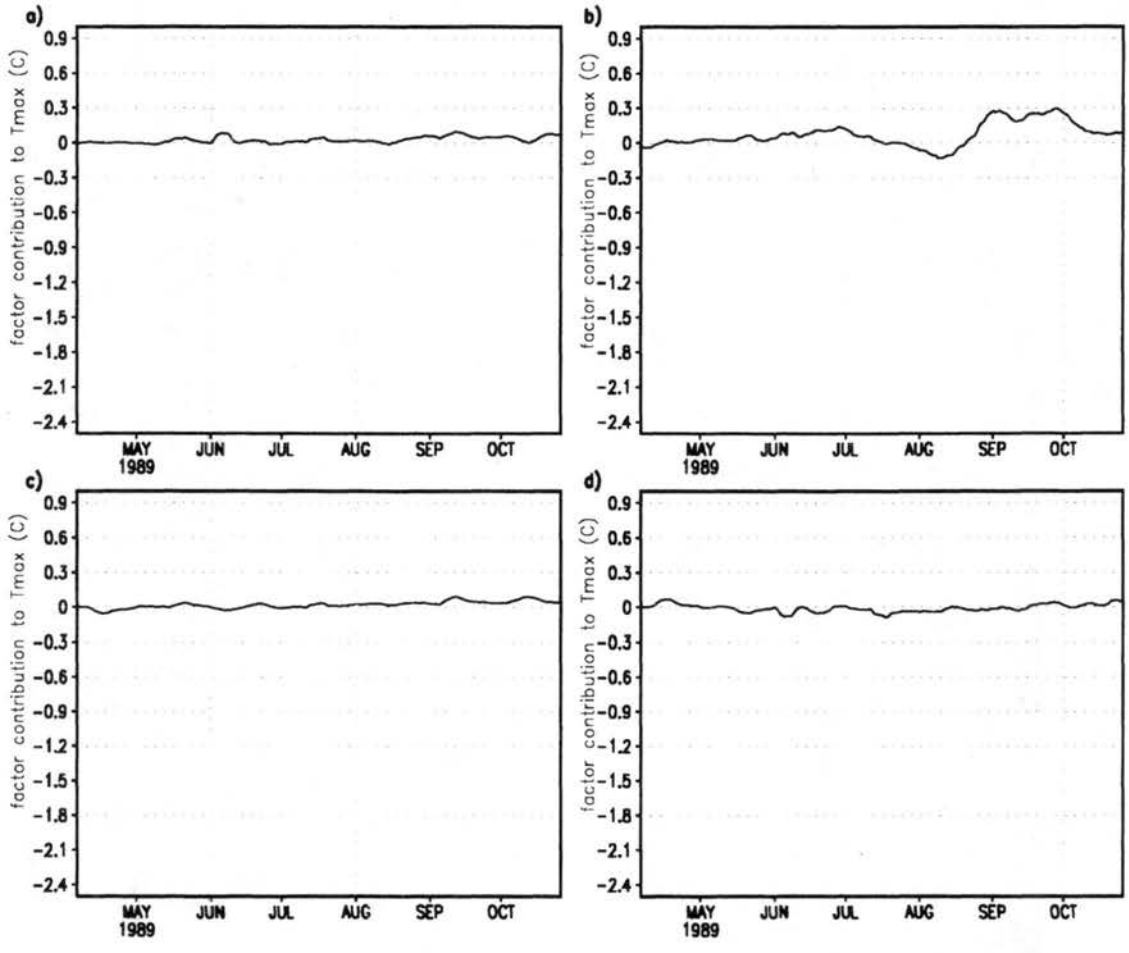

Figure 6.2: Contribution to domain-averaged maximum daily temperature due to a) interaction of natural vegetation and $2\times CO_2$ radiation, b) interaction of natural vegetation and $2\times CO_2$ biology, c) interaction of $2\times CO_2$ radiation and $2\times CO_2$ biology, and d)interaction of natural vegetation, $2\times CO_2$radiation, and $2\times CO_2$ biology.

natural landscape must also be taken into account. Since photosynthesis is driven to a large degree by the CO_2 gradient, the response of the C_3 plants would likely be larger than the C_4 plants, which are considered to be CO_2 saturated at present levels. There is also a clear sign reversal from the beginning of July through mid-August. This could be caused by a relatively dry period observed in 1989 for the eastern half of the domain. Since the C_4 plants generally have a higher water use efficiency, the effect on accumulated biomass would be smaller than in the C_3 crop species present in the current landscape. This would then lead to a lower impact on LAI, subsequently, a lower temperature perturbation. A comparison of tall and short grass responses in the natural vegetation simulations under different CO_2 levels should elucidate further on this. A difference or ratio between the natural simulations run under different CO_2 levels would represent the $2\times CO_2$ biology contribution relative change to the natural landscape. Figure 6.3 compares the ratio of LAI under $2\times CO_2$ to $1\times CO_2$. The green line corresponds to the ratio for short grass (C_3), while the black line is for tall grass (C_4). The curves were from simulations using the natural landscape as the vegetative boundary condition. This figure indicates that

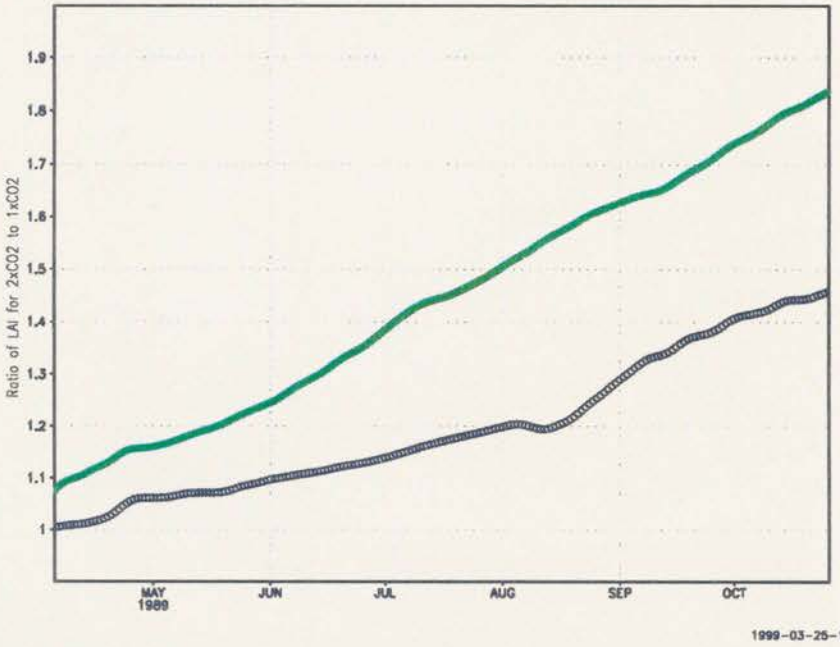

Figure 6.3: The ratio of LAI for tall grass (black line) and short grass (green line) for $2\times CO_2$ to $1\times CO_2$ biology conditions. The data is extracted from the natural vegetation simulations.

the there are considerably different responses by the two vegetation types. For instance,

on 1 August 1989 of the simulation, the short grass exhibits a 50% increase in LAI in the $2\times CO_2$ biology simulation. At the same date, the tall grass indicates a 20% increase in LAI. There are also indications of short-term temporal responses by both vegetation types. It is another example of the model behaving in a nonlinear fashion. Contributing variables could be precipitation, soil water content, temperature, and an integrated effect of the CO_2. Whether these responses continue and their differing slopes continue on a yearly basis remains to be investigated.

The next series of plots are for the daily minimum temperature and are displayed in Figure 6.4 for the control simulation and individual factor contributions. Unlike the maximum daily temperature, which is largely affected by the solar insolation, this field evolves in response to the longwave radiative flux and surface dewpoint temperature. The computation of the longwave radiation takes into account the water and CO_2 content in the atmosphere as well as the different emissivities of the vegetation and soil surface. In addition, there is a dependence on the vegetation and ground temperature raised to the fourth power. Naturally the coverage of the foliage will enter into this computation, and will subsequently affect the computed minimum daily temperatures. The emissivities of the various vegetation classes are also accounted for in the computation. For example, the emissivities of the crops in this model are set to 0.95, while the grasses have values of 0.96. In addition, the temperature of the soil will be affected by soil water content. It is expected the results for the minimum daily temperature contributions will be somewhat harder to interpret than the maximum daily temperature, due to these varying effects.

Figure 6.4a shows the expected seasonal pattern for minimum daily temperature. The minimum occurs early in the simulation, with two localized maximums in early July and August. Unlike the maximum daily temperature, this field does not exhibit a period of relatively constant values. Overall, the field possesses more variability than the maximum daily temperature plots.

Figure 6.4b displays the natural vegetation contribution to the minimum daily temperature field. Compared to Figure 6.1b, the signal contains significantly more short-term fluctuations. This could be anticipated from the results of the previous section, where

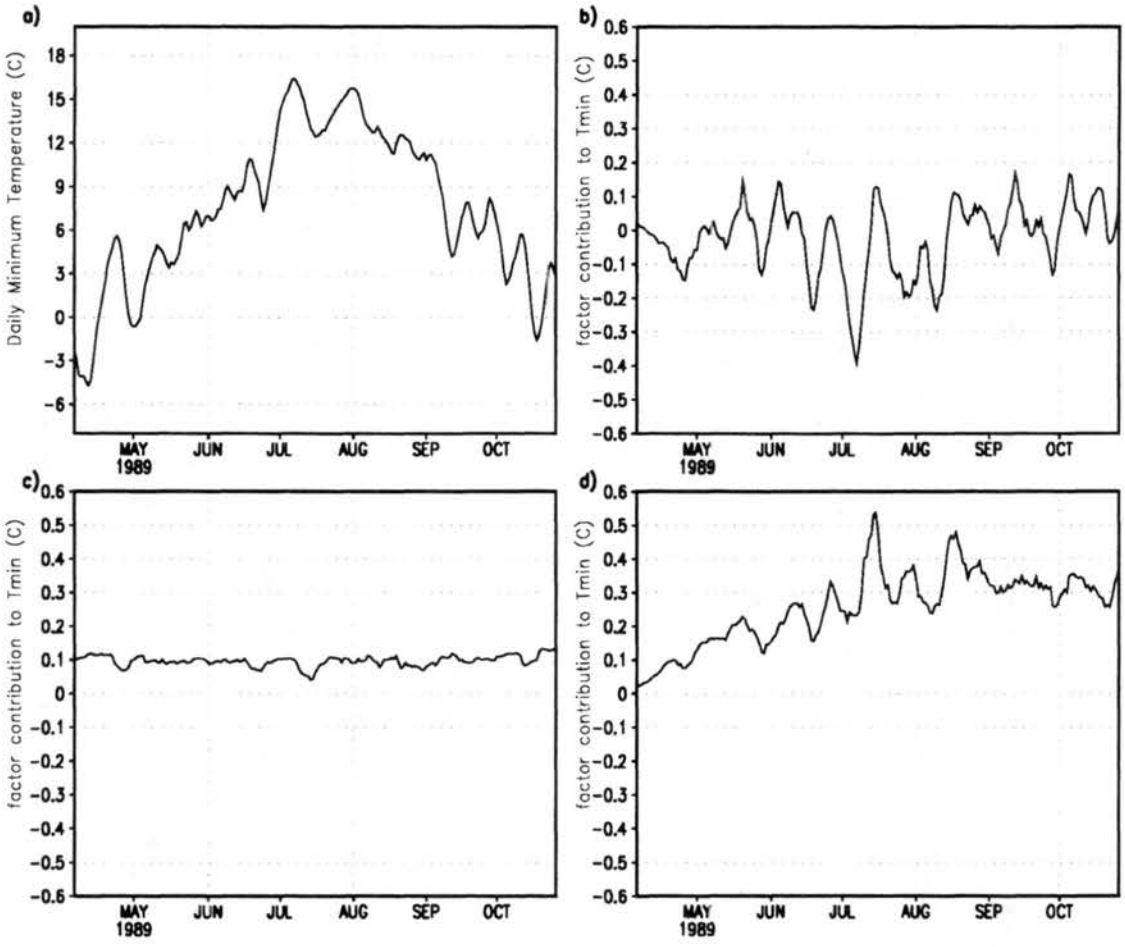

Figure 6.4: a) Domain-averaged minimum daily temperature. Contribution to domain-averaged maximum daily temperature due to b) natural vegetation, c) $2\times CO_2$ radiation, and d) $2\times CO_2$ biology.

the ratio of the mean to the standard deviation is considerably smaller than that for the maximum daily temperature fields. Those results also indicated that the mean was not significantly different than zero and the percent contribution was 0.05%. When a longer averaging period is applied to the data (not shown) a weak seasonal pattern begins to emerge with a minimum in late July of roughly 0.1°C. This is somewhat surprising since the ground coverage by vegetation in the natural simulation was demonstrated to be slightly larger in the natural vegetation case. This is likely due to the higher emissivities in the natural vegetation case.

The $2\times CO_2$ radiation contribution is shown in Figure 6.4c. Fluctuations are evident during strong cooling events, when it is likely that synoptic forcing would dominate the minimum daily temperature. The figure also indicates that the signal is fairly consistent throughout the simulation, with values showing a warming of 0.1°C. This would be expected since the free atmosphere longwave CO_2 was held constant throughout the simulation, hence the lack of a seasonal component.

Figure 6.4d shows the effect of $2\times CO_2$ biology on the minimum daily temperature. This factor also exhibits large temporal fluctuations throughout the season, as was seen in the natural vegetation case. The contribution shows a general trend towards increasing the minimum daily temperature until early September, where it appears to level off at a value of 0.3°C. As in the case of the maximum daily temperature, this is likely due to the harvesting of crops. It is interesting that this contribution appears to be anti-correlated to the strong synoptic cooling events evident in the $2\times CO_2$ radiation field.

We now turn our attention to the factor interactions displayed in Figure 6.5a-d. The upper left panel shows the contribution due to the interaction of natural vegetation and $2\times CO_2$ radiation. This figure shows little contribution due to the interaction. The largest signal appears to be present in the last two months of the simulation, again temporally collocated with the harvest and enhanced fall death periods. Again, this simulation is not subjected to the former.

For the interaction of natural vegetation and $2\times CO_2$ biology, Figure 6.5b shows the largest contribution compared to the other interactions. The peak effect occurs just before

the onset of the harvest and attains a value of nearly 0.2°C. This figure demonstrates little correlation to large-scale synoptic forcing. Overall, this interaction contributes to an increase in the minimum daily temperature, similar to the case of $2\times CO_2$ biology.

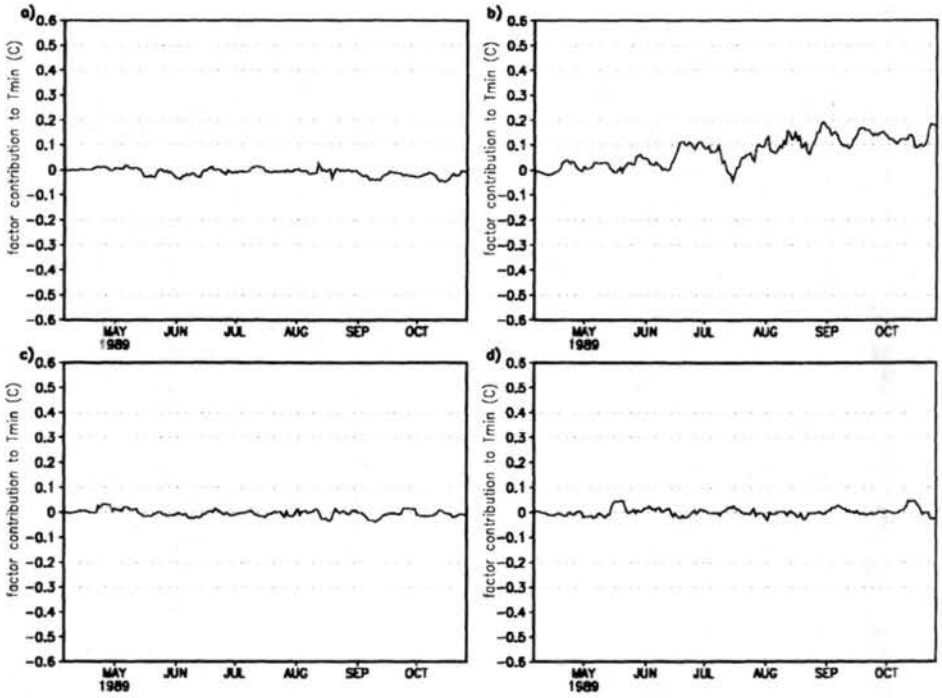

Figure 6.5: Contribution to domain-averaged minimum daily temperature due to a) interaction of natural vegetation and $2\times CO_2$radiation, b) interaction of natural vegetation and $2\times CO_2$ biology, c) interaction of $2\times CO_2$ radiation and $2\times CO_2$ biology, and d)interaction of natural vegetation, $2\times CO_2$ radiation, and $2\times CO_2$ biology.

The last two interaction plots, shown in Figures 6.5c-d exhibit relatively minor contributions to the minimum daily temperature field. Both fluctuate between a positive and negative contribution of less than 0.05°C. This affirms up the results seen in the temporally and domain-averaged analysis presented in the last section, suggesting that it is a very small signal.

The contributions to the biota are examined in the next series of plots. Figure 6.6 shows the control run LAI and individual factor contributions to LAI. The domain-averaged LAI exhibits a rapid spring growth phase, followed by slow steady growth for June and July. Starting in the middle of August, harvesting, senescence, and death begin to dominate. The contribution of natural vegetation, displayed in Figure 6.6b, is fairly

constant from April through September, at which point a decline begins. The enhanced LAI is a likely contributor to the lower maximum daily temperatures. The cooler nighttime temperatures could be due to the different emissivities of the natural vegetation, which are slightly higher.

Figure 6.6c-d show the contribution due to $2\times CO_2$ radiation and $2\times CO_2$ biology, respectively. The $2\times CO_2$ radiation shows a minimal contribution. It appears that there is a seasonal signal, where the contributions are slightly higher during the spring and fall time periods. The $2\times CO_2$ biology exhibits the stronger contribution. At the time it peaks in early September, the contribution is nearly a third of the domain-averaged LAI. It is interesting that the peak is so late in the year. It is likely that soil water status could have been enhanced due to the larger coverage in the $2\times CO_2$ biology simulation. This would allow a longer growth period for the plants. This curve suggests that there is a direct effect on the maximum daily temperature, which was shown to decrease in magnitude after the middle of September.

The next series of plots, Figures 6.7c-d, show the interaction contributions. As with other variables previously analyzed, the effect of the various factors are quite small relative to the $2\times CO_2$ biology effect. In the case of the interaction of natural vegetation and $2\times CO_2$ biology, the figures imply a contribution about a third as large as natural vegetation alone. The effect peaks in mid August, unlike the natural vegetation contribution which peaked in early October. Taken all together, Figures 6.6a-d and 6.7a-d present a contrasting picture of temporal scales. The major effects, and the control simulation itself, all have different seasonal evolutions.

The final set of figures are for the domain-averaged daily transpiration shown in Figures 6.8a-d and 6.11a-d. In Figure 6.8a, the seasonal transpiration signal is exhibited for the control simulation. Superimposed on this is a considerable amount of short-term variability. Notice that the peak is considerably offset from the LAI peak. This is likely due to the onset of water stress related to the seasonal drying of the soil and warm months of July and August when stoma shutdown to a large degree.

The natural contribution is displayed in Figure 6.8b. The figure shows another temporal shift in the maximum relative to the control simulation, which is nearly collocated

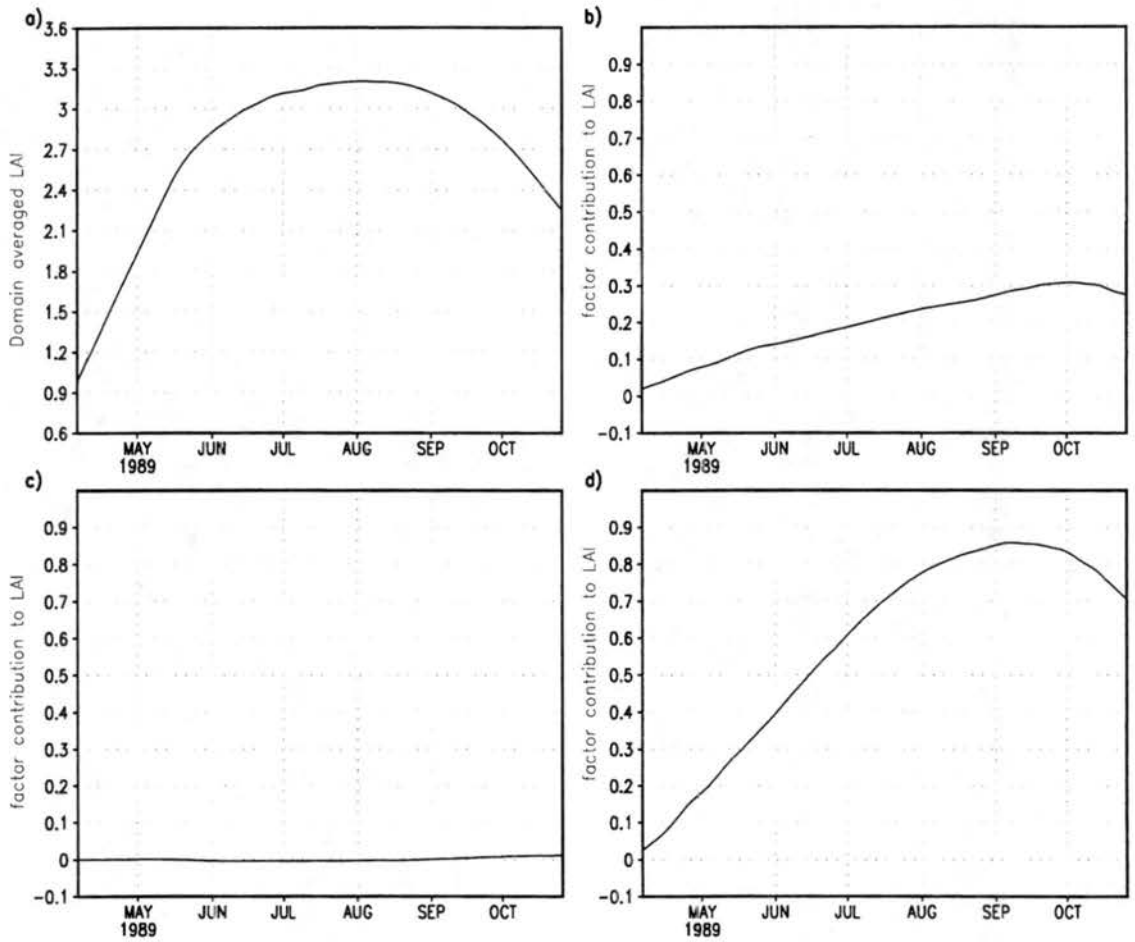

Figure 6.6: a) Domain-averaged LAI. Contribution to domain-averaged LAI due to b) natural vegetation, c) $2\times CO_2$ radiation, and d) $2\times CO_2$ biology.

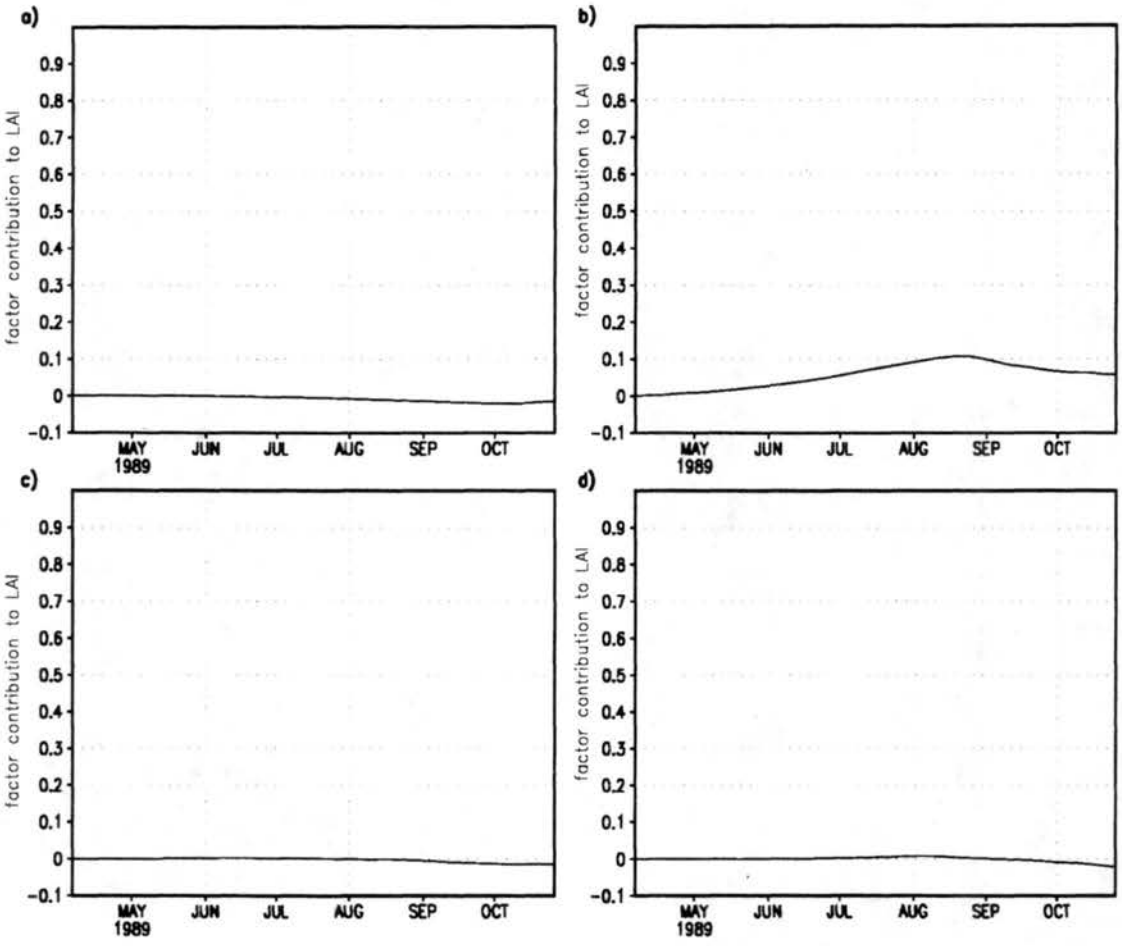

Figure 6.7: Contribution to domain-averaged LAI due to a) interaction of natural vegetation and $2\times CO_2$radiation, b) interaction of natural vegetation and $2\times CO_2$ biology, c) interaction of $2\times CO_2$radiation and $2\times CO_2$ biology, and d)interaction of natural vegetation, $2\times CO_2$ radiation, and $2\times CO_2$ biology.

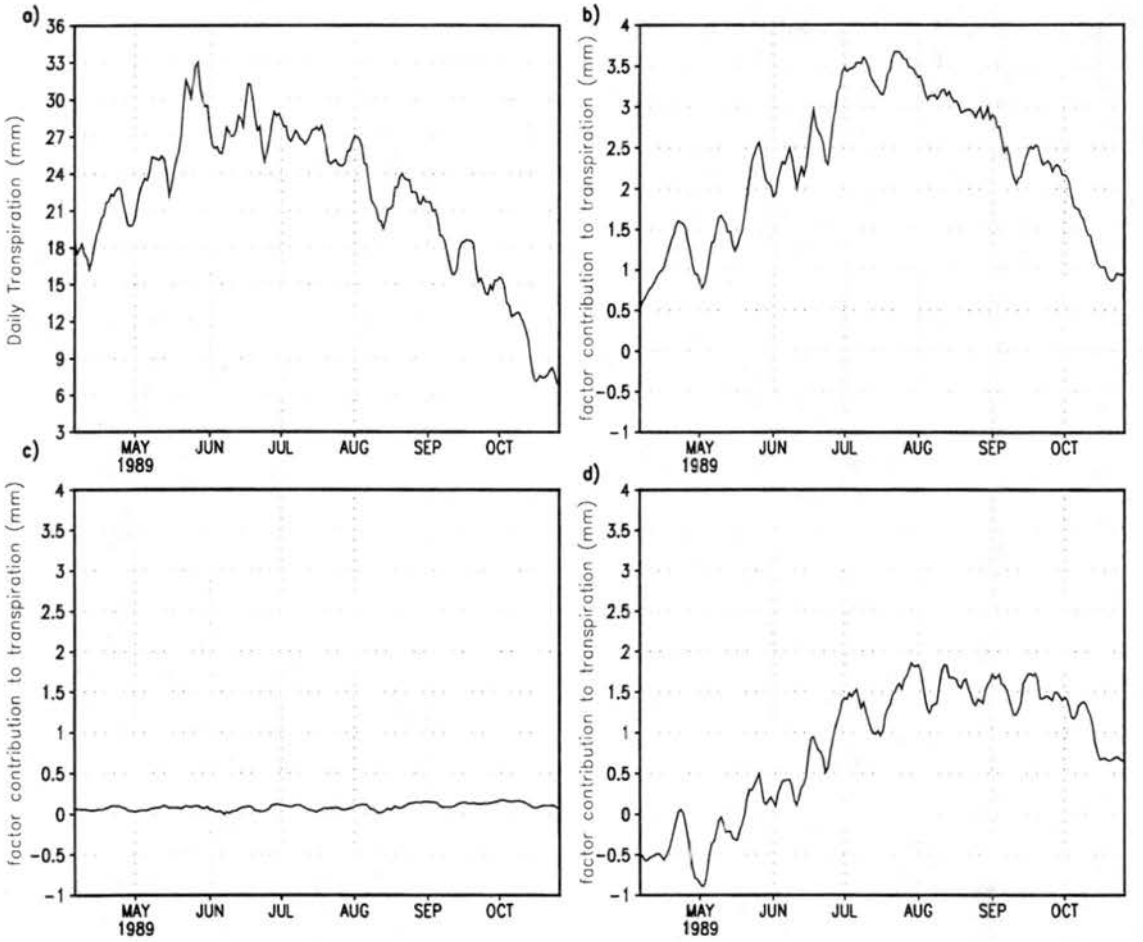

Figure 6.8: a) Contribution to the domain-averaged transpiration for a) the control simulation, and due to b) natural vegetation, c) $2\times CO_2$ radiation, and d) $2\times CO_2$ biology.

with the peak in LAI. The magnitudes of this contribution are the largest of any factor and represent nearly 10% of the control simulation values. The enhanced transpiration is a likely contributor to the lower maximum daily temperatures and higher minimum daily temperatures.

Figure 6.8c corresponds to the domain-averaged daily transpiration for $2\times CO_2$ radiation. The $2\times CO_2$ radiation contribution suggests a nearly uniform enhancement to transpiration for the duration of the simulation. This is related to the larger values of stomatal conductance, which were detailed in Tables 5.10 through 5.13 in Chapter 5. Overall, the effect is quite small.

The $2\times CO_2$ biology contribution to domain-averaged daily transpiration is detailed in Figure 6.8d. Again, there is evidence of a seasonal cycle in this field, with the temporal shift to the latter few months of the simulation. The magnitude of the contribution is about half that of the natural simulation. One might expect that the significant increase in LAI would lead to larger values than those observed for the natural vegetation contribution. However, the higher CO_2 levels also lead to lower stomatal conductance which in turn leads to lower transpiration rates for a given biome type. This appears to more than compensate for the biomass increase. This is demonstrated in Figures 6.9 and 6.10, which show the ratio of the $2\times CO_2$ biology to natural vegetation LAI and transpiration, respectively. This is shown for the short grass (green curve) and tall grass (black curve) classes.

The LAI comparison shows a smaller response in the $2\times CO_2$ biology current vegetation case compared to the $2\times CO_2$ biology natural vegetation case for the short grass for the same gridpoints. There are relatively few points in this analysis, since the shortgrass has been replaced by various crops in the current landscape. The same could be said of tall grass. The response of the tall grass is quite similar to that observed when comparing natural vegetation simulations only. This is likely related to the lower sensitivity of the tall grass to doubled CO_2 levels.

The plots for transpiration, Figure 6.10, reveal why there are temporal differences between the natural and $2\times CO_2$ biology plots. Notice, the short grass curve is initially displaying less transpiration over the short grass for the $2\times CO_2$ biology contribution. Even

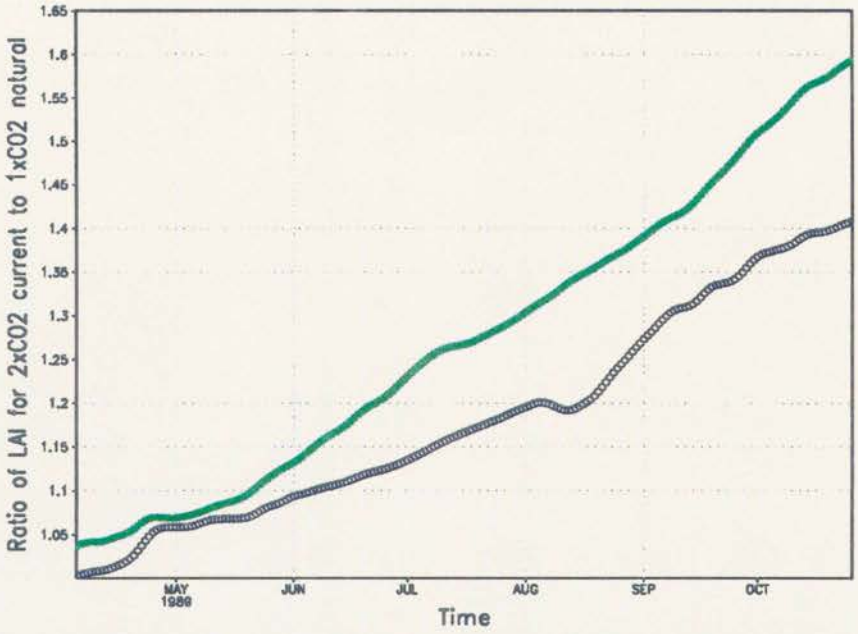

Figure 6.9: The ratio of LAI for tall grass (black line) and short grass (green line) for $2\times CO_2$ biology in the natural vegetation simulation. The data is extracted from points in the natural vegetation corresponding to the same biome type in the current vegetation distribution.

more pronounced is the smaller magnitudes over the tall grass. The $2\times CO_2$ biology contribution is less until early September in this case. Adding these two classes together gives a similar pattern to that observed for the pure $2\times CO_2$ biology contribution. As suggested earlier, the lower stomatal conductance under $2\times CO_2$ biology offsets the transpiration enhancement due to increased LAI.

Finally, the interaction contributions are shown in Figure 6.11a-d. All but the interaction of natural vegetation and $2\times CO_2$ biology are extremely small and hard to discern any seasonal trend. The natural vegetation and $2\times CO_2$ biology interaction leads to a decrease in transpiration. Again, despite increased biomass amounts under $2\times CO_2$ biology the size of the stomatal aperture appears to dominate. Relative to the individual factor contributions of $2\times CO_2$ biology and natural vegetation this interaction effect is still quite small on the domain-averaged scale.

Up to this point it has been demonstrated that the individual and interactive effects of natural vegetation, $2\times CO_2$radiation, and $2\times CO_2$ biology are significantly different than zero on the domain-averaged scale. The analysis has also shown that the pure factor con-

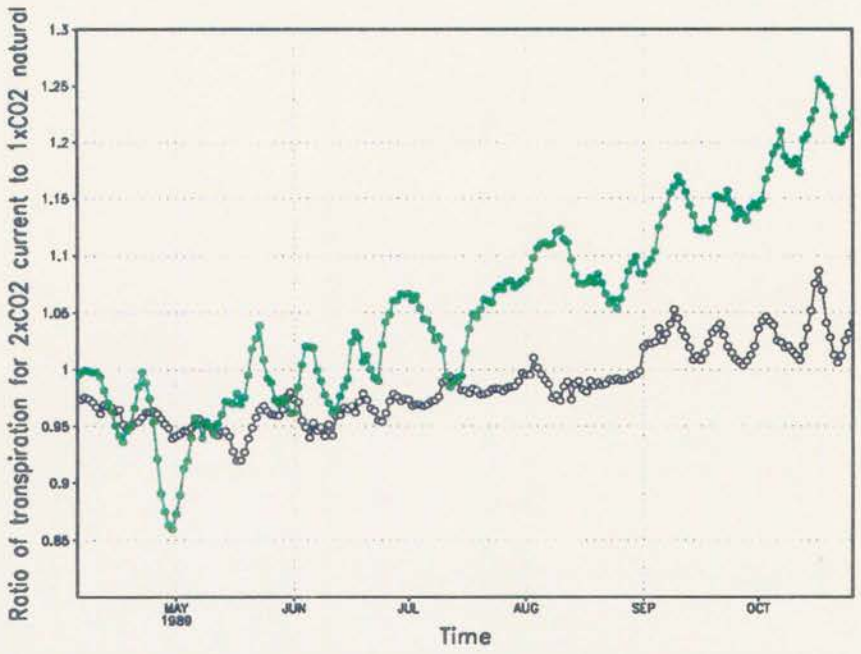

Figure 6.10: The ratio of transpiration for tall grass (black line) and short grass (green line) for $2\times CO_2$ biology in the natural vegetation simulation. The data is extracted from points in the natural vegetation corresponding to the same biome type in the current vegetation distribution.

tributions of natural vegetation and $2\times CO_2$ biology exhibit the strongest contributions on this same scale. In terms of the factor interactions, it has been seen that the natural vegetation and $2\times CO_2$ biology combine to produce the most significant contributions relative to the other interactions. Indeed, in many cases it was found to have a larger magnitude than the factor $2\times CO_2$ radiation. Finally, the different factors and their combinations have exhibited contrasting temporal signals. Possible explanations have been provided for most of these. All of this was done on a domain-averaged scale, which leads us into an exploration of spatial patterns. It is expected that even the factor interactions themselves can have large impacts on smaller spatial scales.

6.1.3 Spatial Analysis of Temporally-Averaged Factor Contributions

In the last section, results on a domain-averaged scale were shown. Although the results were quite interesting, they only tell part of the story. The use of domain averages washes out any spatially explicit differences which would be expected for the various factors and their interactions. Chapter 5 showed spatially explicit tests on the significance

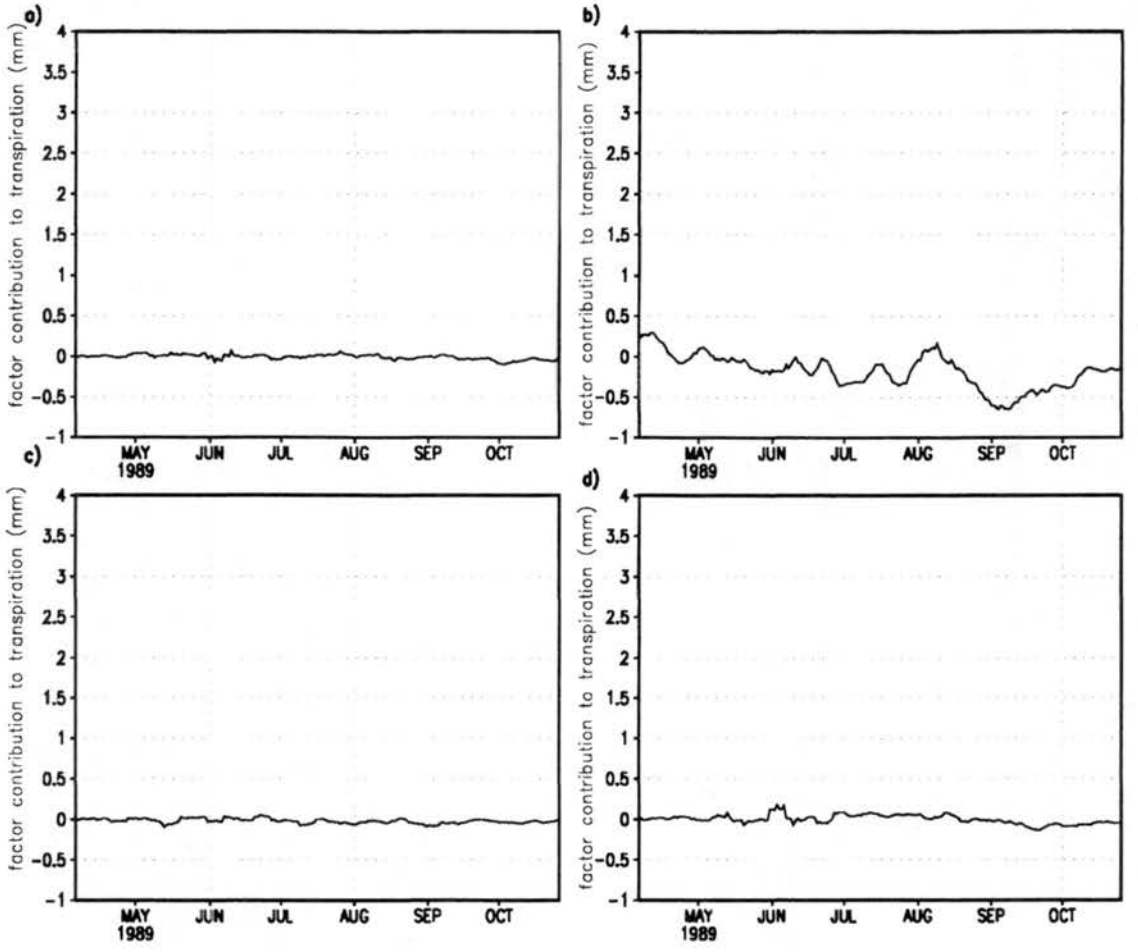

Figure 6.11: Contribution to domain-averaged transpiration due to a) interaction of natural vegetation and $2\times CO_2$ radiation, b) interaction of natural vegetation and $2\times CO_2$ biology, c) interaction of $2\times CO_2$ radiation and $2\times CO_2$ biology, and d) interaction of natural vegetation, $2\times CO_2$ radiation, and $2\times CO_2$ biology.

of the individual factors. The natural vegetation contributions were found to be highly correlated to the underlying vegetation, while the $2\times CO_2$ biology contributions were found to be correlated to a lesser degree to the biome types, and in the case of precipitation, to the topography. The previous section has also demonstrated different responses by biome type for the tall and short grasses. There are also indications of small amplitude contributions due to the $2\times CO_2$ and the factor interactions. It is probable that these contributions were masked to some degree by the domain averaging. This section examines spatially explicit temporal averages will be presented for several variables to demonstrate their contributions throughout the domain.

Figure 6.12a presents a horizontal plot of the temporal-averaged maximum daily temperature for the control simulation. The contours indicate the values of temperature at 2°C intervals. The topographical influence is clearly visible in the western half of the domain. The warmest averages are in the southeastern portion of the domain, and reach a peak of 32°C.

Figure 6.12b is the pure factor contribution due to natural vegetation. As seen previously in the last section, the largest perturbations occur in the areas of the vegetation change. Peak magnitudes in the eastern half of the domain are between $3-6$°C cooler than the control simulation. The mountainous areas in the west exhibit results generally ranging from -0.5 to 0.5°C. In the transition from higher to lower elevations, values are consistently in the 0 to -0.5°C range, with a few positive values interspersed.

The $2\times CO_2$ radiation contribution to the temporally-averaged maximum daily temperature is displayed in Figure 6.12c. The figure exhibits little spatial detail relative to the previous plots. Overall, there is a slight warming contribution between 0 and 0.5°C. A few areas indicate slight cooling of a similar magnitude.

Near domain-wide cooling is shown in Figure 6.12d, and corresponds to the maximum temperature fields due to a $2\times CO_2$ biology contribution. The strongest cooling of -2 to -3°C occurs over the short grass areas in the north central portions of the domain. There is also spatially consistent cooling between -1 to -2°C collocated over the temperate arid shrub regions in the west. An area in central Nebraska exhibits a patch of warming around

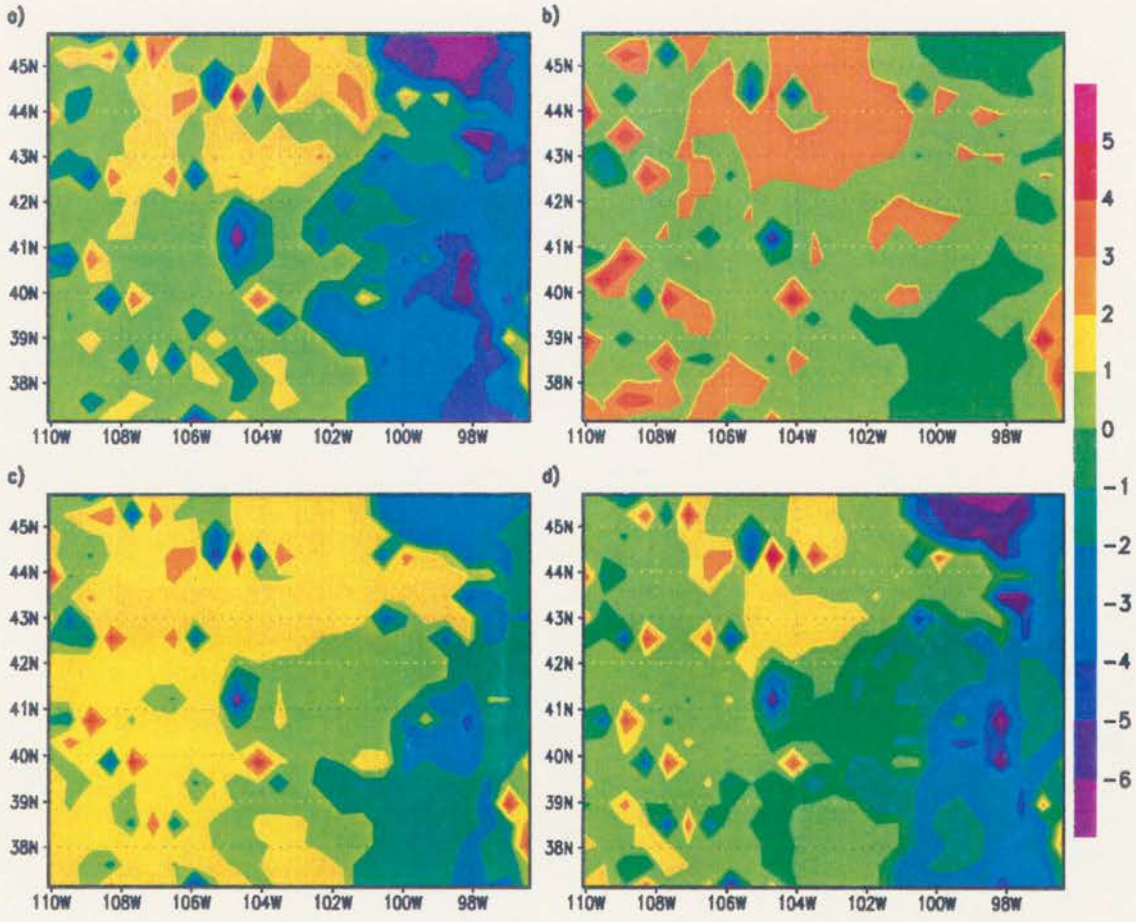

Figure 6.12: a) Horizontal plot of the temporally-averaged maximum daily temperature (C). Color values are represented by the contour labels. Horizontal plots of the temporal average of the contribution to maximum daily temperature due to b) natural vegetation, c) $2\times CO_2$ radiation, and d) $2\times CO_2$ biology. Color values in °C are indicated by the color bar.

0.5°C. This area contains a transition between the grassland/grain/wheat and cornbelt biomes.

The contributions of the various interactions to the temporally-averaged maximum daily temperature are displayed in Figures 6.13a-d. It is apparent that there is a spatially complicated pattern of warming and cooling. This would also explain the small domain averages, where it was found the magnitudes were relatively insignificant. The interaction of natural vegetation and $2\times CO_2$ radiation, (Figure 6.13), indicates the largest contiguous area of cooling occurs over the areas of vegetation change. The largest magnitude of this contribution, however, is over an area where there has been no change, and is between 1 and 2°C. The area is dominated by short grass vegetation under both natural and current landscapes. The slight warming of 0 to 0.5°C also generally occurs over areas where there has not been vegetation change.

Figure 6.13b corresponds to the contribution due to the natural vegetation and $2\times CO_2$ biology interaction. This figure indicates a majority of the domain exhibits warmer temperatures. In general, the areas of vegetation change show slight cooling. The figure also exhibits a larger warm spot over the short grass found in Figure 6.13a. Limited areas do exhibit cooling of -0.5 to -1°C.

The last two panels, Figure 6.13c and d, also exhibit the complicated spatial pattern found in the previous two figures. The interaction of $2\times CO_2$ radiation and biology suggest the same cooling over a large portion of the crop areas. The warm spot in the short grasslands is not as readily apparent. The triple interaction has an effect in contrast to the previous 3 interactions. It appears that is largely anti-correlated to the other interactions. In contrast to the warm spot in the central grasslands, this interaction displays strong cooling in this area. Although the interactions exhibit weaker contributions than the individual factor contributions of natural vegetation and $2\times CO_2$ biology, the sum is not insignificant.

Shown in Figure 6.14 is the combined field of all 4 interactions. The warm spot over the grasslands is now quite large, with a peak of nearly 2.5°C. In close proximity is an area exhibiting cooling of roughly -2°C. There are also areas suggesting a similar amount

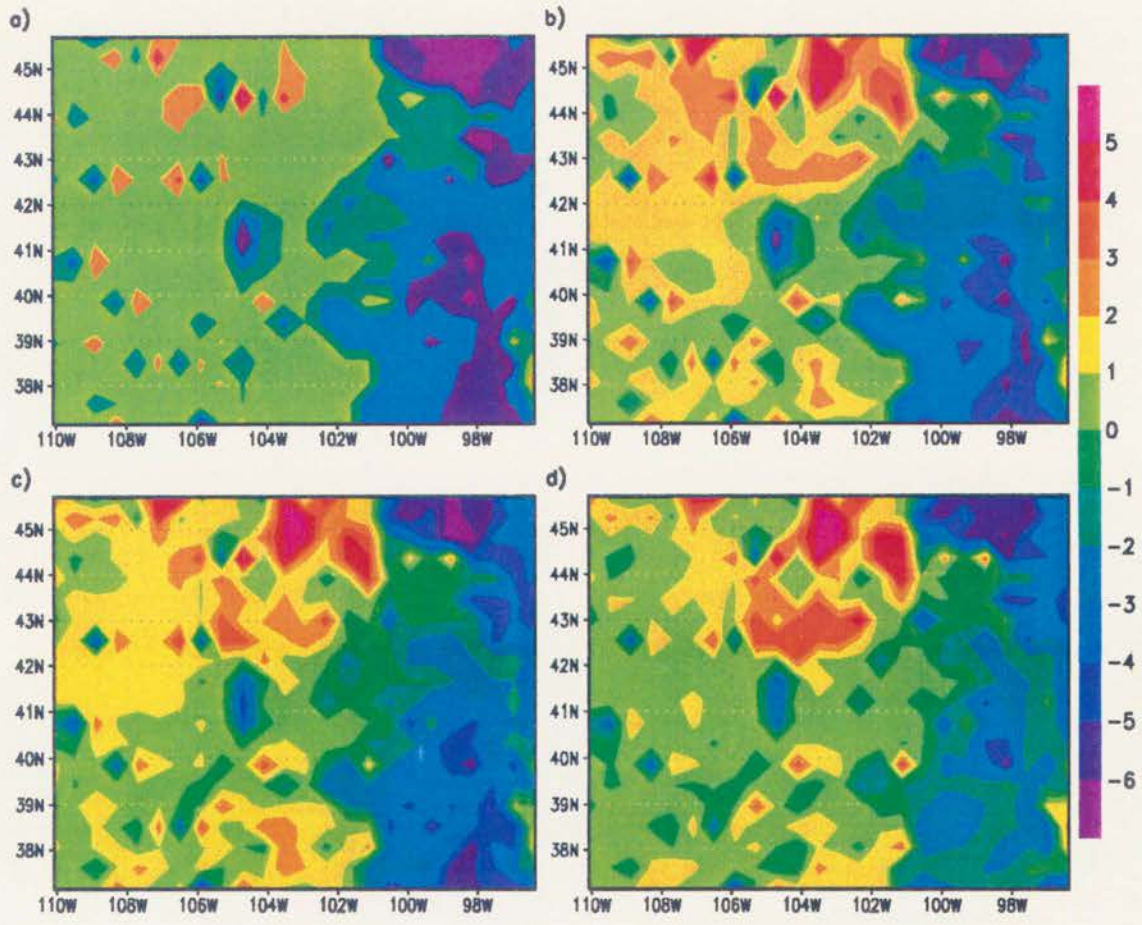

Figure 6.13: Horizontal plots of the temporal average of the contribution to maximum daily temperature due to a) interaction of natural vegetation and $2\times CO_2$ radiation, b) interaction of natural vegetation and $2\times CO_2$ biology, c) interaction of $2\times CO_2$ radiation and $2\times CO_2$ biology, and d) interaction of natural vegetation, $2\times CO_2$radiation, and $2\times CO_2$ biology. Color values are indicated by the color bar. Contour values are in °C.

of cooling in the cropland areas. A domain average of these combined fields yields a 0.1°C warming. Although not as large in terms of magnitude and areal extent as the individual natural vegetation and $2\times CO_2$ biology contributions, highly localized areas emerge where the combined interactions reach an appreciable magnitude. This further suggests these interactions cannot be ignored.

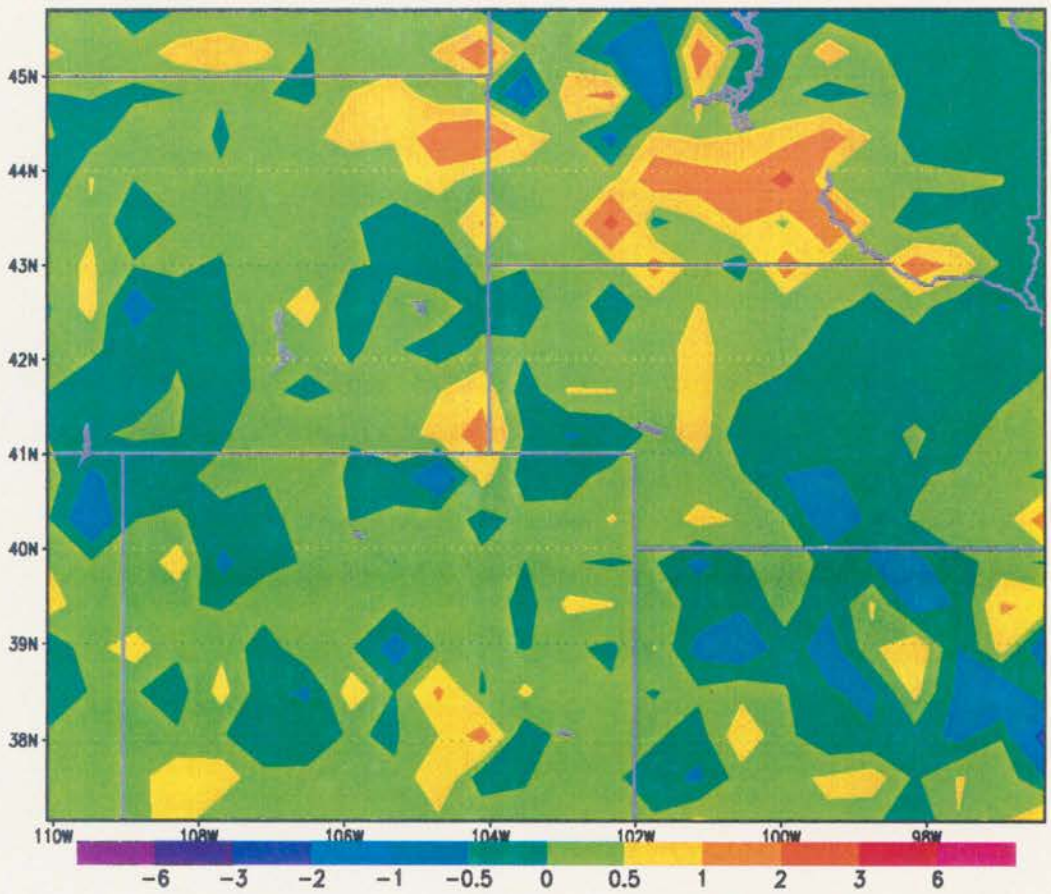

Figure 6.14: a) Horizontal plots of the temporal average of the contribution to minimum daily temperature due to the sum of all four interactions. Color values in °C are indicated by the color bar.

The next series of plots are for the seasonally-averaged minimum daily temperature. The control simulation and individual factor contributions are displayed in Figure 6.15a-d. The control simulation exhibits elevation effects as well as a north-to-south gradient over the plains. Minimums of 2°C are found in the highest elevations and the plains range from $8 - 12$°C.

Figure 6.15b shows the natural vegetation contribution. The figure indicates a warming over the eastern areas of the plains, where the landscape has changed. However there are portions over the central portion of the domain that suggest lower minimum daily temperatures. These areas correspond to tall grass areas that are grassland/grain/wheat biome types in the current landscape. The spots where the landscape change in the west are evident as hotspots, where forest areas have been replaced by crops.

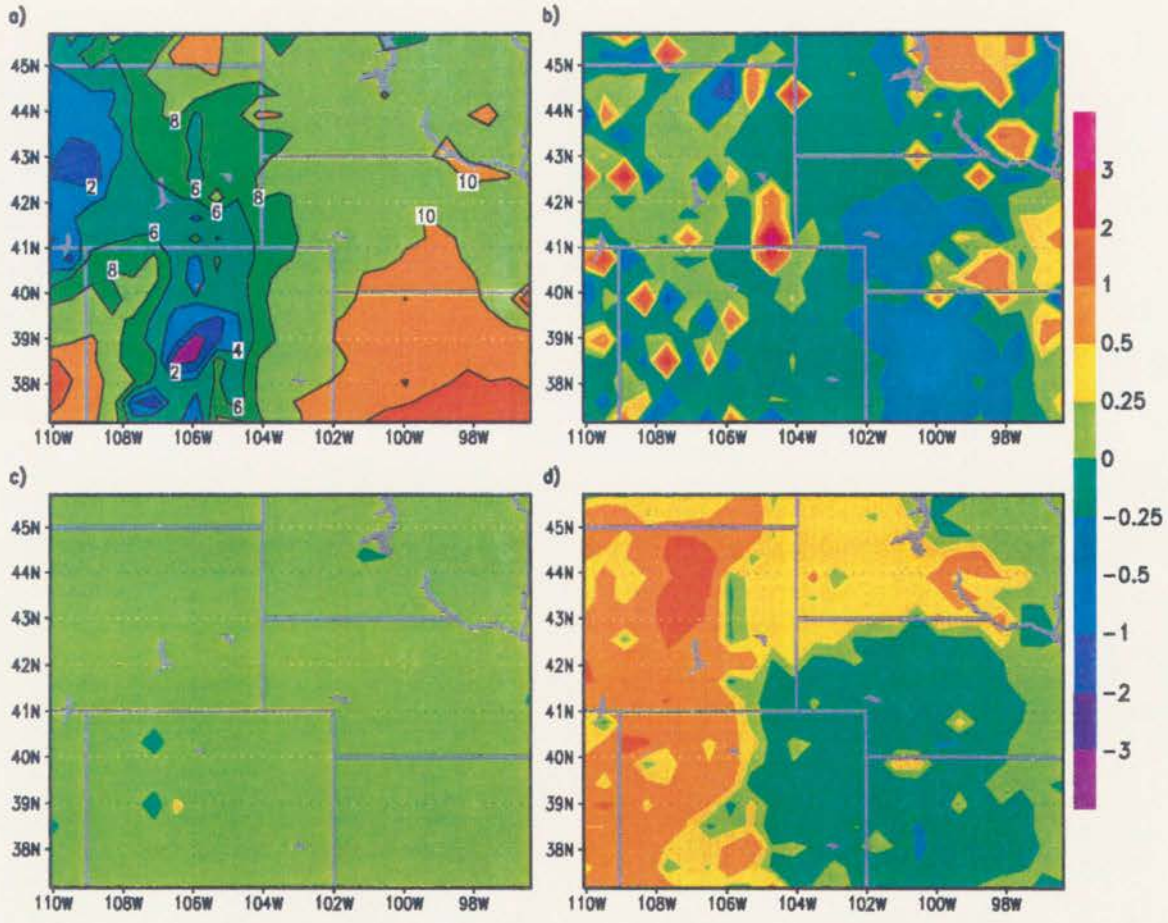

Figure 6.15: a) Horizontal plot of the temporally-averaged minimum daily temperature. Color values are represented by the contour labels. Horizontal plots of the temporal average of the contribution to minimum daily temperature due to b) natural vegetation, c) $2\times CO_2$ radiation, and d) $2\times CO_2$ biology. Color values in °C are indicated by the color bar.

The contribution due to $2\times CO_2$ radiation is shown in Figure 6.15b. The figure indicates relatively little spatial variability. This would be expected considering the constant

forcing in the longwave radiation parameterization. The domain average is $-0.1°C$ with a standard deviation less than half that magnitude.

Figure 6.15d displays the $2\times CO_2$ biology contribution. Nearly three quarters of the domain indicates a warming of $0.25 - 2°C$. Curiously the southeastern quadrant exhibits a decrease in the minimum daily temperature. A scatter plot of the contributions to LAI versus the contributions to minimum daily temperature should demonstrate if there is a threshold that is related to warming or cooling of temperatures. This is shown in Figure 6.16. It is clear that values of LAI enhancement less than 0.2 are likely to exhibit a cooler minimum daily temperatures. Since the fractional coverage is related to the ratio of LAI to a theoretical maximum LAI, it is likely this contribution is too small below the threshold of 0.2 to make a positive contribution to minimum daily temperature. As seen in Figure 6.19d, which shows the $2\times CO_2$ biology contribution to LAI, the figure indicates the cooler area exhibits LAI contributions less than 0.25. The one warm spot in the middle of this cool area indicates an LAI contribution greater than 0.2. This still does not completely explain why this area is cooler. Referring back to the plot for contribution to maximum daily temperature, we see that this area is generally cooler to begin with. Thus the relative cooling at night may be less, but the area is already -0.5 to $-2°C$ cooler to begin with.

The interaction plots for daily minimum temperature contributions are displayed in Figure 6.17a-d. The interaction of natural vegetation and $2\times CO_2$ biology, Figure 6.17b, exhibits the largest contribution, ranging from -0.5 to $2°C$. The hotspots in the western part of the domain are collocated with points that are different from the current vegetation distribution. The triple interaction field is again anti-correlated to a large degree, when compared to the other interactions. This is demonstrated in the scatter plot (Figure 6.18), which displays the contribution to minimum daily temperature due to interaction of $2\times CO_2$ radiation with $2\times CO_2$ biology versus the contribution due to the triple interaction. The distribution is nearly centered on the line with a slope of -1. The figure also indicates the relative magnitudes of the interactions which are concentrated in a range from -0.05 to $0.05°C$. These two interactions would be expected to cancel each other out, given their distribution. Overall the factors taken by themselves exhibit fairly small contributions.

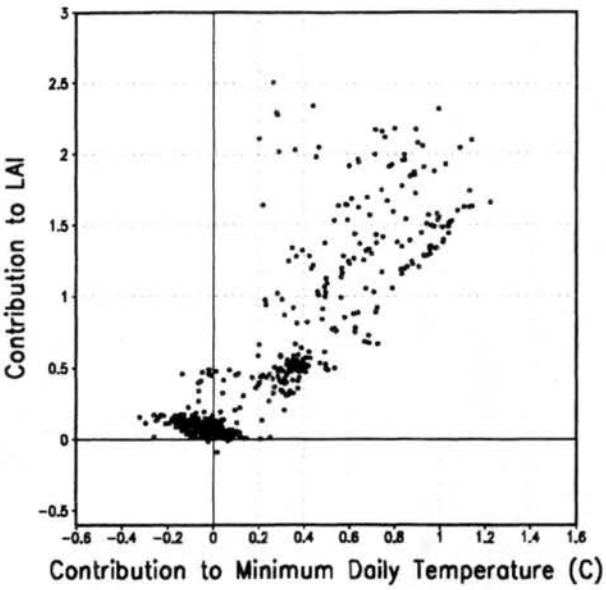

Figure 6.16: Scatter plot of the contribution to LAI versus the contribution to minimum daily temperature due to $2\times CO_2$ biology.

Figure 6.19a-d displays the seasonally-averaged LAI for the control simulation and the seasonally-averaged contributions to LAI due to the individual factors. A strong east-west gradient in LAI is clear as one moves eastward from the mountains to the plains. The plains exhibit values in the 0.25 to 1 range, while the mountains exhibit values up to 10.

The contribution of natural vegetation shown in Figure 6.19b shows a mixed response in the mountains. The larger contribution, between 1 and 3, are over areas of deforestation. There are also several cells with a negative contribution of the same magnitude. They are generally forest areas or temperate arid shrub in the current vegetation distribution. Nearly all cells in the eastern portion of the domain that were crops under the current distribution exhibit an LAI enhancement under natural vegetation. It must be kept in mind that for a couple of months in the season, these are areas that would be bare fields in the current distribution. Finally, large tracts of unchanged vegetation, beginning in the Front Range of the Rockies and extending over the Central Plains also show an increase. The opposite occurs in large areas in the mountains. This raises the question of whether the meteorology has been altered enough that it is beginning to show-up in the biota.

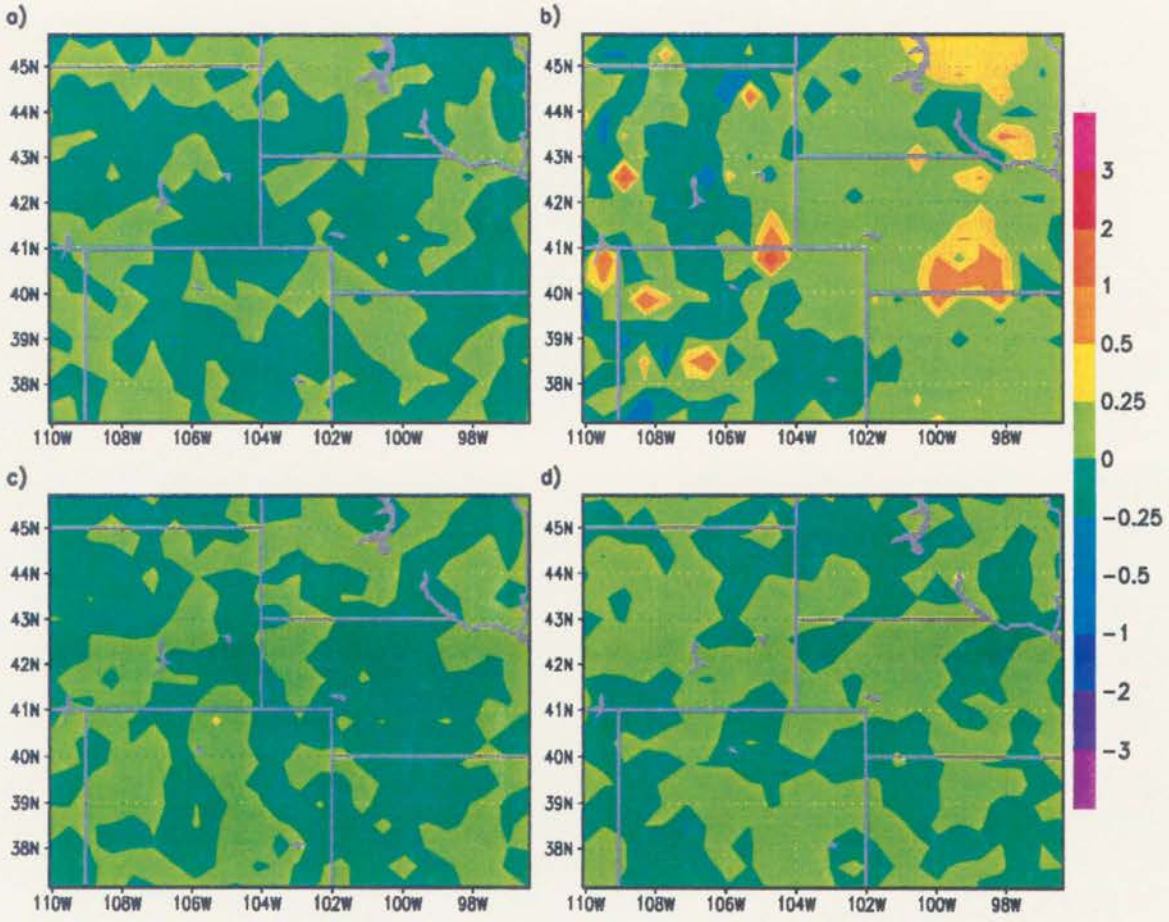

Figure 6.17: Horizontal plots of the temporal average of the contribution to minimum daily temperature due to a) interaction of natural vegetation and $2\times CO_2$radiation, b) interaction of natural vegetation and $2\times CO_2$ biology, c) interaction of $2\times CO_2$ radiation and $2\times CO_2$ biology, and d) interaction of natural vegetation, $2\times CO_2$radiation, and $2\times CO_2$ biology. Color values in °C are indicated by the color bar.

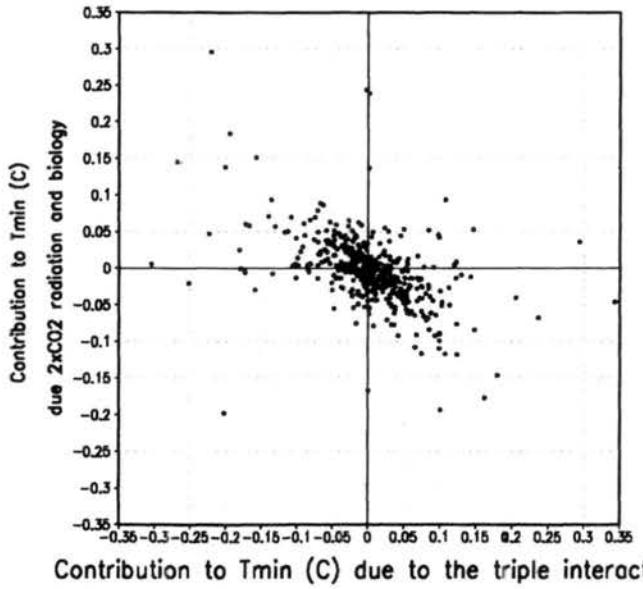

Figure 6.18: Scatter plot of the contribution to minimum daily temperature due to interaction of $2\times CO_2$ radiation with $2\times CO_2$ biology versus the contribution due to the triple interaction. The axis cover a range from -0.35 to $0.35°C$.

The $2\times CO_2$ radiation impact is displayed in Figure 6.19c. The impact appears minimal, with most areas ranging from a -0.1 to 0.1 LAI change. Curiously, there are a pair of coupled maxima and minima located in north central Colorado. The reason for this response is not currently understood, but could be related to changes in precipitation described in Chapter 5.

Figure 6.19d shows the contribution to LAI due to the $2\times CO_2$ biology factor. The largest change is exhibited over the forest areas in the west. The short grass biome also suggests a fairly large response. The plains and croplands show the smallest enhancement. This is somewhat misleading however. The smaller values over the crop areas are still quite large relative to the LAI shown in the control simulation.

The factor interactions, and their contribution to LAI, are displayed in Figure 6.17a-d. The interaction of natural vegetation and $2\times CO_2$ biology again exhibits the largest amplitudes, ranging from -3 to 3. The increases in the east are collocated with areas of change and achieve a peak magnitude of 1. A pattern similar to the natural vegetation contribution also emerges in the mountainous regions of the domain. The interactions

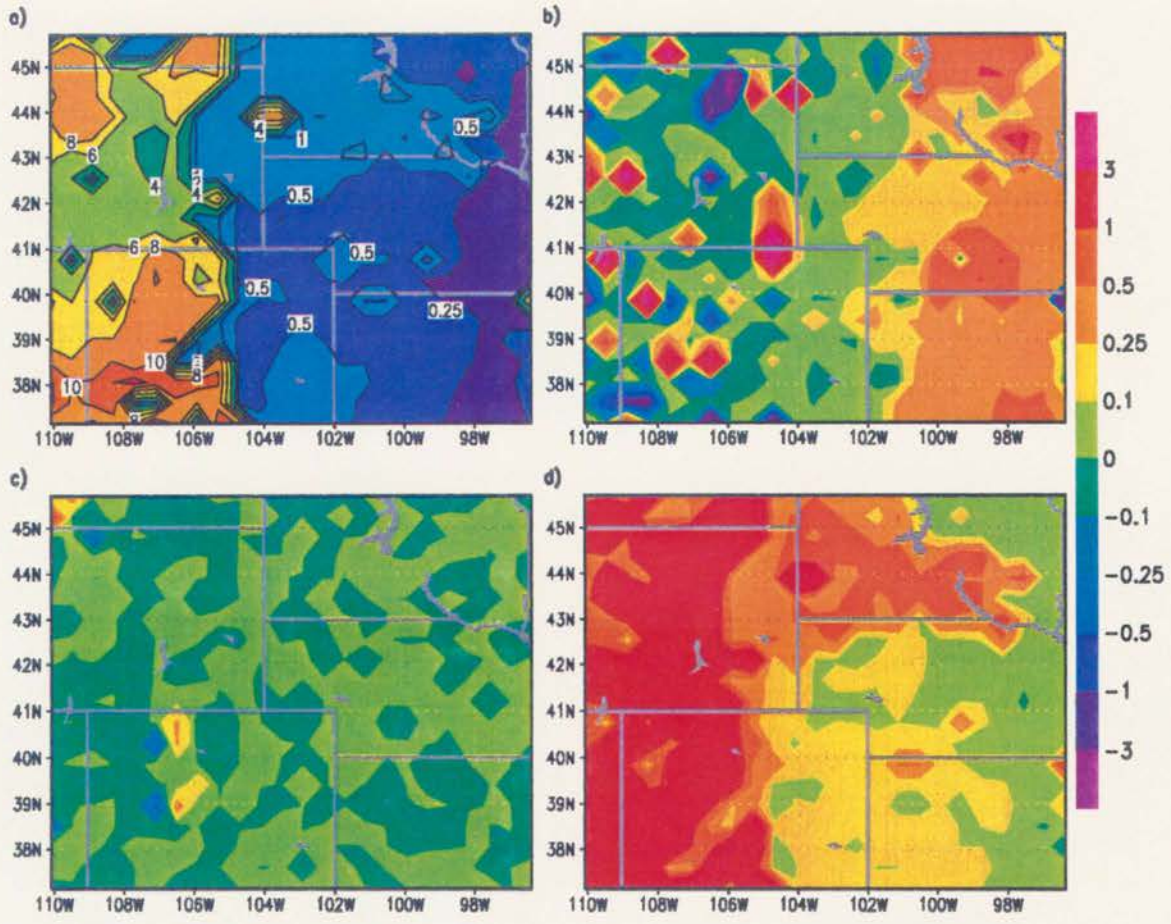

Figure 6.19: a) Horizontal plot of the temporally-averaged LAI. Color values are represented by the contour labels. Horizontal plots of the temporal average of the contribution to LAI due to b) natural vegetation, c) $2\times CO_2$ radiation, and d) $2\times CO_2$ biology. Color values are indicated by the color bar.

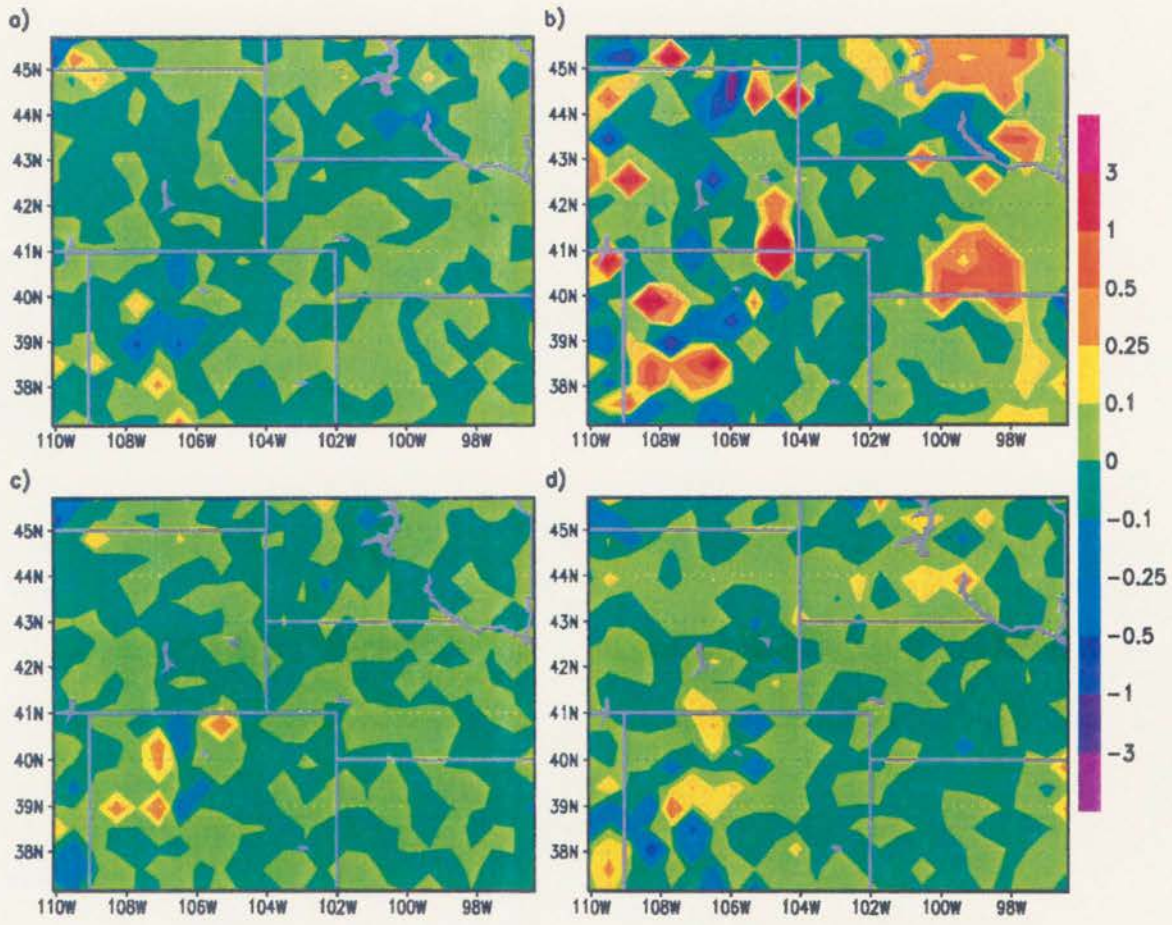

Figure 6.20: Horizontal plots of the temporal average of the contribution to LAI due to a) interaction of natural vegetation and $2\times CO_2$ radiation, b) interaction of natural vegetation and $2\times CO_2$ biology, c) interaction of $2\times CO_2$ radiation and $2\times CO_2$ biology, and d) interaction of natural vegetation, $2\times CO_2$ radiation, and $2\times CO_2$ biology. Color values are indicated by the color bar.

of natural vegetation with $2\times CO_2$ radiation, and $2\times CO_2$ radiation with $2\times CO_2$ biology show regions of a large, highly localized contributions. It is likely attributable to the nonlinear nature of the modeling system. Finally the triple interaction is exhibiting the anticorrelation displayed in the previous fields and suggests minimal contributions.

The precipitation has been shown to exhibit large fluctuations and spatial and temporal displacements in the previous analysis of the last chapter. The daily precipitation of the control simulation is displayed in Figure 6.21a. The figure displays the small values of precipitation observed in the western portion of the domain. The topographical effects are clearly visible over the Rockies in central Colorado. The enhanced precipitation is also clear over the plains and is also associated with storm tracks as the systems move out over the plains from the Rockies.

Figure 6.21b shows the contribution to daily precipitation due to natural vegetation. The figure indicates a decrease in precipitation over the eastern crop areas of the domain. It was surmised in the last chapter that this was mainly due to a decrease in the maximum daily temperature which would impact deep cumulus cloud convection. The decrease is around 10–25% of the daily-averaged totals of the control simulation. A north-to-south strip of increased daily precipitation is present in the central portion of the domain, and exhibits an increase of a similar percentage. The area in southeastern Wyoming, where the vegetation has changed, exhibits a strong decrease in precipitation, reaching nearly 50% of the control run values. The western portion of the domain shows weaker perturbations that tend to cancel out. In Figure 6.21c, the $2\times CO_2$ radiation contribution is plotted. As in many of the previous fields, the figure suggests little spatial variability due to this factor. Overall, the factor tends to increase the daily precipitation. Figure 6.21d represents the contribution from $2\times CO_2$ biology to the daily precipitation. The figure indicates that there is a near domain-wide decrease of 5 to 15%. As stated earlier, this is likely related to decreased maximum daily temperatures.

The interactions of the factors, and their input to the daily precipitation totals is displayed in Figure 6.22a-d. As exhibited in previous fields, their contributions form a spatially complicated pattern. Figure 6.22b shows that the natural vegetation interaction

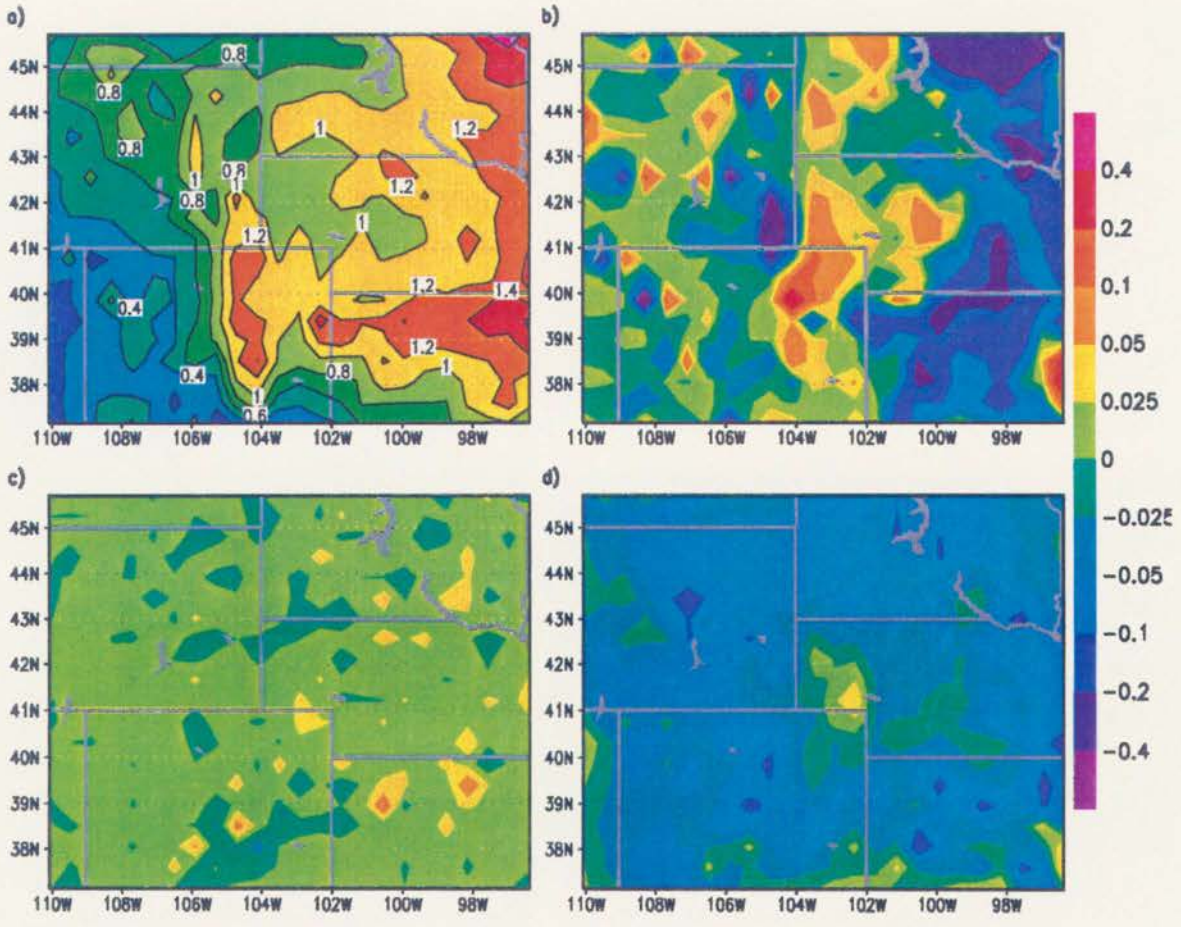

Figure 6.21: a) Horizontal plot of the temporally-averaged daily precipitation (mm). Color values are represented by the contour labels. Horizontal plots of the temporal average of the contribution to daily precipitation (mm) due to b) natural vegetation, c) $2\times CO_2$ radiation, and d) $2\times CO_2$ biology. Color values are indicated by the color bar.

with $2\times CO_2$ biology provides the largest contribution in terms of magnitudes. The magnitudes of large positive contributions are generally contained in small, localized regions. It is also apparent that the areas of decrease are spatially larger and correspond to areas where vegetation has not changed, implying the interaction itself is communicated to other areas of the domain. The triple interaction, which is again anticorrelated to the $2\times CO_2$ radiation and $2\times CO_2$ biology interaction, also indicates predominantly precipitation decreases, with magnitudes similar to the natural vegetation interaction with $2\times CO_2$ biology. There is also no apparent connection to landscape change for this interaction.

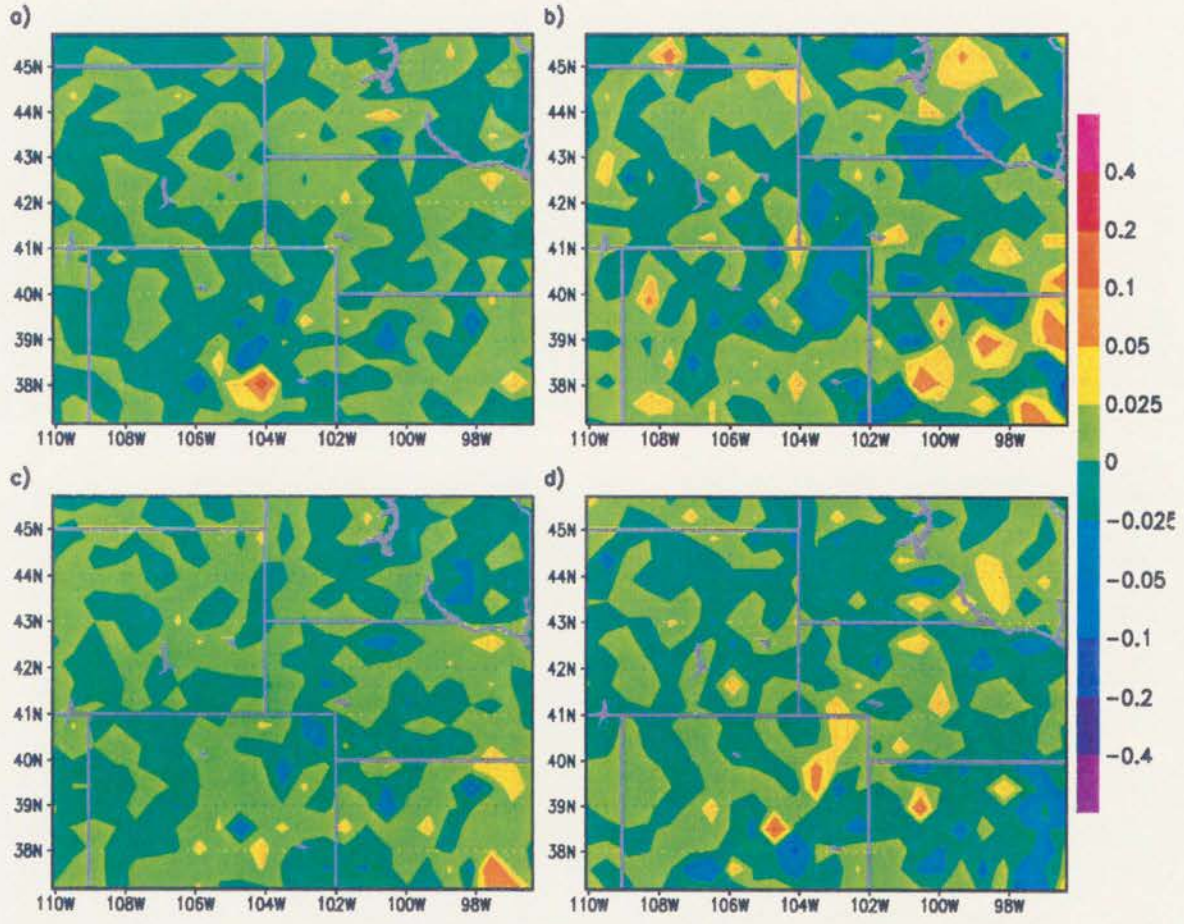

Figure 6.22: Horizontal plots of the temporal average of the contribution to daily precipitation (mm) due to a) interaction of natural vegetation and $2\times CO_2$ radiation, b) interaction of natural vegetation and $2\times CO_2$ biology, c) interaction of $2\times CO_2$ radiation and $2\times CO_2$ biology, and d) interaction of natural vegetation, $2\times CO_2$ radiation, and $2\times CO_2$ biology. Color values are indicated by the color bar.

Recall in the last chapter that the latent and sensible heat fluxes were examined for significance in the individual factor tests. Given the results of this section, with varying spatial patterns and contributions for several variables, it might be instructive to examine the heat fluxes in terms of the Bowen ratio, the ratio of sensible to latent heat flux. Figure 6.23a-d displays the seasonally-averaged Bowen ratio for the control simulation and the individual factor contributions. Scanning Figure 6.23a from left to right. the control simulation exhibits a fairly strong decline in Bowen ratio, falling from 2.5 to 1. Not shown is the domain-averaged Bowen, which shows a seasonal increase in the ratio from 0.5 to 4.

Figure 6.23b displays a strong contribution due to the natural vegetation. The area of greatest landscape change, the eastern portion of the domain, indicates a relatively large decrease in the ratio. The decreases are on the order of the control simulation values. It has been mentioned before that this area exhibits more transpiration as well as higher LAI values. This would lead to the simulated decreases. The gridpoints in the western half of the domain showing large changes in magnitude correspond to those points with different surface vegetation. Other than these extreme point values, the western region shows little contribution, with values ranging from -0.1 to 0.1.

The contribution of the $2\times CO_2$ radiation displays a complicated spatial pattern of rather small contributions, similar to other fields examined. The $2\times CO_2$ biology input to the Bowen ratio exhibits fairly large positive and negative values. The pattern is similar to the previous variables examined, such as minimum daily temperature and daily precipitation. It also tends to reinforce earlier suggestions that the croplands enhanced biomass and proportionally larger weighting in transpiration has been more than offset by the decreased stomatal conductance. At the same time the short grasslands to the north and the forested areas of the west exhibit the opposite trend, where the transpiration has been enhanced by the increased biomass.

The interaction contributions to the Bowen ratios are displayed in Figures 6.24a-d. In contrast to the previous variables examined, the $2\times CO_2$radiation interaction with $2\times CO_2$ biology contribution stands out in Figure 6.24c. In some areas they are nearly as large as the control simulation values themselves. It is likely that the large magnitudes are a

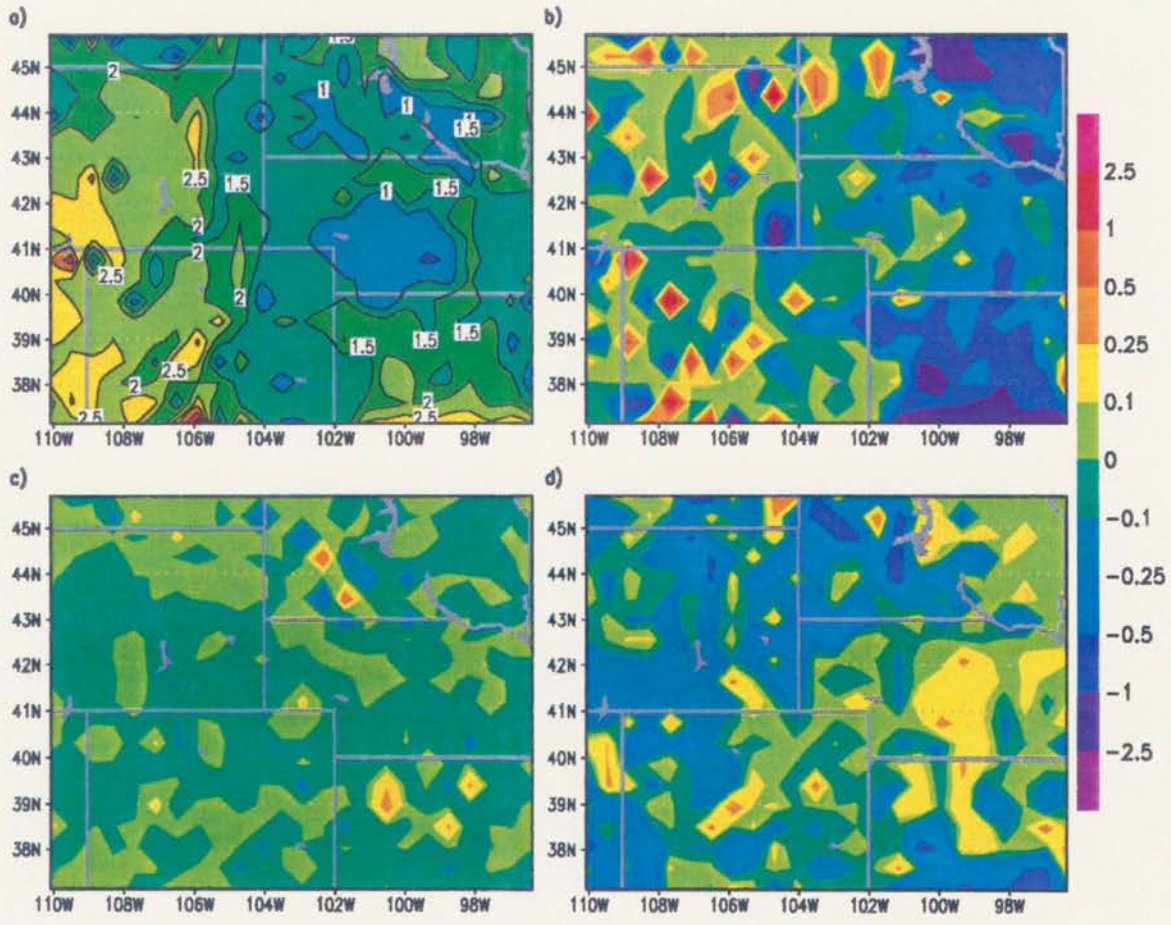

Figure 6.23: a) Horizontal plot of the temporally-averaged Bowen ratio at 18 GMT for the control simulation. Color values are represented by the contour labels. Horizontal plots of the temporal average of the contribution to Bowen ratio at 18 GMT due to: b) natural vegetation, c) $2\times CO_2$ radiation, and d) $2\times CO_2$ biology. Color values are indicated by the color bar.

result of taking a ratio, which will tend to magnify small differences that occur in the denominator. The rest of interactions also show some fairly strong contributions to this ratio and display a complex spatial pattern, seemingly not correlated to the individual factor patterns themselves.

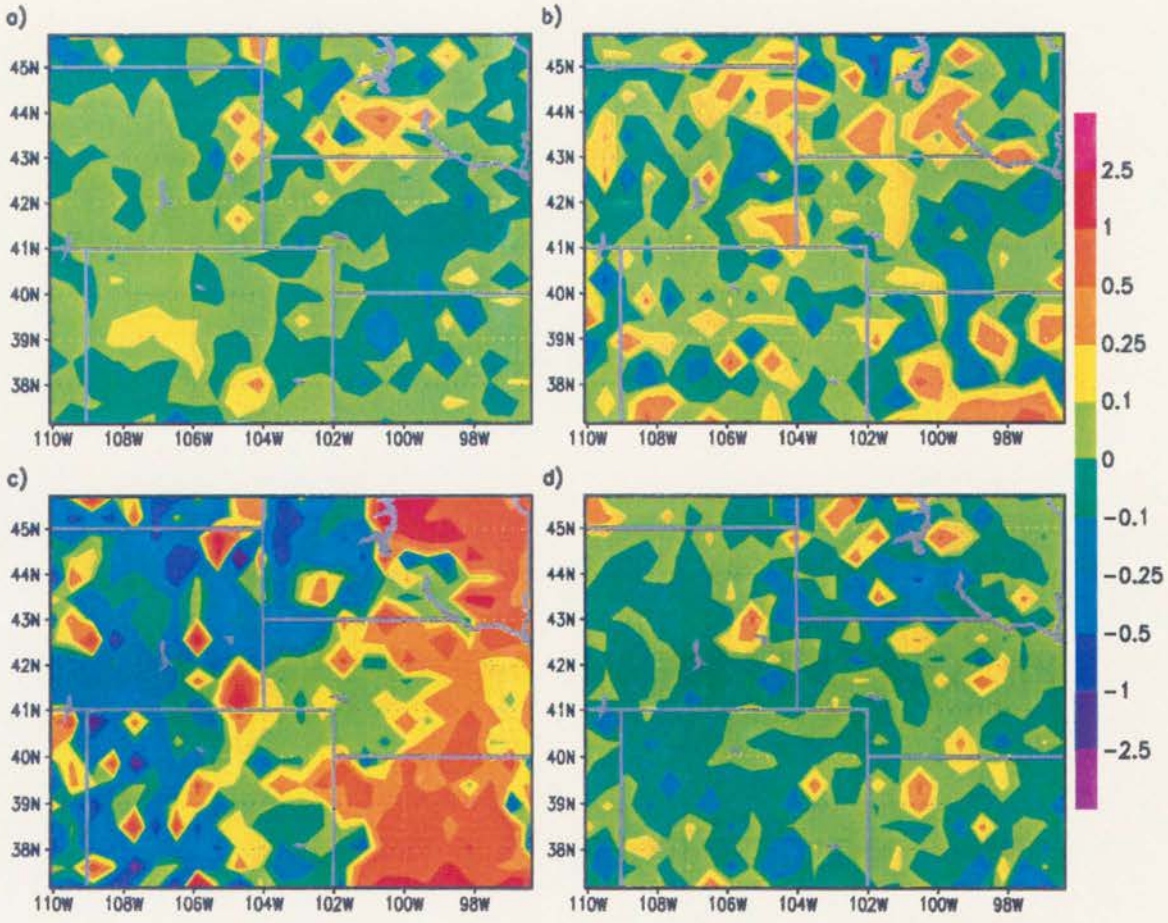

Figure 6.24: Horizontal plots of the temporal average of the contribution to Bowen ratio at 18 GMT due to a) interaction of natural vegetation and $2\times CO_2$ radiation, b) interaction of natural vegetation and $2\times CO_2$ biology, c) interaction of $2\times CO_2$ radiation and $2\times CO_2$ biology, and d) interaction of natural vegetation, $2\times CO_2$ radiation, and $2\times CO_2$ biology. Color values are indicated by the color bar.

This section has shown several interesting results. The importance of including factor interactions has been shown. This was demonstrated for the maximum daily temperature, where their summation was presented. The results have also indicated that contributions on smaller scales can be quite large. Other factors, which might be thought of as extremely

important, have been shown to be quite small ($2\times CO_2$ radiation). All of the results considered together illustrate the highly nonlinear problem of modeling this coupled system, and that all factors and their interactions should be taken into account.

6.2 Monthly Assessments

Up to this point, the focus has been on separating the different factors and their interactions, and putting them in perspective by comparison with the control simulation. There is an underlying theme in this study that has not been directly addressed. This theme is "what have been the possible effects of human impact on landscape and atmospheric CO_2 levels?". Through past experience dealing with this topic it has been the feeling of the author that landscape change has been a major driver in any perceived climate change. This began with a masters thesis concerning atmospheric dispersion. It was found that the predicted dispersion and meteorological variables were not acceptable until the vegetation was explicitly included in the calculations. Further sensitivity studies also suggested highly divergent solutions when different vegetation was applied to the model. In this section, the combined effects of landscape change, $2\times CO_2$radiation, and $2\times CO_2$ biology are briefly examined. Instead of the current landscape under current atmospheric CO_2 levels assuming the role of the control simulation, the natural landscape under current atmospheric CO_2 levels is used. A difference between this simulation and current landscape simulations under present and doubled CO_2, will provide the models sensitivity to these contrasting environments. Since all three simulations have already been included in this study, the exercise will be easy. The impact on maximum daily temperatures will be the only variable examined. Keep in mind that this is not a factor separation, but a difference field for the simulations. If the natural vegetation under current atmospheric CO_2 levels was substituted in the previous analysis, the factors and their contributions could be ascertained explicitly.

Shown in Figure 6.25a is the seasonally-averaged difference between the natural vegetation, with current CO_2 levels for both radiation and biology, with the current vegetation under the same CO_2 levels for both radiation and biology. Negative values indicate a

warming under the current scenario, since the difference is natural minus current. The figure indicates that the majority of the domain has experienced warming. The elevated temperatures in the east, over the croplands, show increases above 5°C. Limited areas in the western portion of the domain suggest weak to moderate cooling.

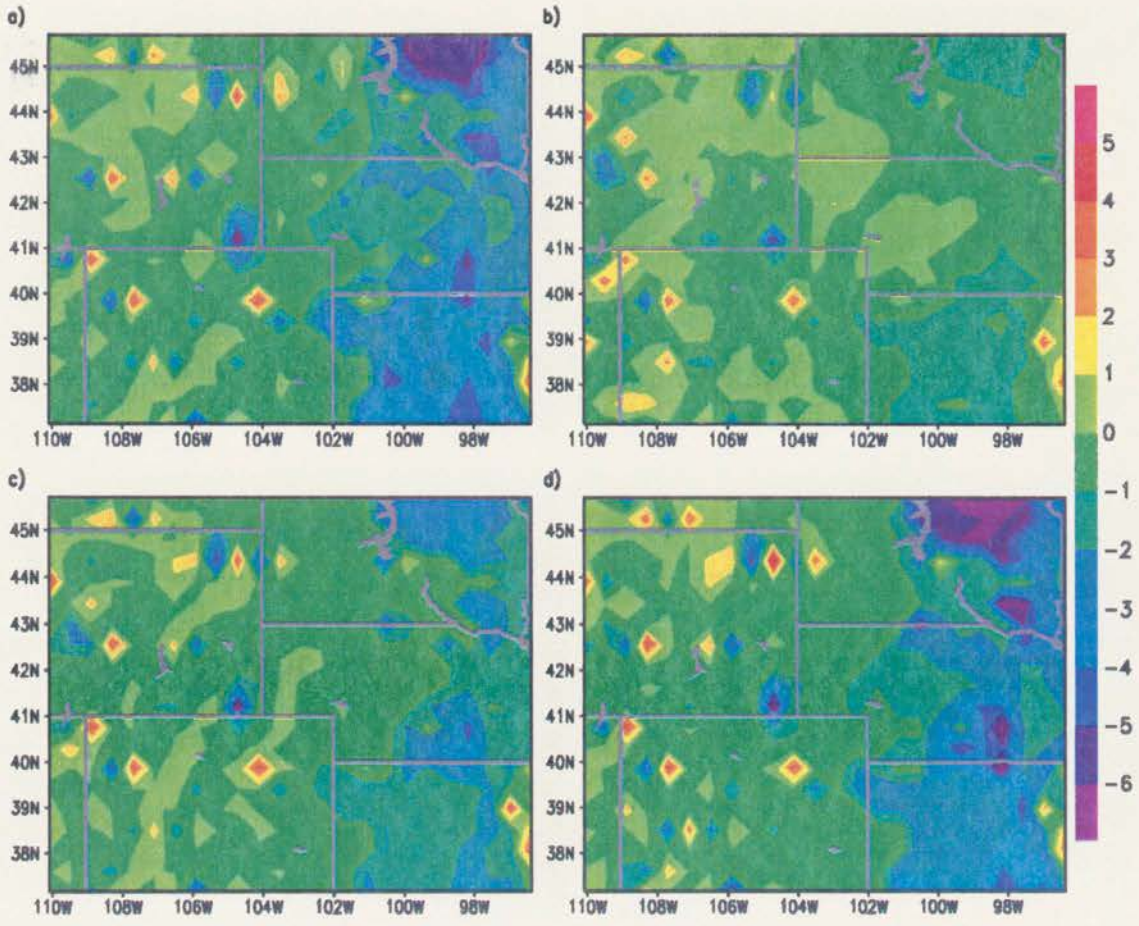

Figure 6.25: The monthly-averaged maximum daily temperature difference between the natural vegetation simulation and a current vegetation using $1\times CO_2$ simulation for a) seasonal average, b) April, c) May, and d) June. Color values in °C are indicated by the color bar.

Examining the April temperature differences, the domain again implies a general warming. The cooling displayed in the west for the seasonal average is large in areal extent. Warming is also exhibited in western South Dakota and west central Nebraska. The crop areas to the east show considerably less warming. Proceeding into the May averages, the elevated temperatures in the east begin to strengthen. It is likely that

sparsely vegetated fields are contributing considerable ground heat. The areas of lower temperatures have decreased from the past month. By the month of June the warming has increased considerably from the past month. It is apparent that the crops are exhibiting the strongest increase. The wheat fields of North Dakota are quite distinctive. The figure also shows that the areas of cooling have continued to recede. Moving on to July, a similar trend as June continues. The eastern farmlands are now readily apparent from north to south. The peak magnitudes have now exceeded 6°C. The areas displaying cooler temperatures in the west have remained largely unchanged at this point in the season. Examining the August figure, cooler temperature regions have expanded, while the eastern half of the domain has remained relatively constant. The plot for September indicates a reversal in the west, with cool temperature areas again shrinking. At the same time, the extent of warmer temperatures in the east has lessened slightly. The final plot for October indicates another reversal in terms of the areal coverage of cooler temperatures with further expansion.

These figures present an interesting progression. General perceptions and scientific study would also agree with the general warming trend. The interesting feature of this quick examination is that the only difference was in the underlying landscape. This was not a product of CO_2 enhancement. The figures also demonstrate that the differences are indicated over a larger areal extent than the areas of altered biomes. Now consider what would happen if another set of factors where added to the current simulation.

The previous analyses concerning the effect of doubled CO_2 has been well documented throughout the last two chapters. The analyses implied that the radiative effects were minimal, while the effect communicated to the biota was substantial. The current predictions of GCMs paint an entirely different picture in terms of the dominant forcing, although some recent work has begun to recognize the importance of the biotic feedback. Recalling the analysis that indicated the biotic effect was to cool the entire domain, and the radiative forcing will heat the domain, mixed results might be expected. However, results also suggested that the interaction of the vegetation change, $2\times CO_2$ radiation and $2\times CO_2$ biology can not be neglected as insignificant. Any model without a level of sophistication necessary to link these processes could be missing important components.

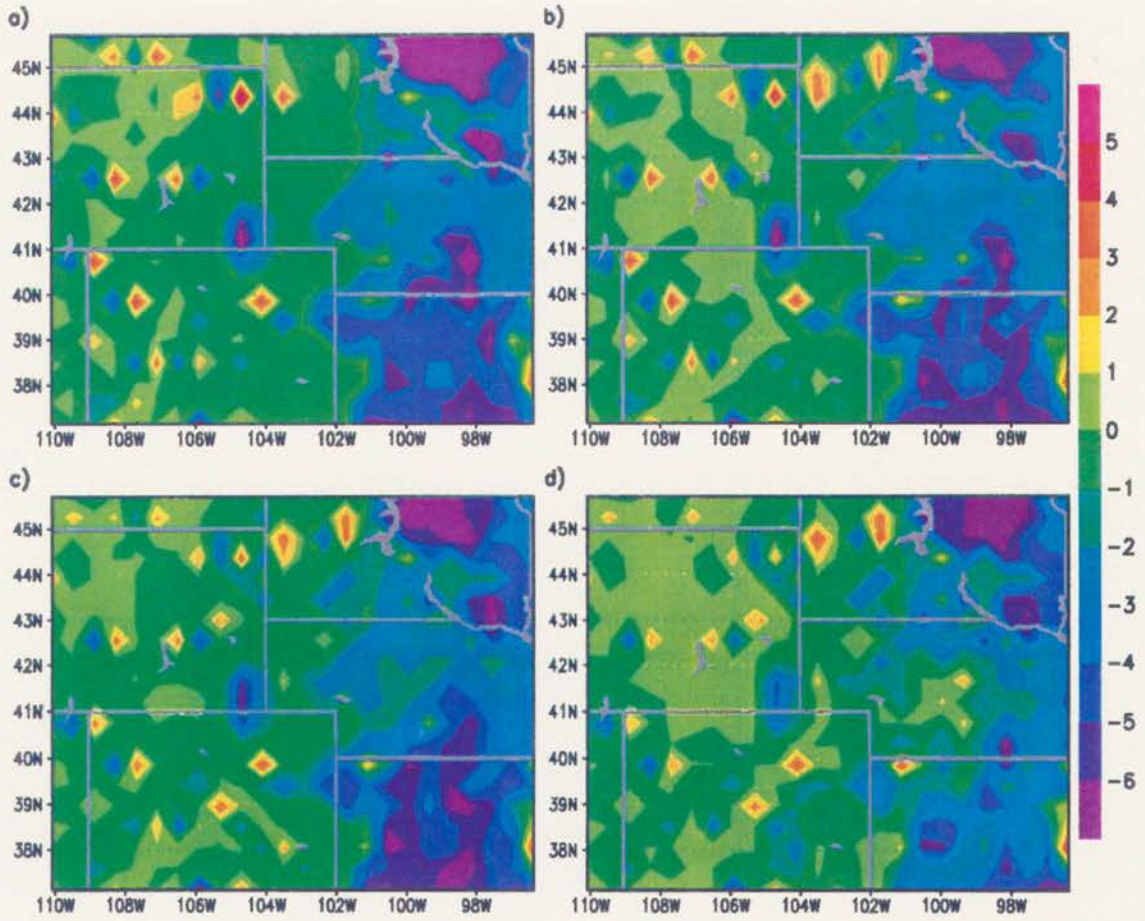

Figure 6.26: The monthly-averaged maximum daily temperature difference between the natural vegetation simulation and a current vegetation using $1\times CO_2$ simulation for a) July, b) August, c) September, and d) October. Color values are indicated by the color bar.

The results for the difference between the natural vegetation simulation, with current CO_2 levels for both radiation and biology, with the current vegetation under the same CO_2 levels for both radiation and biology are shown in Figures 6.27a-d and 6.28. The progression is the same as the last series of figures. The seasonal average is a contrast to

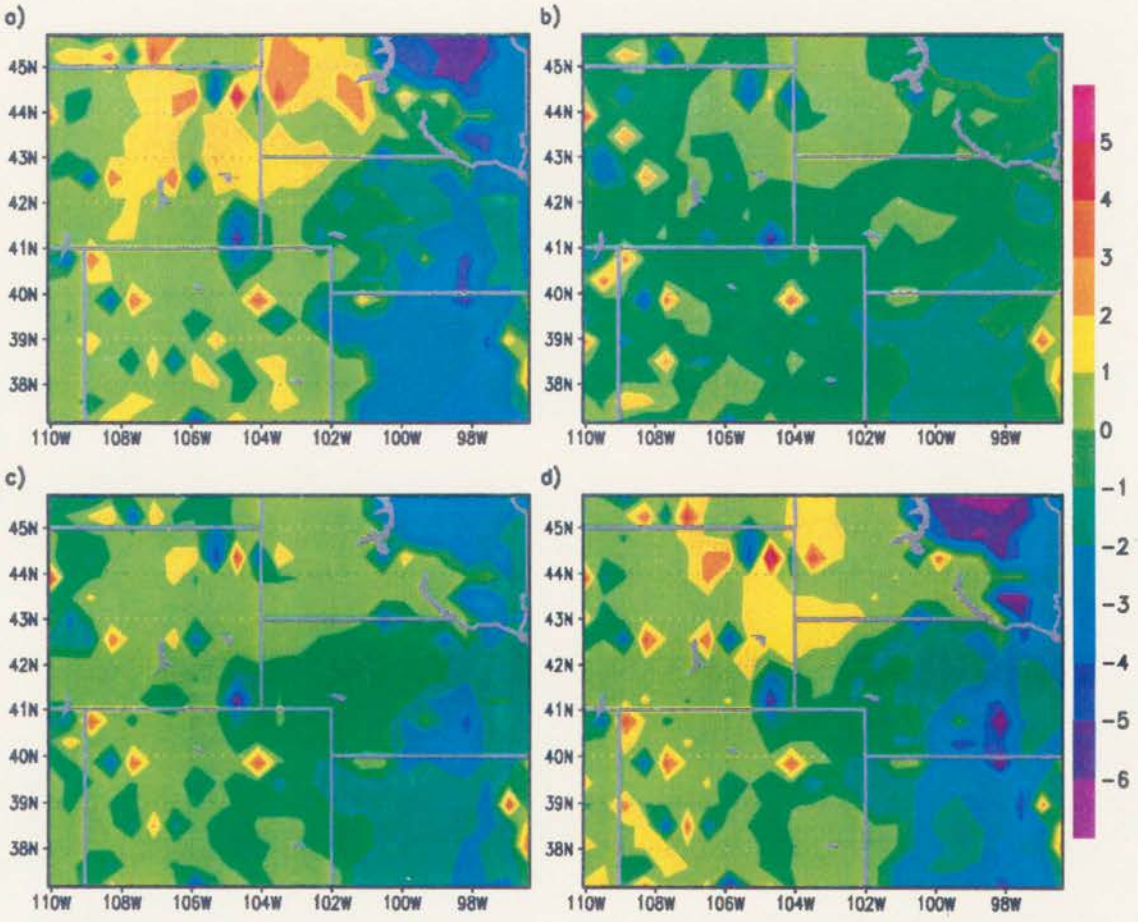

Figure 6.27: The monthly-averaged maximum daily temperature difference between the natural vegetation simulation and a current vegetation doubled CO_2 simulation for a) seasonal average, b) April, c) May, and d) June. Color values in °C are indicated by the color bar.

the previous analysis, and is displayed in Figure 6.27a. There is significantly greater areas indicating weak to strong cooling. The areas in the northwest quadrant of the domain show magnitudes great than 2°C, while the rest of the western portion of the domain suggest cooling between 0 and 1°C. There are still a few patches where warming is indicated. The areas over crops also show a lessening in the strength of the warming signal, as well

a shrinking areal extent. This is likely dominated by the $2\times CO_2$ biotic factor, which was shown in the previous sections of this study. The April average maximum daily temperature field has more area with higher temperatures than did the current CO_2 level experiment. The warmer patches in the east are quite similar to the previous set of results. By the month of May, the enhanced areal extent of warming is no longer apparent in the western portion of the domain. In fact, there is a reversal, with the area of cooler temperatures relative to the natural vegetation simulation substantially larger than the current CO_2 level experiment. It is also visible that the warming signal over the farmlands in the east remains similar to the previous results. The June averages suggest roughly the same area of cooling as was exhibited in the previous month, but the magnitudes have increased in some areas. There are now pockets on the 1 to 2°C range. As before, the signal over the croplands remains similar in magnitude and spatial pattern when compared to the same month in the previous analysis. The July pattern is a marked contrast to the prior analysis. It is clear that a majority of the domain area is now displaying cooling, with the majority of that area greater than 1°C. In addition, the warming areas over the croplands are now exhibiting smaller magnitudes of warming compared to Figure 6.26. A similar comparison can be made for August. At this time the magnitude of cooling has continued to increase, while the converse is true of the eastern farmlands. The month of September indicates a slight reversal of these trends, with limited shrinkage in the areal extent of cooled areas relative to June. The agricultural areas continue to exhibit a similar pattern to the previous month. The last month, October, shows that areas of higher magnitude cooling have increased further, and the cooling has begun to show up further eastward. The warming signal of the eastern farmlands has also decreased substantially relative to the previous results.

The two analyses have shown sharp contrasts in their seasonal evolution. The current vegetation simulation under current CO_2 levels indicate a general warming trend relative to a natural landscape simulation under the same CO_2 levels. When the CO_2 levels were doubled in the current landscape simulation, a strong cooling was present in a large portion of the domain, although the agricultural regions in the east still exhibited warmer

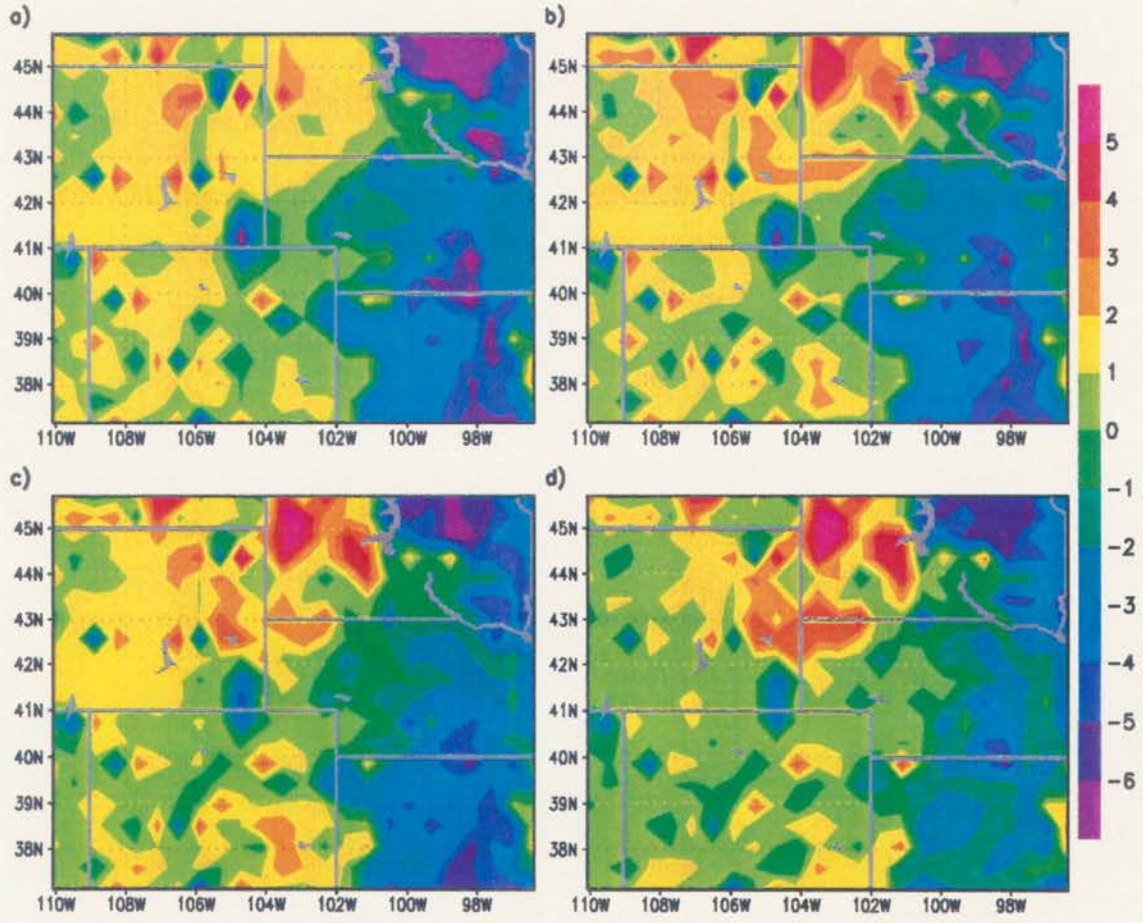

Figure 6.28: The monthly-averaged maximum daily temperature difference between the natural vegetation simulation and a current vegetation doubled CO_2 simulation for a) July, b) August, c) September, and d) October. Color values in °C are indicated by the color bar.

temperatures. In general the doubled CO_2 levels sharpened the thermal gradient across the domain. Naturally, these results are not intended to represent a climate simulation, but are presented to demonstrate the models sensitivity to various factors and imply the relative importance of including their interaction.

Chapter 7

SUMMARY AND CONCLUSIONS

A new modeling system has been developed and is detailed throughout Chapter 2 of this dissertation. The coupling of a mechanistic plant model to a climate version of the RAMS model was accomplished through a linkage in the surface parameterization of ClimRAMS. The level of detail in the plant model has enhanced the ability of ClimRAMS to investigate sensitivities to biotic changes. The detailed parameterizations in the plant model that are also coupled to prognosed and diagnosed atmospheric variables include:

- C_3 and C_4 photosynthesis pathways dependent on prognosed atmospheric and plant variables,
- atmospheric and biological stomatal feedback and control,
- dynamic allocation to roots, shoots and leaves through temporal changes temperature and water status,
- continual surface energy budget interaction between the plant and atmosphere affecting the status of both,
- a new root model that allows multi-layer water uptake and effluence which affects the surface energy budget, transpiration, and soil water status,
- root growth algorithm that allows the plant to forage for water resources, and
- detailed 9-level canopy radiation model to calculate canopy-surface-soil reflectance and whole canopy transmission.

The ClimRAMS model has been adapted here to facilitate long-term integrations on a regional scale. This coupling allows the investigation of the mutual adjustment of plant and meteorological fields on these scales.

In Chapter 3, a set of hypotheses were designed to test the interaction of biosphere and atmosphere due to a set of well-defined factors, and their interactions. In order to identify the contribution of these, a factor separation technique was presented that allowed linear and nonlinear components to be extracted from a series of simulations consisting of various combinations of the factors.

An objective technique to spatially initialize the plant model was then developed to provide consistency between the different landscapes employed in this study. This included the LAI, shoot and root biomass, as well as root length and weight density distributions. A spring green-up algorithm was also introduced to simulate the rapid growth rates observed during the springtime. The chapter concluded with a description of a soil moisture initialization technique and bottom soil boundary conditions; the latter being a new addition to ClimRAMS.

In Chapter 4, the task of validating the coupled modeling system was undertaken. The variables considered were maximum daily temperature, minimum daily temperature, precipitation, and LAI. They were subjected to a variety of analyses, including standard distribution statistics, such as correlation coefficient, mean, variance, standard deviation, skewness, and Kurtosis.

Excellent agreement was found in the temperature fields, with correlation coefficients upwards of 0.89 for the domain averages. It was also found that both modeled maximum and minimum daily temperatures were not significantly different from the observations for the KS and F tests. The t test indicated significantly different means for the maximum daily temperature, while the minimum daily temperature t test showed no significant difference. The temperatures fields also exhibited good agreement when point-by-point correlations were calculated. Some bias was identified in certain regions, mainly the western and southeastern portions of the domain, and likely causes were identified.

The most difficult field to predict, precipitation, showed mixed results. The correlation was only 0.35, but the model was shown to reproduce the events in a temporal

analysis. It was found that the model tended to underpredict precipitation, especially during the summer. Faults and possible corrections for the precipitation parameterizations were also suggested.

An indicator of biomass, LAI, was also subjected to the same tests. The correlation between the observations and modeled data was 0.9, and the t and F tests indicated the mean and variance were not significantly different. The model was found to slightly underpredict the biomass. Spatially-explicit analysis also concluded the model had displayed good agreement over most of the domain. The chapter also found good agreement when comparisons were made over different biome types.

In Chapter 5, the job of testing the significance of the individual factors was performed. The analysis was directed at answering the following hypothesis stated in Chapter 3.

- Significant differences in the domain-averaged prognosed meteorological and biological fields will be observable between the control simulation and factor simulations when
  - landcover is changed from current to potential vegetation,
  - radiative forcing is changed from $1\times CO_2$ to $2\times CO_2$, and
  - biological CO_2 levels are doubled.
- Significant differences will be found between the control simulation and factor simulations at individual gridpoints due to the factor contributions.
- Landcover-induced changes will exhibit more significant differences and higher magnitudes of contributions than either CO_2 effect.

This included domain-averaged and spatially-explicit analysis. It was found that for the domain averages that the landscape change exhibited the most significant differences for daily and hourly variables. This was followed by the biological $2\times CO_2$ contribution, with the $2\times CO_2$ radiation exhibiting one significant difference. The results also indicated a strong diurnal contribution from landscape, and to a lesser degree from $2\times CO_2$ biology.

From these results, it can be concluded that the first hypothesis is true at the $\alpha = 0.05$ level in an overall sense. The results also indicate that the contribution due to $2\times CO_2$ radiation was minimal in this analysis. In analyzing the spatial distributions it was found that significant differences were apparent on a point-by-point basis due to all three factors. The t test results demonstrated that the natural vegetation contribution exhibited the most significant results for the meteorological variables analyzed as well as transpiration. It was also found that the $2\times CO_2$ biology contribution exhibited the most significant differences for the biological variables. Again, the $2\times CO_2$ radiation effect was found to be minimal on a grid percentage basis. The variance test displayed similar results to the t test. The KS test exhibited an exception to these results. Here, the test statistics indicated that the $2\times CO_2$ biology contribution produced the highest percentage of cells for significance tests on the total accumulated precipitation and daily precipitation. These results suggest the second hypothesis is also true at the $\alpha = 0.05$ level. The final hypothesis addressed in this chapter was demonstrated for the meteorological variables. However, the biological variables indicated the most significant differences were due to $2\times CO_2$ biology. In retrospect, this is not very surprising. It was also concluded in the chapter that there is a balance between temperature and transpiration fields and their effects on different precipitation-forcing mechanisms.

The factor interactions were separated and compared with the individual contributions in Chapter 6. The first series of tests demonstrated significant differences from the null hypothesis ($\alpha = 0.05$), that the means are significantly different from zero. It was found that nearly all factors and factor interaction contributions were found to be significant. The only exceptions were for minimum daily temperature, daily precipitation, LAI, transpiration, and total accumulated carbon for the triple interaction, daily precipitation for the interaction of natural vegetation and $2\times CO_2$ biology, and minimum daily temperature and daily precipitation for the interaction of $2\times CO_2$ biology and $2\times CO_2$ radiation. This was meant to address the hypothesis stated as:

- Significant differences in the domain-averaged prognosed meteorological and biological fields will be observable between the factor interactions and the null hypothesis due to the nonlinear interactions between:

- landcover and doubled CO_2 biology
- radiative forcing at $2\times CO_2$ and landcover.

Shown alongside the significant tests were the percentage of grid cells also exhibiting significant differences. This supported the hypothesis stated in Chapter 3.

- Significant differences will be found due to the factor interactions at individual gridpoints due to the factor interaction contributions.

Chapter 6 also demonstrated that localized nonlinear reactions could be as large as the individual factors contributions. This was another hypothesis stated in Chapter 3. This was not demonstrated for all interactions and factors, but was seen in the domain-averaged percent contribution to selected variables and factors. The same results suggested that the natural vegetation contributed the largest percentage for some variables, while $2\times CO_2$ exhibited the largest contribution in the majority of variables. This implies that the hypothesis:

- landcover-induced changes will exhibit more significant differences and higher magnitudes of contributions than either CO_2 effect,

cannot be accepted at the $\alpha = 0.05$ level for all variables. The analysis also indicated that the temporal response of the factors and factor interactions was generally contrasting for different variables, and quite dissimilar between factors. Chapter 6 further demonstrated that the response of the biota to $2\times CO_2$ varied over biome types, and had significant impacts on the variables.

The chapter next focused on showing the relative magnitudes for the various factors and interactions in a spatially explicit manner. The results indicated that the factor interactions could be larger than the factors on an individual gridpoint basis. It was also concluded that factors and interactions produced spatially complicated patterns with relatively large impacts in some regions of the domain. For example, Figure 6.19 showed that the impact of $2\times CO_2$ biology was pronounced in the west, while the natural vegetation factor was largely confined to the eastern plains.

As a final example of the model's sensitivity to factors and interactions, two series of monthly-averaged maximum daily temperature fields were presented. The first series represented the effect of vegetation change. It was concluded that the model predicted a general warming trend over the integration period, and contained a strong seasonal and localized component. In the next series, $2\times CO_2$ biology and $2\times CO_2$ radiation were added to the current vegetation factor, and a difference with the natural vegetation simulation was again conducted. This difference field would represent the contribution of all 3 pure factors and their interactions. The results indicated that varying degrees of cooling would be experienced nearly domain wide, with the exception being the farmlands in the eastern portion of the domain. It was concluded that the likely contributor was the enhanced biomass due to $2\times CO_2$ biology. This was based on the previous factor separation results concerning $2\times CO_2$ biology and natural vegetation.

It is hoped that this dissertation will provide fodder for considerable discussion and aid in creating an air of objectivity when climate and landuse issues are addressed. The results should not be taken out of context as proving or disproving the prevalent hypothesis of greenhouse or global warming. That problem is beyond the scope of this model at the present time. This study is presented as an alternative method to help quantify the different forces governing regional climate, through a mechanistic, detailed, and objective approach.

REFERENCES

Anderson T., and D. Darling, 1952: Asymptotic theory of certain "goodness of fit" criteria based on stochastic processes, *Annals of Mathematical Statistic*, **23**, 193-212.

Asrar, G., M. Fuchs, E.T. Kanemasu, and J.L. Hatfield, 1984: Estimating absorbed photosynthetic radiation and leaf area index from spectral reflectance in wheat. *Agron. J.*, **76**, 300-306.

Avissar, R., 1995: Recent advances in the representation of land-atmosphere interactions in general circulation models. *Rev. Geophys.*, Supplement, 1005-1010, U.S. National Report to International Union of Geodesy and Geophysics 1991-1994.

Avissar, R. and Y. Mahrer, 1988: Mapping frost-sensitive areas with a three-dimensional numerical model. Part I: Physical and Numerical Aspects. *J. Appl. Meteor.*, **27**, 400-413.

Ball, J.T., I.E. Woodrow, and J.A. Berry, 1987: *A model predicting stomatal conductance and its contribution to the control of photosynthesis under different environmental conditions.* In: I. Biggins (editor), Progress in Photosynthesis Research. Vol IV. Martinees Nijhof, Dordrecht, 221-224.

Bazzaz, F.A., 1990: The response of natural ecosystems to the rising global CO_2 levels. *Annu. Rev. Ecol. Syst.*, **21**, 167-196.

Bazzaz, F.A., and W.E. Williams, 1991: Atmospheric CO_2 concentrations within a mixed forest: implications for seedling growth. *Ecology*, **72**, 12-16.

Berry, J.A. and G.D. Farquhar, 1978: The CO_2 concentrating function of C_4 photosynthesis: a biochemical model. In: D. Hall, J. Coombs and T. Goodwin (Editors), *Proc.*

of the 4th international Congress on Photosynthesis. Biochemical Society, London, pp. 119-131.

Chase, T.N., R.A. Pielke, T.G.F. Kittel, R. Nemani, and S.W. Running, 1996: The sensitivity of a general circulation model to global changes in leaf area index. *J. Geophys. Res.*, **101**, 7393-7408.

Chen, J., 1983: The reciprocity relation for reflection and transmission of radiation by crops and other plane-parallel scattering media. *Remote Sens. Environ.*, **13**, 475-486.

Chen, D.-X., M.B. Coughenour, A.K. Knapp, and C.E. Owensby, 1994: Mathematical simulation of C_4 grass photosynthesis in ambient and elevated CO_2. *Ecological Modelling*, **73**, 63-80.

Chen, D.-X., and M.B. Coughenour, 1994: GEMTM: a general model for energy and mass transfer of land surfaces and its application at the FIFE sites. *Agr. and Forest Meteor.*, **68**, 145-171.

Chen, D.-X. and J.H. Lieth, 1992: Two-dimension model of water transport in the rootzone and plant for container-grown chrysanthemum. *Agric. Forect Meteor.*, **59**, 129-148.

Chen, D.-X. and J.H. Lieth, 1993: A two-dimensional, dynamic model for root growth distribution of potted plants. *J. Am. Soc. Hort. Sci.*, **118**, 181-187.

Claussen, M., 1994: On coupling global biome models with climate models. *Climate Res.*, **4**, 203-221.

Claussen, M., 1998: On multiple solutions of the atmosphere-vegetation system in present-day climate. *Global Change Biol.*, **4**, 549-559.

Claussen, M., V. Brovkin, A. Ganopolski, C. Kubatzki, and V. Petoukhov, 1998: Modeling global terrestrial vegetation – climate interaction. *Phil. Trans. Roy. Soc. London*, **353**, 53-63.

Collatz, G.J., Ribas-Carbo, M. and Berry, J.A., 1992: Coupled photosynthesis-stomatal conductance model for leaves of C_4 plants. Aust. J. Plant Physiol., 19, 519-538.

Cotton, W.R. and R.A. Pielke. 1995: *Human impacts on weather and climate.* Cambridge University Press, New York, 288 pp.

Cotton, W.R., J.F. Weaver, and B.A. Beitler, 1995: An unusual summertime downslope wind event in Fort Collins, Colorado, on 3 July 1993. *Wea. Forecasting*, **10**, 786-797.

Dalu, G.A., R.A. Pielke, M. Baldi, and X. Zeng 1996: Heat and momentum fluxes induced by thermal inhomogeneities. *J. Atmos. Sci.*, **53**, 3286-3302.

Dawson, T.E., 1993: Hydraulic lift and water use by plants: implications for water balance, performance, and plant-plant interactions. *Oecolegia.*, **95**, 565-574.

Eastman, J.L., 1993: A numerical study and tracer evaluation of transport and diffusion in a lake breeze. M.S. Thesis. Department of Atmospheric Science, Colorado State University, 112 pp.

Fahquhar, G.D., S. von Caemmerer, and J.A. Berry, 1980: A biochemical model of photosynthetic CO_2 assimilation in leaves of C_3 species. *Planta*, **149**, 78-90.

Foley, J.A., 1994: The sensitivity of the terrestrial biosphere to climate change: a simulation of the middle Holocene. *Global Biogeochemical Cycles*, **8**, 505-525.

Gardner, W.R., 1960: Dynamic aspects of water availability to plants. *Soil Sci.*, **89**, 63-73.

Goudriaan, J., 1977: *Crop Micrometeorology: a simulation study.*, Pudoc, Wageningen, The Netherlands, 249 pp.

Henderson-Sellers, A. and K. McGuffie, 1995: Global climate models and "dynamic' vegetation changes. *Global Change Biology*, **1**, 63-75.

Hillel, D., H. Talpaz, and H. van Keulen, 1976: A macroscopic scale model of water uptake by nonuniform root system and of water and salt movement in the soil profile. *Soil Sci.*, **121**, 240-255.

Idso, S.B., 1992: Shrubland expansion in the American Southwest. *Climate Change*, **22**, 85-86.

Jackson, R.B., J. Canadell, J.R. Ehleringer, H.A. Mooney, O.E. Sala, E.D. Schulze, 1996: A global analysis of root distributions for terrestrial biomes. *Oecologia*, **108**, 389-411.

Johnson, I.R. and J.H.M Thornley, 1985: Temperature dependence of plant and crop processes. *Ann. Bot.*, **55**, 1-24.

Kalney, E., M. Kanamitsu, R. Kistler, W. Collins, D. Deaven, L. Gandin, M. Iredell, S. Saha, G. White, J. Woollen, Y. Zhu, M. Chelliah, W. Ebisuzaki, W. Higgins, J. Janowiak, K.C. Mo, C. Ropelewski, J. Wang, A. Leetmaa, R. Reynolds, R. Jenne, and D. Joseph, 1996: The NCEP/NCAR 40-year reanalysis project. *Bull. Ammer. Meteor. Soc.*, **77**, 437-471.

Kittel, T.G.F., N.A. Rosenbloom, T.H. Painter, D.S. Schimel, and VEMAP Modeling Participants, 1995: The VEMAP integrated database for modeling United States ecosystem/vegetation sensitivity to climate change. *J. of Biogeo.*, **22**, 857-862.

Klemp, J.B. and R.B. Wilhelmson, 1978a: The simulation of three-dimensional convective storm dynamics. *J. Atmos. Sci.*, **35**, 1070-1096.

Klemp, J.B. and R.B. Wilhelmson, 1978b: Simulations of right- and left-moving storms produced through storm. *J. Atmos. Sci.*, **35**, 1097-1110.

Kuo, H.L. and W.H. Raymond, 1980: A quasi-one-dimensional cumulus cloud model and parameterization of cumulus heating and mixing effects. *Mon. Weather Rev.*, **101**, 547-553.

Küchler, A.W., 1964: Potential natural vegetation of the conterminous United States. *Special Publication No. 36.* American Geophysical Society. 116 p. With separate map at 1:3,168,000.

Lee, T.J., 1992: The impact of vegetation on the atmospheric boundary layer and convective storms. Ph.D. Dissertation. Department of Atmospheric Science, Colorado State University, 137 pp.

Lewis, T.J. and K. Wang, 1998: Geothermal evidence for deforestation induced warming: Implications for the climatic impact of land development. *Geo. Rev. Letters*, **25**, 535-538.

Liston, G.E. and R.A. Pielke, 1999: A climate version of the Regional Atmospheric Modeling System. In preparation.

Ott, R.L., 1993: *An introduction to statistical methods and data analysis.* (Belmont, CA, Duxbury Press), Fourth Edition, 1051 pp.

Mahrer, Y. and R.A. Pielke, 1977: A numerical study of the airflow over irregular terrain. *Beitrage zur Physik der Atmosphare*, **50**, 98-113.

Mintz, Y. and Y. Serafini, 1981: Global fields of soil moisture and land-surface evapotranspiration. NASA Goddard Space Flight Center Tech. Memo. 83907, Research review - 1980/81:178-180.

Nemani, R. and S.W. Running, 1989: Testing a theoretical climate-soil-leaf area hydrologic equilibrium of forests using satellite data and ecosystem simulation. *Agric. Forest Meteorol.*, **44**, 245-260.

Norman, J.M., R. Garcia, S.B. Verma, 1992: Soil surface CO_2 fluxes and carbon budget of a grassland. *J. Geophys. Res.*, **97**,18845-18853.

Otterman, J., 1977: Anthropogenic impact on the albedos of earth. *Climatic Change*, **1**, 137-155.

Pielke, R.A., 1998: Climate prediction as an initial value problem. *Bull. Amer. Meteor. Soc.*, **79**, 2743-2746.

Pielke, R.A. and X. Zeng, 1994: Long-term variability of climate. *J. Atmos. Sci.*, **51**, 155-159.

Pielke, R.A., G.E. Liston, J.L. Eastman, L. Lu, and M. Coughenour, 1999a: Seasonal weather prediction as an initial value problem. *J. Geophys. Res.*, in press.

Pielke, R.A., R.L. Walko, L. Steyaert, P.L. Vidale, G.E. Liston, and W.A. Lyons, 1999b: The influence of anthropogenic landscape changes on weather in south Florida. *Mon. Wea. Rev.*, in press.

Reynolds, J.F. and B. Acock, 1985: Predicting the response of plants to increasing carbon dioxide: a critique of plant growth models. *Ecol. Modelling*, **29**, 107-129.

Sivillo, J.K., J.E. Ahlquist, and Z. Toth, 1997: An ensemble forecasting primer. *Wea. Forecasting*, **12**, 809-818.

Smagorinsky, J., S. Manabe, and J.L. Holloway, Jr., 1965: Numerical results from a nine-level general circulation model of the atmosphere. *Mon. Wea. Rev.*, **93**, 727-798.

Stein, U. and P. Alpert, 1993: Factor separation in numerical simulations. *J. Atmos. Sci.*, **50**, 2107-2115.

Texier, D., N. de Noblet, S.P. Harrison, A Haxeltine, D. Jolly, S. Joussaume, F. Laarif, I.C. Prentice, and P. Tarasov, 1997: Quantifying the role of biosphere-atmosphere

feedbacks in climate change: Coupled model simulations for 6000 years BP and comparison with paleodata for northern Eurasia and northern Africa. *Climate Dynamics*, **13**, 865-882.

Tremback, C.J. and R. Kessler, 1985: A surface temperature and moisture parameterization for use in mesoscale numerical models. Preprints, 7th Conference on Numerical Weather Prediction, 17-20 June 1985, Montreal, Canada, AMS.

Tripoli, G.J. and W.R. Cotton, 1980: A numerical investigation of several factors contributing to the observed variable intensity of deep convection over South Florida. *L. Appl. Meteor.*, **19**, 1037-1063.

Uccellini, L.W., R.A. Petersen, K.F. Brill, P.J. Kocin, and J.J. Tuccillo, 1987: Synergistic interactions between an upper level jet streak and diabatic process that influence the development of a low-level jet and secondary coastal cyclone. *Mon. Wea. Rev.*, **115**, 2227-2261.

Vidale, P.L., R.A. Pielke, A. Barr, L.T. Steyaert, 1997: Case study modeling of turbulent and mesoscale fluxes over the BOREAS region. *J. Geophys. Res.*, **102**, 29167-29188.

Vitousek, P.M., H.A. Mooney, J. Lubchenco, and J.M. Melillo, 1997: Human domination of Earth's ecosystems. *Science*, **277**, 494-499.

Ziegler, C.L., T.J. Lee, and R.A. Pielke, 1997: Convective initiation at the dryline: A modeling study. *Mon. Wea. Rev.*, **125**, 1001-1026.

Walko, R.L., W.R. Cotton, M.P. Meyers, J.Y. Harrington, 1995a: New RAMS cloud microphysics parameterization Part I: the single-moment scheme. *Atmos. Res.*, **38**, 29-62.

Walko, R.L., C.J. Tremback, R.A. Pielke, and W.R. Cotton, 1995b: An interactive nesting algorithm for stretched grids and variable nesting ratios. *J. Appl. Meteor.*, **34**, 994-999.

Waring, R. and S.W. Running, 1998: *Forest ecosystems.* Academic Press, London, 370 pp.